VILNIUS UNIVERSITY

ŠARŪNAS MIKOLAITIS

EVOLUTIONARY EFFECTS OF CHEMICAL COMPOSITION IN RED GIANTS OF OPEN CLUSTERS

Doctoral Dissertation
Physical Sciences, Physics (02 P)

Vilnius, 2012

Doctoral Dissertation was completed during 2007–2011 at Vilnius University, Institute of Theoretical Physics and Astronomy

Scientific supervisor:

Habil. Dr. Gražina Tautvaišienė (Vilnius University, Institute of Theoretical Physics and Astronomy, Physical sciences, Physics – 02 P)

VILNIAUS UNIVERSITETAS

ŠARŪNAS MIKOLAITIS

EVOLIUCINIAI CHEMINĖS SUDĖTIES EFEKTAI PADRIKŲJŲ SPIEČIŲ RAUDONOSIOSE MILŽINĖSE

Daktaro Disertacija
Fiziniai mokslai, fizika (02 P)

Vilnius, 2012

Daktaro disertacija rengta 2007–2011 metais Vilniaus universiteto Teorinės fizikos ir astronomijos institute

Mokslinis vadovas:

Habil. dr. Gražina Tautvaišienė (Vilniaus universiteto Teorinės fizikos ir astronomijos institutas, fiziniai mokslai, fizika – 02 P)

Table of Contents

Introduction

Open clusters are important tools for studying of the Galactic disk as well as for understanding of stellar evolution (c.f., Friel et al. 2002; Bragaglia et al. 2008; Jacobson, Friel & Pilachowski 2009; Santos et al. 2009). This characterisation comes from the unique physical characteristics of their origin. Open clusters are physically related multi-object systems of stars bounded together by the gravitational force. Stars inside the open cluster populate a limited region of space, usually much smaller than their distance from the Sun, so that they are all roughly at the same heliocentric distance. They are believed to originate from large clouds of cosmic gas and dust in the Milky Way (or other parent galaxy), and are orbiting the Galaxy through the Galactic disk. In many clouds visible as bright diffuse nebulae, the star formation still takes place and we can observe the formation of new young star clusters. The process of formation takes only a considerably short time compared to the lifetime of a cluster, thus all member stars are of similar age. Since all stars in a cluster are formed from the same diffuse nebula, they are of similar initial chemical composition. Due to these features, open clusters attract a great interest of scientists (Paunzen 2008). The open cluster database WEBDA (Mermilliod & Paunzen 2003) states that about 2100 Galactic open clusters are identified and nearly a half of them have been observed so far in at least one photometric system. A number of stars per cluster goes from several tens in the poorest objects, to several thousands in the most populous clusters. Usually the Galactic open clusters that contain more than 100 stars are considered as populous.

Uniform groups of stars are better tools for understanding whether and how a slope of the radial metallicity distribution in a galaxy changes with time, since the statistics of the uniform multi-object system is much better, and their ages, distances and metallicities are more accurately derived than for field stars.

On the other hand, stars inside an open cluster can be treated separately. The basic theory states that evolution of a new star is predetermined by its initial mass. So, stars of open clusters have three constant basic parameters (age, initial compo-

Figure 0.1: The image of the cluster NGC 2506. The cluster consists of several hundreds 11th to 20th magnitude stars, thickly located across a region of about 8 arcmin in diameter (kindly provided by Observatorio Antilhue, Chile)

sition and distance) and one that varies from star to star (mass). This makes open clusters to be excellent laboratories for investigations of stellar evolution as well. Since cluster members were initially of approximately identical chemical composition, all changes in stellar atmospheres of evolved stars are related to internal and external processes of stellar evolution (see, e.g., Pallavicini 2003 and references therein). Changes of carbon and nitrogen abundances are most often seen in evolved stars. The enhancement of CN molecular bands and altered carbon isotope ratios in evolved stars of open clusters were reported already 30 years ago (e.g. Pagel 1974; McClure 1974). However, the detailed analyses of abundances in stars of open clusters from high-resolution spectra are still necessary for understanding of processes of the dredge-up and extra-mixing affecting the chemical composition of atmospheres in evolved low-mass stars. Detailed spectral analyses of carbon, nitrogen and oxygen elements in stars of open clusters are still rather scarce (Gilroy 1989; Gilroy & Brown 1991; Luck 1994; Gonzalez & Wallerstein 2000; Tautvaišienė et al. 2000, 2005; Origlia et al. 2006; Smiljanic et al. 2009 etc.). This thesis work is

a part of the effort to determine detailed elemental abundances in open clusters. In particular, we concentrate here on carbon and nitrogen, and also derive abundances of more than 20 other chemical elements.

Aims of the study

The main aim of the study is dedicated for the analysis of mixing tracers and possible extra mixing evidences in photospheres of evolved stars. Convection, the only mechanism of internal mixing taken into account by standard stellar evolution models, is not able to account for carbon and nitrogen abundance alterations seen in clump stars of open clusters. Extra-mixing processes may become efficient on the red giant branch when stars reach the so-called red giant branch (RGB) luminosity bump, and may modify the surface abundances. Alterations of $^{12}C/^{13}C$ and $^{12}C/^{14}N$ ratios depend on stellar evolutionary stage, mass and metallicity. This study aims to test theoretical models.

The secondary goal is a contribution of observational data to the study of present properties of the Galactic disc, its history and evolution. By collecting new spectroscopic data for open clusters, we aim to contribute to the analysis of chemical composition gradients in the Galactic disk in the radial direction.

Tasks of the study

- Determination and interpretation of abundances for mixing sensitive elements: carbon, nitrogen and C/N and $^{12}C/^{13}C$ ratios in stars of open clusters NGC 2506, NGC 6134, NGC 6253, IC 4651, and Collinder 261. Comparison of observational data with theoretical models of mixing.

- Determination of abundances of oxygen, α-elements, iron group and heavier chemical elements in open clusters NGC 2506, NGC 6134 and IC 4651, and comparison with studies of abundance gradients in the Galaxy.

Scientific novelty

- There is a very small number of clusters with known abundances of mixing sensitive elements as carbon, nitrogen and their elemental and isotopic ratios. The analysis of C, N, C/N and $^{12}C/^{13}C$ adds important data points for theoretical investigations of mixing and extra-mixing in atmospheres of evolved stars. Only one of selected clusters (NGC 6134) had the C/N and $^{12}C/^{13}C$ ratios for three other stars determined. Other four clusters gain this information for the first time.

- For the first time the detailed analysis of the chemical composition is done for the open cluster NGC 2506 and a number of stars in other investigated clusters.

Practical importance

Theory and modelling of extra-mixing processes in evolved low and intermediate mass stars can be tested just by using observational results. In this field of investigations, the data from open clusters are more welcomed because of uniform chemical and spatial properties of cluster stars.

High-resolution spectroscopy of open clusters with different metallicities, turn-off masses and distances will be standard reference points for the investigation of stellar and Galactic chemical evolution.

Results and statements presented for defence

- Derived photospheric abundances of up to 26 chemical elements, and $^{12}C/^{13}C$ and $^{12}C/^{14}N$ ratios in evolved stars of five open clusters.

- The $^{12}C/^{13}C$ ratios in helium-core-burning clump stars for the clusters with turn-off masses lower than 2 $M_{\odot}$ are in agreement with the Cool-bottom processing (CBP) model and the Thermohaline mixing (TH) model.

- The observed $^{12}C/^{13}C$ ratios of the helium-core-burning stars in the open cluster NGC 6134 support the observational evidences of extra-mixing in stars

heavier than 2.5 $M_{\odot}$ and are in disagreement with the theoretical models of mixing which state that extra-mixing is not possible for stars with turn-off mass higher than 2.5 $M_{\odot}$.

- In the open clusters NGC 2506 and NGC 6253, the $^{12}C/^{13}C$ ratios in core-helium-burning stars are lower than in the first ascent giants, located above the RGB luminosity bump. This could be caused by the further material mixing during a very violent helium flash event.

Personal contribution

The author made the reduction of spectra of observed stars in five open clusters, updated the software used for the analysis, determined the main atmospheric parameters (clusters NGC 2506, NGC 6253) and chemical composition of the programme stars. The author interpreted the chemical composition results and drew conclusions.

Publications on the subject of the dissertration

1. Tautvaišienė G., **Mikolaitis Š.**, Puzeras E., 2009, *E-infrastructure in Baltic States and its application in astrophysics*, Memorie della Societ Astronomica Italiana, Vol. 80, 534–539.

2. **Mikolaitis Š.**, Tautvaišienė G., Gratton R., Bragaglia A., Carretta E., 2010, *Chemical composition of evolved stars in the open cluster NGC 6134*, Monthly Notices of the Royal Astronomical Society, Vol. 407, 1866–1874.

3. **Mikolaitis Š.**, Tautvaišienė G., 2011, *Stellar energy flux modelling under gridified software SYNTSPEC*, EAS Publications Series, Vol. 45, 413–416.

4. **Mikolaitis Š.**, Tautvaišienė G., Gratton R., Bragaglia A., Carretta E., 2011, *Chemical composition of evolved stars in the open cluster IC 4651*, Monthly Notices of the Royal Astronomical Society, Vol. 413, 2199–2206.

5. **Mikolaitis Š.**, Tautvaišienė G., Gratton R., Bragaglia A., Carretta E., 2011, *Chemical composition of evolved stars in the open cluster NGC 2506*, Monthly Notices of the Royal Astronomical Society, Vol. 416, 1092–1098.

6. Tautvaišienė, **Mikolaitis Š.**, 2012, *Carbon and Nitrogen As Tracers of Stellar Evolution in Red Clump Stars of Open Cluster*s, Astrophysics and Space Science Proceedings, Part 2, 229–230.

7. **Mikolaitis Š.**, Tautvaišienė G., Gratton R., Bragaglia A., Carretta E., 2012, *C, N, O abundances and carbon isotope ratios in evolved stars of the open clusters Collinder 261 and NGC 6253*, Astronomy & Astrophysics, Vol. 541, 137–144.

Presentations at the international conferences

1. Tautvaišienė G., Pałak B., **Mikolaitis Š.**, *The Stellar Spectra Modeling As An Example Of Data- And Compute-Intensive Application Running On The Balticgrid Project Testbed*, "EGEE07 Conference", Budapest (Hungary), 04 – 06 April, 2007 (live demo presentation).

2. **Mikolaitis Š**. & Tautvaišienė G., *The Synthetic spectra modeling under GRIDCOM interface*, "European Week of Astronomy and Space Science Science, Royal Astronomical Society National Astronomy Meeting and European Astronomical Society Joint European and National Astronomy Meeting 2009", Hatfield (United Kingdom), 20 – 23 April, 2009.

3. **Mikolaitis Š**. & Tautvaišienė G., *The Synthetic spectra modeling application SYNTSPEC under GRIDCOM interface*, "EGEE09 Conference", Barcelona (Spain), 21 – 25 September, 2009.

4. **Mikolaitis Š**. & Tautvaišienė G., *Stellar energy flux modeling under SYNTSPEC application*, "ELSA conference 2010, Gaia: at the frontiers of astrometry", Sévres (France), 7 – 11 June, 2010.

5. Tautvaišienė G. & **Mikolaitis Š.**, *CNO Elements as Tracers of Stellar Evolution in Red Clump Stars of Open Clusters*, "JENAM 2010", Lisbon (Portugal),

6 – 12 September, 2010.

6. **Mikolaitis Š**. & Tautvaišienė G., *Synthetic stellar energy flux modeling under gridified software SYNTSPEC*, "Seventh International Conference on Atomic and Molecular Data and Their Applications 2010", 2010 Vilnius (Lithuania), 21 – 25 September.

7. Tautvaišienė G. & **Mikolaitis Š.**, *Tracers of Stellar Chemical Evolution in Red Clump Stars of Open Clusters* "Science Innovation and Gender", 2011 Vilnius (Lithuania), 24 – 25 November.

Thesis outline

The dissertation consists of five main parts: Introduction, four Chapters, and References.

Chapter 1 presents the programme open clusters and relevant observational data.

Chapter 2 introduces to the methods of differential analysis, models of stellar atmospheres, the software packages and developments, and uncertainties of the analysis.

Chapter 3 provides the results obtained for the programme stars, and their analysis, presents the comparison of mixing sensitive elements with theoretical models and describes the abundances in the light of the Galactic radial composition.

In Chapter 4 the main results and conclusions are summarised.

Chapter 1

Cluster data

The programme clusters were selected from the target list of the Bologna Open Clusters Chemical Evolution project (BOCCE). The BOCCE project aims to improve our understanding of mixing processes and chemical composition gradients according to Galactocentric radial distances. It builds up a large sample of open clusters for which the age, distance, and metallicity are derived in the most precise and homogeneous way, avoiding spurious effects due to inhomogeneous treatments. The BOCCE project collected about 30 clusters evenly distributed in age, metallicity, and galactocentric distance bins to allow for a reliable derivation of possible trends. For this reason the BOCCE group is undertaking a long-term project of accurate photometry and high-resolution spectroscopy. The project goal is to derive ages, distances, reddening, and element abundances in open clusters of various ages and Galactic locations, and eventually to infer from them the evolution of the metallicity radial distribution. Age, distance, and reddening are obtained by deriving the CMDs from deep, accurate photometry and applying to them the synthetic CMD method described by Tosi et al. (1991). Accurate chemical abundances are obtained from high-resolution spectroscopy, applying to all clusters the same method of analysis and the same metallicity scale (see Bragaglia & Tosi 2006). Positions of the BOCCE project clusters in the Galactic plane (Bragaglia & Tosi 2006), together with open clusters studied in this thesis work, are shown in Fig. 1.1.

Stars in chosen clusters were selected on a basis of their evolutionary phases derived from the photometric data. Red clump stars (i.e. stars in the core-helium-burning phase) were the main targets. Among the evolved population, they are the most homogeneous group, and their temperatures are, in general, high enough that, even at the high metallicity expected for open clusters, model atmospheres can well reproduce the real atmospheres. Only objects for which membership information

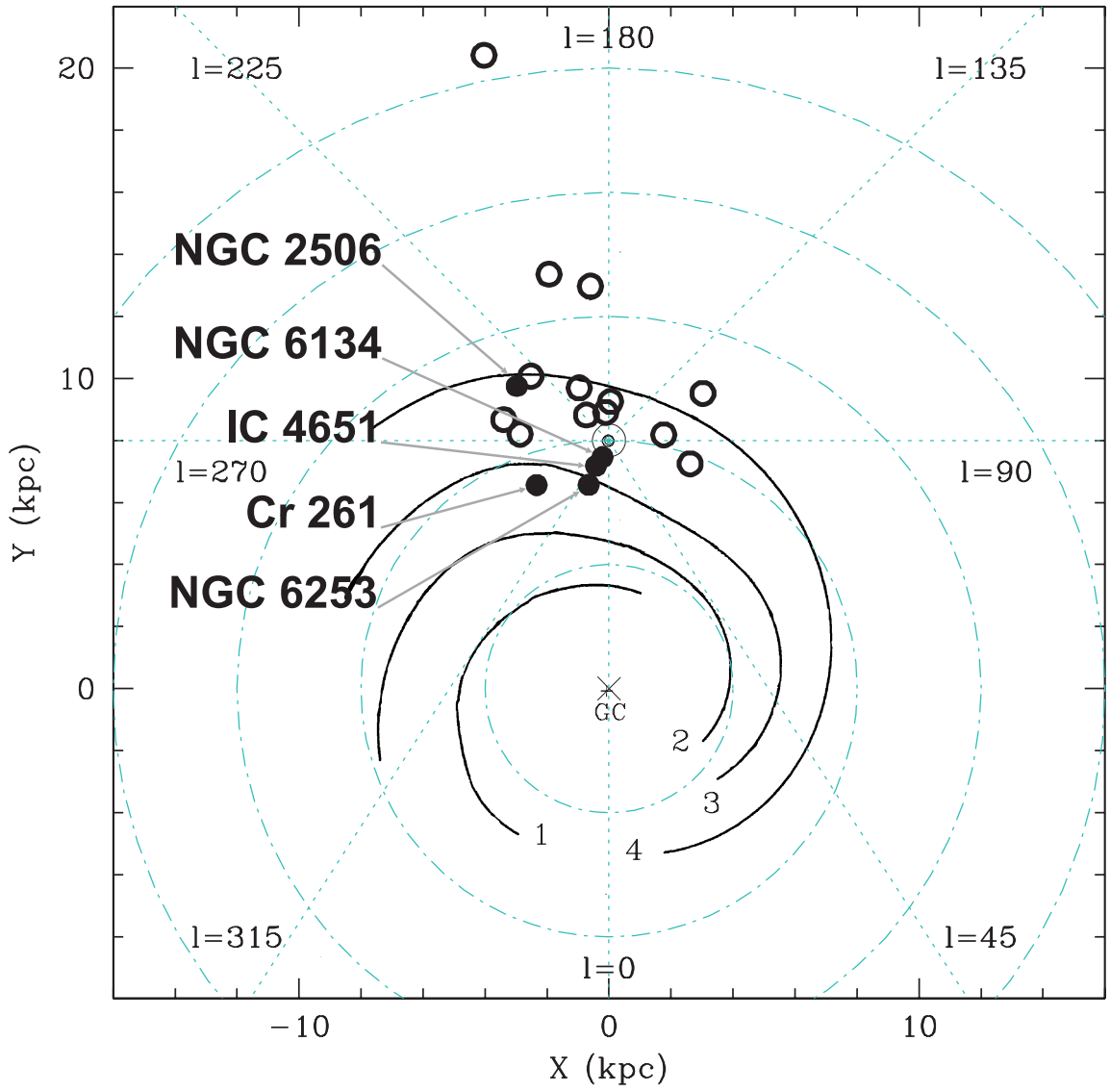

Figure 1.1: Positions of open clusters on the Galactic plane from Bragaglia & Tosi (2006). Green filled circles mark clusters of this work, opened circles present other clusters of the BOCCE project. Positions of the Sun and the Galactic centre are shown. A sketch of the spiral arms (respectively: 1 = Norma, 2 = Scutum-Crux, 3 = Sagittarius-Carina, 4 = Perseus).

was available from astrometry were considered (NGC 2506, Chiu & van Altena 1981), and/or radial velocity (NGC 2506: Friel & Janes 1993, Minniti 1995; NGC 6134: Claria & Mermilliod 1992; IC 4651: Mermilliod 1995).

Table 1.1: Parameters of the programme stars in open clusters NGC 2506, NGC 6253, NGC 6134, IC 4651 and Collinder 261.

Star*	V mag	$B-V$ mag	$b-y$ mag	S/N	Phase	RV km s^{-1}
			NGC 2506			
438	13.234	0.944	–	85	Clump	+84.64 ±0.3
443	13.105	0.952	–	77	Clump	+84.66 ±0.2
456	13.977	0.919	–	35	RGB	+83.68 ±0.3
459	11.696	1.100	–	110	RGBtip	+81.62 ±0.6
* Star numbers, V and $B-V$ from Marconi et al. (1997);						
			NGC 6134			
39	12.20	1.273	0.811	56	Clump	−25.34 ±0.3
69	12.36	–	0.811	200	Clump	−25.19 ±0.3
75	12.39	1.284	0.820	200	Clump	−26.34 ±0.3
114	12.07	1.310	0.841	80	Clump	−24.94 ±0.6
129	12.25	1.314	0.838	200	Clump	−25.46 ±0.3
157	12.25	1.268	0.820	80	Clump	−25.26 ±0.2
* Star numbers from Mermilliod (1995), V and $B-V$ from Claria & Mermilliod (1992), $b-y$ from Bruntt et al. (1999);						
			NGC 6253			
2509	12.685	1.314	0.877	120	Clump	−28.71 ±0.3
2885	12.656	1.352	0.891	180	Clump	−28.13 ±0.3
3595	12.388	1.292	0.866	85	Clump	−28.76 ±0.4
4510	12.759	1.296	0.873	150	Clump	−28.44 ±0.3
* Star numbers, V and $B-V$ from Bragaglia et al. (1997), $b-y$ from Twarog, Anthony-Twarog & De Lee (2003);						

Table 1.1: Continued

Star*	V mag	$B-V$ mag	$b-y$ mag	S/N	Phase	RV km s^{-1}
			IC 4651			
27	10.86	1.23	0.749	100	Clump	-30.17 ± 0.6
56	8.95	1.68	1.064	100	RGBtip	-29.56 ± 0.3
72	10.41	1.33	0.801	100	RGB	-30.82 ± 0.2
76	10.94	1.17	0.708	100	Clump	-29.86 ± 0.3
146	10.94	1.14	0.702	100	Clump	-27.88 ± 0.4
* Star numbers, V and $B-V$ from Lindoff (1972), $b-y$ from Anthony-Twarog & Twarog (2000);						
			Collinder 261			
1045	13.547	1.487	–	85	RGB	-25.56 ± 0.3
1080	13.952	1.435	–	70	Clump	-25.31 ± 0.3
1485	13.680	1.577	–	85	RGB	-27.63 ± 0.3
1871	12.350	2.060	–	130	RGBtip	-26.85 ± 0.3
2001	13.932	1.356	–	75	Clump	-25.37 ± 0.3
2105	12.908	1.517	–	95	RGB	-25.34 ± 0.3
* Star numbers, V and $B-V$ from Phelps, Janes & Montgomery (1994), $b-y$ from Gozzoli et al. (1996);						

1.1 Cluster parameters

1.1.1 NGC 2506

In this work, our first target of investigation is the open cluster NGC 2506 ($\alpha_{2000} = 08^h0.02^m, \delta_{2000} = -10°46.2'; l = 230.564°, b = +09.935°$). The Galactic orbit of this cluster was determined by Carraro & Chiosi (1994). It was found that the orbit of NGC 2506 has a small eccentricity ($e = 0.03$) and epicyclical amplitude ($\Delta R =$ 0.84 kpc), suggesting that it has not moved far away from the site of formation. The orbit remains confined at radial distances between 10.7 and 11.6 kpc, and along the z-direction does not extend beyond 0.6 kpc.

Since the first studies by van der Bergh & Sher (1960) and Purgathofer (1964), NGC 2506 has quite many references in the literature. Relative proper motions for

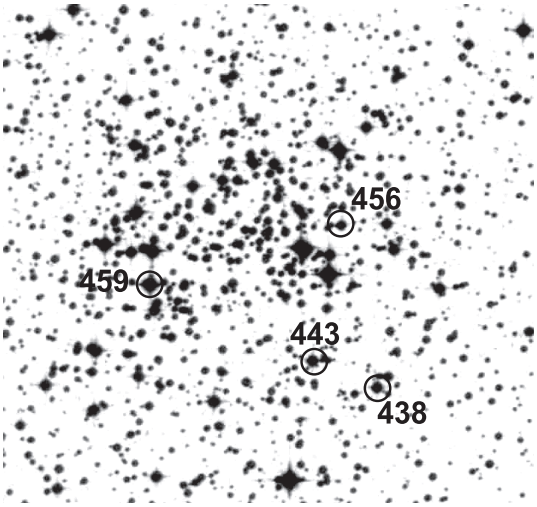

Figure 1.2: Field of 7.5 x 7.5 arcmin^2 centered on NGC 2506, with the programme stars indicated by their numbers according to Marconi et al. (1997).

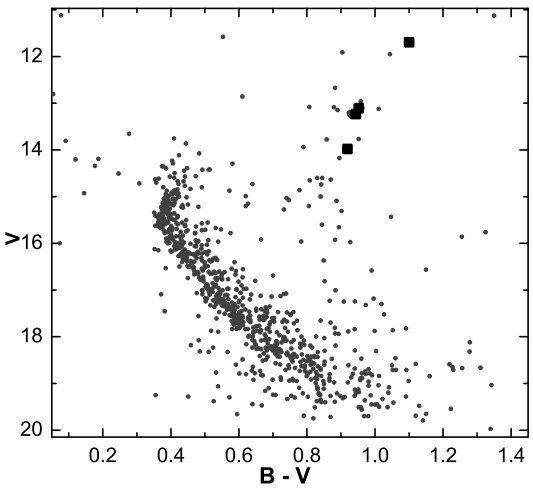

Figure 1.3: The colour-magnitude diagram of the open cluster NGC 2506. The stars investigated in this work are indicated by the filled squares. The diagram is based on *UBVRI* photometry by Marconi et al. (1997).

724 stars in the region of NGC 2506 have been determined and probabilities of membership derived by Chiu & van Altena (1981). According to the recent studies, NGC 2506 is a mildly elongated cluster containing about 1090 stars (Chen, Chen & Shu 2004), its generally accepted age is $t = 1.7$ Gyr (Marconi et al. 1997), the turn-off mass $M = 1.69\ M_{\odot}$ (Carretta et al. 2004), its Galactocentric and Heliocentric distances are $R_{gc} = 10.38$ kpc and $d = 3.26$ kpc respectively (Bragaglia & Tosi 2006).

A high resolution spectroscopic observation of NGC 2506 was already obtained already 30 years ago by Geisler (1984). For the star NGC 2506 22012, a surprisingly low metallicity ([Fe/H]$= -0.67$)[1] was determined and [Mg/Fe] and [Si/Fe] were found to be rather large (0.8 dex). Metallicity determinations using Washington system photometry were also presented for this cluster in the same paper, with value of -0.93 dex using the $M - T_1$ colour index and of -0.51 dex using $C - M$. Later photometric observations of this cluster indicated quite a low metallicity as

[1] In this work we use the customary spectroscopic notation:

$$[X/Y] \equiv \log_{10}\left(\frac{N_{\rm X}}{N_{\rm Y}}\right)_{\rm star} - \log_{10}\left(\frac{N_{\rm X}}{N_{\rm Y}}\right)_{\odot} \tag{1.1}$$

well. A value of $[Fe/H] = -0.55$ relative to the Hyades was determined from UBV and DDO photoelectric photometry and B and V photographic photometry by McClure, Twarog & Forrester (1981). Using the same observational data and a new calibration, Piatti, Claria & Abadi (1995) have determined $[Fe/H] = -0.48$. From Washington photoelectric photometry $[Fe/H] = -0.58$ was determined by Geisler, Claria & Minniti (1992). However, a higher metal abundance of -0.20 dex was obtained from high resolution spectroscopy by Carretta et al. (2004), as averaged from two stars. Parameters of the programme stars are presented in Table 1.1 and log of observations in Table 1.2. Two stars of this thesis work, (438 and 443) belong to the red clump, the star 456 is a first-ascent giant, and the star 459 is an red giant branch (RGB)-tip giant (see Fig. 1.3 for the colour-magnitude diagram of NGC 2506 with these stars indicated). Fig. 1.2 shows a finding chart of the observed stars.

1.1.2 NGC 6134

The open cluster NGC 6134 is an intermediate-age, moderately concentrated open cluster (Trumpler class II3m) located almost on the galactic plane ($\alpha_{2000} = 16^h27.8^m$, $\delta_{2000} = -49^\circ09.4'.9; l = 324.91^\circ, b = -0.20^\circ$). The first extensive photometric study was published by Lindoff (1972) who derived a colour excess $E(B-V) = 0.45$, a distance of about 700 pc, and an age of about 0.7 Gyr. These values were based only on UBV photographic data. Kjeldsen & Frandsen (1991) published UBV CCD data for 66 stars at the centre of the cluster and obtained $E(B-V) = 0.46$ and $m-M = 11.25$.

Coravel radial velocity measurements and photometry in the UBV and CMT_1T_2 system of 24 red giants, supplemented by *DDO* observations of 11 stars, were carried out by Claria & Mermilliod (1992) for membership and binarity analysis, who identified 17 red giant members and 6 spectroscopic binaries. The mean cluster radial velocity was found to be -26.0 ± 0.24 km s^{-1}, the reddening $E(B-V) = 0.35 \pm 0.02$, and the distance about 760 pc. The weighted mean value of [Fe/H] $= -0.05 \pm 0.12$ was evaluated from the UV excesses. Strömgren photometry was analysed by Bruntt et al. (1999). They determined $E(b-y) = 0.263 \pm 0.004$ ($E(B-V) = 0.365$), [Fe/H]$= 0.28 \pm 0.02$, and age=0.69 ± 0.10 Gyr. The colour-magnitude diagram (Bruntt et al. 1999) shows a "clump" of core-He-burning stars,

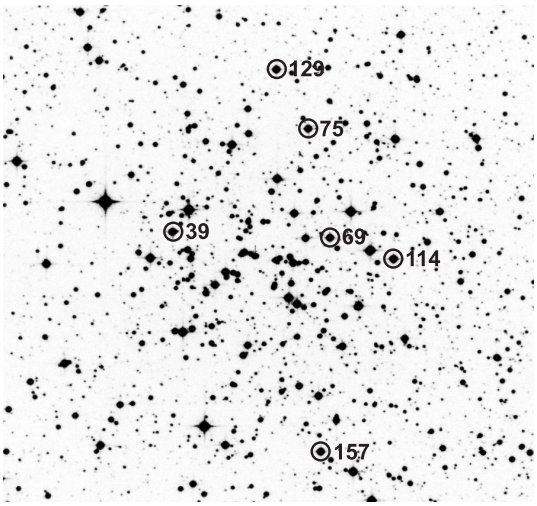

Figure 1.4: Field of 10×10 arcmin^2 centered on NGC 6134, with the programme stars indicated by their numbers according to Mermilliod (1995).

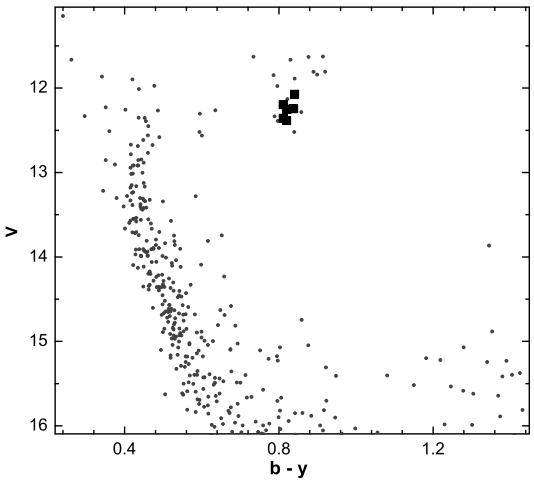

Figure 1.5: The colour-magnitude diagram of the open cluster NGC 6134. The core-He-burning 'clump' stars analysed are indicated by the filled squares. The diagram is based on Strömgren photometry by Bruntt et al. (1999).

several RGB stars, and a main sequence. From *BVRI* CCD observations Ahumada (2002) has determined a colour excess $0.29 < E(B-V) < 0.37$, age of 1.26 Gyr, and a distance of about 1080 ± 50 pc, which is larger than in the previous analyses.

Precise iron abundances from high resolution spectra for six stars in this cluster have been determined by Carretta et al. (2004). An overall metallicity $[\mathrm{Fe/H}] = 0.15 \pm 0.03$ with $rms = 0.07$ was found. Carretta et al. also computed the reddening from the spectroscopically derived temperatures and from the Alonso, Arribas & Martínez-Roger (1999, 2001) colour-temperature relations, finding $E(B-V) = 0.363 \pm 0.014$, in very good agreement with Bruntt et al. (1999). Using the same spectra and method of analysis, in this thesis work we continued detailed abundance investigations for the clump stars NGC 6134 39, 69, 75, 114, 129, and 157. Elemental abundances in three other clump stars of this cluster (NGC 6134 30, 99, and 202) have been investigated recently by Smiljanic et al. (2009).

Fig. 1.4 shows a finding chart of the observed stars and their evolutionary status is indicated by their position in the CMD (Fig. 1.5). All of these stars belong to the red clump of the cluster. The log of observations is presented in Table 1.2 and parameters of the programme stars are in Table 1.1. In the Carretta et al. (2004)

paper all the main atmospheric parameters for the observed stars were determined. For convenience we present them in this work as well (Table 3.1).

1.1.3 NGC 6253

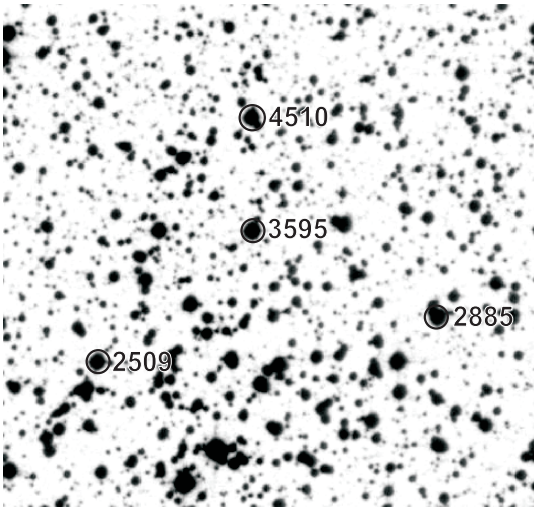

Figure 1.6: Field of 5 × 5 arcmin^2 centered on NGC 6253, with the programme stars indicated by their numbers according to Bragaglia et al. (1997).

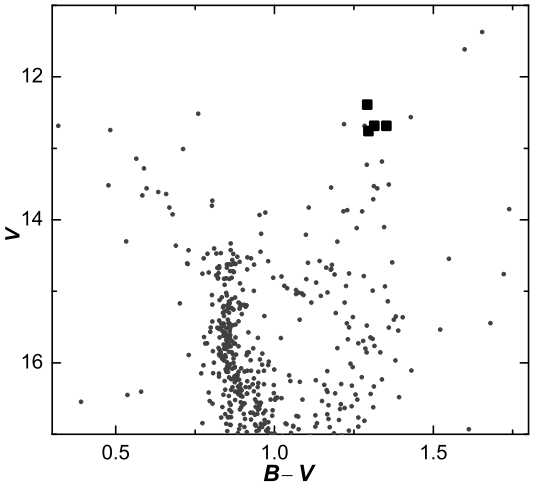

Figure 1.7: The colour-magnitude diagram of the open cluster NGC 6253. The stars investigated in this work are indicated by the filled squares. The diagram is based on $UBVI$ photometry by Bragaglia et al. (1997).

NGC 6253 (galactic coordinates $l = 335°.45, b = -6°.26$) is also quite old open cluster of 3–5 Gyr (Piatti et al. 1998; Bragaglia & Tosi 2006; Montalto et al. 2009) and located in the inner part of the Galaxy, at 6.6 kpc from the Galactic centre. The most interesting signature of this open cluster is its high metallicity. Recent high-resolution spectral determinations of [Fe/H] are the following: +0.43 dex (Anthony-Twarog et al. 2010), +0.36 dex (Sestito, Randich & Bragaglia 2007), +0.46 dex (Carretta, Bragaglia & Gratton 2007). Since mixing processes depend on stellar metallicitys, it is important to have C/N and $^{12}C/^{13}C$ ratios determined in metal-abundant evolved stars. By now, less than a handful of open clusters with similarly high metal-abundance have been detected in our Galaxy (e.g., NGC 6791,

Gratton et al. 2006; NGC 2632, Pace, Pasquini & François 2008). This makes NGC 6253 a very attractive target for our study. All stars observed in NGC 6253 belong to the red clump of the cluster (see Fig. 1.7). Fig. 1.6 shows a finding chart of the observed stars. Parameters of the programme stars are presented in Table 1.1 and log of observations in Table 1.2.

1.1.4 IC 4651

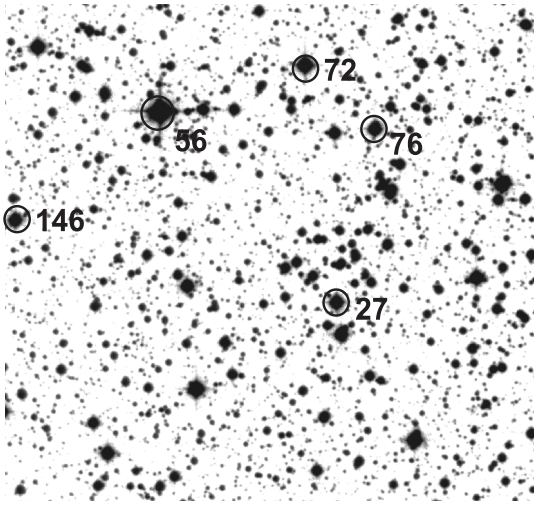

Figure 1.8: Field of 8 x 8 arcmin^2 centered on IC 4651, with the programme stars indicated by their numbers according to Lindoff (1972).

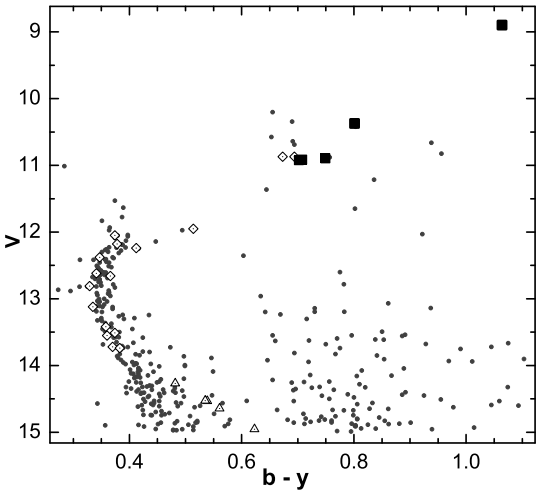

Figure 1.9: The colour-magnitude diagram of the open cluster IC 4651. The stars investigated in this work are indicated by the filled squares. The stars of two other high-resolution spectral abundance studies are shown in this plot as well: the work of Pace, Pasquini & François (2008) is marked by triangles and of Pasquini et al. (2004) – by diamonds. The diagram is based on Strömgren photometry by Anthony-Twarog & Twarog (2000).

The open cluster IC 4651 ($\alpha_{2000} = 17^h24.8^m, \delta_{2000} = -49°56.0'; l = 340.088°, b = -07.907°$) is an intermediate-age (1.7 Gyr) open cluster located 140 pc below the Galactic plane and 7.1 kpc form the Galactic centre (Pasquini et al. 2004). Mei-

bom, Andersen & Nordström (2002) provided calculations of the space motion and the Galactic orbit of the cluster. The orbital eccentricity is $e = 0.19$ and the mean radius of Galactocentric orbit is 8.6 kpc, its maximum distance from the Galactic plane is 190 pc . Results of extensive photometric studies were published first by Eggen (1971) and Lindoff (1972) and later on by Anthony-Twarog & Twarog (1987, 2000) and Anthony-Twarog et al. (1988). However, the most recent photometric study was performed by Meibom (2000) and Meibom, Andersen & Nordström (2002). They combined photometric observations and radial velocity measurements for the 44 single member stars down to $V = 14.5$ mag and determined $E(B-V) = 0.10$ mag, the distance $d = 1.01 \pm 0.05$ kpc, and the mean radial velocity equal to -30.76 ± 0.20 km s^{-1}. It was found that 37 per cent of giant members are spectroscopic binaries with periods up to 5000 days, and 52 per cent of the main-sequence and turn-off members are binaries with periods less than 1000 days. The estimated total mass of IC 4651 is $\approx 630 M_{\odot}$ (Meibom, Andersen & Nordström 2002). The turn-off mass of the IC 4651 stars $M = 1.69 M_{\odot}$ was obtained by Carretta et al. (2004) reading the turn-off values on the Girardi et al. (2000) isochrones for solar metallicity at the age of the cluster of 1.7 Gyr as determined by Meibom, Andersen & Nordström (2002).

There were several photometric studies that evaluated the metallicity of IC 4651. Based on $uvby - H_{\beta}$ photometry, $[\mathrm{Fe/H}] = 0.23 \pm 0.02$ was found by Anthony-Twarog & Twarog (1987), $[\mathrm{Fe/H}] = 0.18 \pm 0.05$ by Nissen (1988), and $[\mathrm{Fe/H}] = 0.077 \pm 0.012$ by Anthony-Twarog & Twarog (2000). High resolution spectroscopic data started to appear in the beginning of the millennium. Bragaglia et al. (2001) determined the mean metallicity of five evolved stars $[\mathrm{Fe/H}] = 0.16 \pm 0.01$. Pasquini et al. (2004) provided the cluster metallicity $[\mathrm{Fe/H}] = 0.10 \pm 0.03$ from the analysis of 22 faint main sequence stars of the cluster. Abundances of the iron peak, α-elements and lithium were investigated in their study as well. Carretta et al. (2004) found the average $[\mathrm{Fe/H}] = 0.11 \pm 0.01$ for 5 evolved stars of the cluster, which we analyse further in this our work. Pace, Pasquini & François (2008) provided the abundance measurements of Fe, Ca, Na, Ni, Ti, Al, Cr, Si for 20 solar-type stars belonging to IC 4651 and found $[\mathrm{Fe/H}] = 0.12 \pm 0.05$. And finally, Santos et al. (2009) derived the mean metallicity $[\mathrm{Fe/H}] = 0.15 \pm 0.02$ for IC 4651 from five dwarf stars. In our work for the open cluster IC 4651, the detailed abundance

analysis of almost 30 chemical elements is done. Abundances of such key chemical elements as ^{12}C, ^{13}C, N, O as well as representatives of *s*- and *r*-processes are determined. The finding chart of the investigated stars is given in Fig. 1.8. The colour-magnitude diagram of the open cluster IC 4651 is show in Fig. 1.9 with the stars investigated in Pasquini et al. (2004), Pace, Pasquini & François (2008) and this work indicated by different symbols. Main photometric parameters, S/N ratios, evolutionary phases are presented in Table 1.1 and log of observations in Table 1.2.

1.1.5 Collinder 261

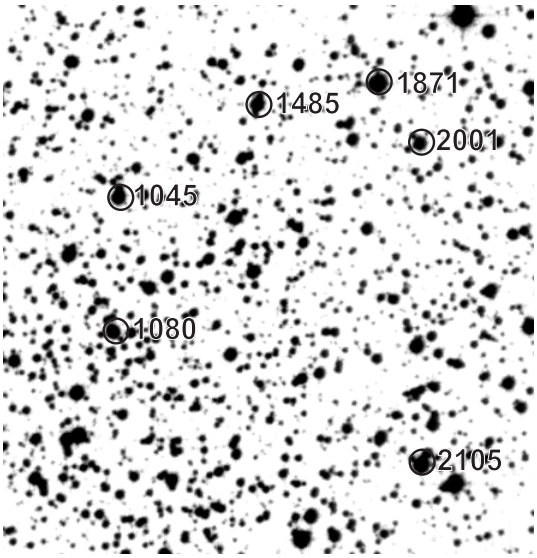

Figure 1.10: Field of 7 × 7 arcmin^2 centered on Collinder 261, with the programme stars indicated by their numbers according to Phelps, Janes & Montgomery (1994).

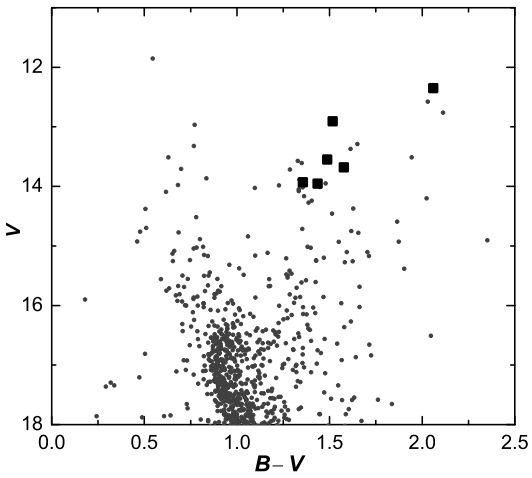

Figure 1.11: The colour-magnitude diagram of the open cluster Collinder 261. The stars investigated in this work are indicated by the filled squares. The diagram is based on *BVI* photometry by Gozzoli et al. (1996).

Collinder 261 (Cr 261; galactic coordinates $l = 301°.68, b = -5°.53$) is one of the oldest open clusters in the Galaxy. Its age is 5–10 Gyr, depending on the adopted stellar evolution models (Janes & Phelps 1994; Mazur, Krzeminski & Kaluzny 1995; Gozzoli et al. 1996; Carraro, Ng & Portinari 1998), but the recent investigation of Bragaglia & Tosi (2006) has defined a most probable age around 6 Gyr.

Unlike the majority of old open clusters, which are located in the outer Galactic disk, this cluster is in the inner part, at 7.5 kpc from the Galactic centre and 235 pc below the plane. Despite the old age, the metallicity of this cluster, determined from high-resolution spectral studies, is close to solar: $[\mathrm{Fe/H}] = -0.03$ (Carretta et al. 2005; De Silva et al. 2007), -0.22 dex (Friel et al. 2003), $+0.13$ dex (Sestito et al. 2008). De Silva et al., who investigated 12 red giants in Cr 261 using Very Large Telescope (VLT) UVES spectra, emphasised that this cluster is very chemically homogeneous – the intrinsic scatter was estimated to be less than 0.05 dex. The chemical homogeneity of Cr 261 makes this cluster an extremely interesting target for the investigation of mixing sensitive elements like carbon isotopes and nitrogen, which have not been studied in previous studies. Two stars (1080 and 2001) belong to the red clump of the cluster, three stars (1045, 1485 and 2105) are first-ascent giants, and the star 1871 is an RGB-tip giant (see Fig. 1.11 for the colour-magnitude-diagram and Fig. 1.10 for the finding chart). The log of observations, main photometric parameters and S/N ratios are presented in Tables 1.1 and 1.2.

1.2 Observations

1.2.1 FEROS spectrograph

The most of the spectra were obtained with the spectrograph FEROS (Fiber-fed Extended Range Optical Spectrograph) mounted at the 1.5 m telescope in La Silla (Chile). The resolving power is $R = 48\,000$ and the wavelength range is λ 3700–8600 Å. There was a possibility of reducing data at the telescope using a dedicated on-line data reduction package in the MIDAS environment, so the wavelength calibrated spectra were obtained immediately. Multiple exposures for the same star were summed. Samples of the spectra are presented in Fig. 1.12.

1.2.2 UVES spectrograph

Some spectra of stars in two clusters were obtained with the UVES spectrograph (UV-Visual Echelle Spectrograph) on the Unit 2 of the VLT ESO-Paranal telescope. The spectral coverage is λ 3560–4840 Å and 5550–9460 Å, and the resolving power

is $R = 43\ 000$. The UVES data were reduced with the standard pipeline which produces extracted, wavelength calibrated, and merged spectra. Samples of the spectra are presented in Fig.1.12. The observational data (instrument, coordinates, date and time of observation, exposure time) for individual stars are presented in Table 1.2.

Table 1.2: Log of observations. The identification numbers for cluster NGC 2506 are those of Marconi et al. (1997), for the cluster NGC 6253 are used from Bragaglia et al. (1997), NGC 6134 are used from the BDA (Mermilliod 1995), IC 4651 from Lindoff (1972) and Cr 261 are from Phelps, Janes & Montgomery (1994). Coordinates are at J2000, and exposure times are in seconds.

ID	Inst.	Ra	Dec	Date obs.	UT	Exptime
		hh:mm:ss	deg:mm:ss	yyyy-mm-dd	hh:mm:ss	s
			NGC 2506			
438	FEROS	7:59:51.79	-10:48:46.51	2000-04-28	01:51:57	3600
	FEROS			2000-04-29	00:02:56	3600
443	FEROS	7:59:55.77	-10:48:22.73	2000-04-29	01:06:30	3600
	FEROS			2000-04-29	02:12:58	3600
456	FEROS	7:59:54.06	-10:46:19.50	2000-04-30	00:56:38	3600
	FEROS			2000-04-30	02:00:05	2400
	FEROS			2000-05-01	01:34:51	2700
459	FEROS	8:00:05.84	-10:47:13.33	2000-04-28	00:43:04	3600
			NGC 6134			
69	UVES	16:27:39.49	-49:08:39.30	2002-07-20	00:09:57	1800
75	UVES	16:27:42.27	-49:06:36.10	2002-07-18	01:25:11	2400
129	UVES	16:27:46.07	-49:05:29.60	2002-07-19	23:36:34	1800
39	FEROS	16:27:57.68	-49:08:36.20	2000-05-01	07:45:47	1800
	FEROS			2000-05-01	08:18:58	1800
114	FEROS	16:27:32.10	-49:09:02.00	2000-04-30	08:04:09	2700
	FEROS			2000-04-30	08:55:42	3229
157	FEROS	16:27:40.05	-49:12:42.20	2000-05-01	08:56:11	2400
	FEROS			2000-05-01	09:39:14	2400

Table 1.2: Continued

ID	Inst.	Ra	Dec	Date obs.	UT	Exptime
		hh:mm:ss	deg:mm:ss	yyyy-mm-dd	hh:mm:ss	s
			NGC 6253			
2509	UVES	16:59:15.91	-52:42:26.07	2002-07-16	02:07:04	1800
2885	UVES	16:58:53.28	-52:41:54.04	2002-07-16	02:12:40	2400
3595	FEROS	16:59:05.80	-52:41:04.09	2001-04-25	07:40:59	4200
	FEROS			2001-04-25	08:53:33	4200
4510	UVES	16:59:06.03	-52:39:56.06	2002-07-19	23:37:52	1800
			IC 4651			
27	FEROS	17:24:50.13	-49:56:55.89	2000-04-28	08:05:27	1800
56	FEROS	17:25:09.02	-49:53:57.21	2000-04-28	09:39:59	600
72	FEROS	17:24:54.22	-49:53:07.58	2000-04-28	09:15:05	1200
76	FEROS	17:24:46.78	-49:54:06.94	2000-04-28	08:39:43	1800
146	FEROS	17:25:23.63	-49:55:47.11	2000-04-29	09:25:29	1500
	FEROS			2000-04-29	09:54:04	1500
			Collinder 261			
1045	FEROS	12:38:08.49	-68:21:15.01	2000-05-01	03:16:43	3600
	FEROS			2000-05-01	03:16:43	3600
1080	FEROS	12:38:07.42	-68:22:30.82	2000-05-01	05:42:01	3600
	FEROS			2000-05-01	06:45:03	3600
1485	FEROS	12:37:55.55	-68:20:14.36	2000-04-29	04:37:56	3600
	FEROS			2000-04-29	05:41:30	3600
1871	FEROS	12:37:43.60	-68:19:55.06	2000-04-29	03:27:25	3600
2001	FEROS	12:37:38.68	-68:20:25.87	2000-04-29	06:48:44	3600
	FEROS			2000-04-30	03:45:22	3600
	FEROS			2000-04-30	04:48:33	3600
2105	FEROS	12:37:34.82	-68:23:24.99	2000-04-30	06:09:47	3600
	FEROS			2000-04-30	06:09:47	3600

Figure 1.12: Small samples of stellar spectra of programme stars in three clusters. An offset of the 0.5 base in relative flux is applied for clarity.

Chapter 2

Method of analysis

2.1 Differential analysis

The analysis technique requires a number of input data in order to derive abundances of chemical elements: values of main atmospheric parameters (effective temperature, surface gravity in logarithmic scale, microturbulence velocity, and general metallicity); a grid of stellar atmosphere models for interpolation of an exact model; physical atomic and molecular parameters.

In the presented work a differential analysis technique was used. This allowed to eliminate uncertainties related to atomic data, simplifications in model atmospheres, assumptions of local thermodynamic equilibrium (LTE). We have performed the differential abundance analysis for each programme star relative to the Sun as a standard star. It is a typical practice to use the Sun as a standard star.

2.2 Models of stellar photosphere

A stellar interior is a dense and hot plasma environment where energy is produced by fusion processes. It radiates a specific flux of energy, that is spread within all range of electromagnetic waves. The atmosphere is the part of a star which modifies the energy flux distribution over the wavelength range. The atomic and molecular matter of the photosphere redistributes the initial energy flux through all the spectrum employing absorption, re-emission, scattering processes and paints a unique shape of flux image of a specific star. The stellar atmosphere consists of low density gas (see an example of the modeled Solar densities in the second column of Table 2.1). The Ideal Gas Law may be chosen to describe main physical parameters of gas: pressure, density and temperature.

Table 2.1: Example of ATLAS atmosphere models for a solar-type star.

Nr	ρx $\frac{g}{cm^2}$	T K	P_g $0.1Pa$	N_e cm^{-3}	κ_{ross} $\frac{g}{cm^2}$	g_{rad} $\frac{cm}{s^2}$	v_t $\frac{cm}{s}$
1	$5.128\ 10^{-4}$	3709.1	$1.405\ 10^{+1}$	$2.797\ 10^{+9}$	$2.600\ 10^{-4}$	$7.028\ 10^{-2}$	$1.5\ 10^{+5}$
2	$6.711\ 10^{-4}$	3732.6	$1.839\ 10^{+1}$	$3.602\ 10^{+9}$	$3.019\ 10^{-4}$	$7.387\ 10^{-2}$	$1.5\ 10^{+5}$
3	$8.535\ 10^{-4}$	3754.9	$2.339\ 10^{+1}$	$4.517\ 10^{+9}$	$3.483\ 10^{-4}$	$7.641\ 10^{-2}$	$1.5\ 10^{+5}$
4	$1.064\ 10^{-3}$	3778.6	$2.917\ 10^{+1}$	$5.568\ 10^{+9}$	$4.009\ 10^{-4}$	$7.802\ 10^{-2}$	$1.5\ 10^{+5}$
...							
52	$2.473\ 10^{+0}$	5504.6	$6.776\ 10^{+4}$	$1.198\ 10^{+13}$	$2.545\ 10^{+1}$	$5.827\ 10^{-1}$	$1.5\ 10^{+5}$
53	$2.848\ 10^{+0}$	5650.2	$7.805\ 10^{+4}$	$1.554\ 10^{+13}$	$3.098\ 10^{+1}$	$7.002\ 10^{-1}$	$1.5\ 10^{+5}$
54	$3.248\ 10^{+0}$	5843.7	$8.900\ 10^{+4}$	$2.190\ 10^{+13}$	$4.021\ 10^{+1}$	$9.037\ 10^{-1}$	$1.5\ 10^{+5}$
...							
70	$7.378\ 10^{+0}$	9631.9	$2.021\ 10^{+5}$	$4.840\ 10^{+15}$	$5.619\ 10^{+1}$	$5.417\ 10^{+0}$	$1.5\ 10^{+5}$
71	$7.681\ 10^{+0}$	9813.4	$2.104\ 10^{+5}$	$5.740\ 10^{+15}$	$6.752\ 10^{+1}$	$5.181\ 10^{+0}$	$1.5\ 10^{+5}$
72	$8.021\ 10^{+0}$	9977.4	$2.197\ 10^{+5}$	$6.688\ 10^{+15}$	$7.936\ 10^{+1}$	$5.099\ 10^{+0}$	$1.5\ 10^{+5}$

A grid of stellar atmosphere models ATLAS was used for the analysis (Kurucz 1993; Sbordone et al. 2004). The ATLAS grid contains 7600 stellar atmosphere models for a wide range of metallicities, effective temperatures and gravities. The metallicities, [A/H], cover the range from –5.0 to +1.0 dex with a step of 0.5 dex, the gravities, log g, range from 0.0 to +5.0 with $\Delta\log g = 0.5$. The range of effective temperatures, $T_{\rm eff}$, from 3500 K to 50000 K is covered with uneven spacing (Kurucz 1993; Sbordone et al. 2004). The modelled spectra cover a spectral range from 100 nm in ultraviolet to 10 μm in infrared, with a non-uniform wavelength spacing. These classical one dimensional models of atmosphere were computed with several assumptions described by Castelli (1988):

- The thickness of the atmosphere is very small compared to the radius of a star. The atmospheric layers are plane-parallel, making all physical variables to be a function of only one space coordinate.
- Magnetic fields, granules, spicules, cells, and spots are ignored. All layers are homogeneous.
- The Hydrostatic equilibrium is accepted. The atmosphere is static. The grav-

itational attraction is balanced by the pressure. There are no relative motions of layers, expansion is not allowed.

- The Steady state approximation is accepted. The state of gas and the transport of the radiation are constant.
- The Local thermodynamic equilibrium is accepted. The gas depends only on the local values of the radiation field. It has no connection to the radiation in other layers. Each layer has its own temperature
- Radiative and convective flux of energy is constant with depth in the atmosphere. The flux is constant throughout the atmosphere.
- The atomic abundances are specified and constant throughout the atmosphere.

The one dimensional ATLAS models are assembled of 72 layers, that describe the physical properties of the stellar atmosphere layer by layer. An example of the ATLAS model structure is shown in Table 2.1. Here ρx is the mass depth variable in $\mathrm{g \cdot cm^{-2}}$ and equal to $\int_0^x \rho(x)dx$. T is modelled temperature estimate in the layer in K. P_g is the gas pressure, measured in 0.1 Pa. The electron number density is N_e ($\mathrm{cm^{-3}}$). The fifth column is the Rosseland mass absorption coefficient κ_ross with the dimension $\mathrm{g \cdot cm^{-2}}$. The radiative acceleration is g_rad ($\mathrm{cm \cdot s^{-2}}$) and the final column is the microturbulence velocity, adopted for the layer, v_t in ($\mathrm{cm \cdot s^{-1}}$). The more exact properties of main parameters for the models are reached by the interpolation procedures inside the software packages, described in further sections.

2.3 Software and developments

The software description is divided into two parts. First, the main software packages, that are historically used by the BOCCE scientific group, are described, and secondly, the local developments and adaptations.

2.3.1 Main software packages

The BOCCE group uses three packages for common work: ROSA, WIDTH and SYNTH.

ROSA is a scientific tool for the spectral processing: continuum placing, normalisation, equivalent width measurement and other treatments (Gratton 1988). The package includes the automatic equivalent width measurement software developed by the Padova Astronomical observatory group.

WIDTH is a package for the calculation of elemental abundances from measured equivalent widths. This software package includes the interpolation of ATLAS models, interpolating them towards more accurate atmospheric parameters of stars. Therefore this software package requires input data of several types. (1) Atmospheric parameters for exact interpolation of ATLAS models: effective temperature $T_{\rm eff}$ (K), surface gravity in logarithmic scale, log g, total metallicity [A/H] and microturbulence velocity $v_{\rm t}$ ($\rm m \cdot s^{-1}$). (2) The list of specific physical line parameters for a specific transition: line central wavelength λ (Å), excitation potential E.P. (eV), oscillator strength f, statistically weighted by the weight of the lower level of the transition g in logarithmic scale log gf, collisional damping constant $\Gamma_{\rm coll}$ and a measured equivalent width EW (mÅ). The output of the WIDTH is a list of abundance estimates for each line $\log\varepsilon_{\rm el} = \log N_{\rm el} - \log N_{\rm H}$ of the element or ion, together with the averaged abundance, and standard deviation σ_{el}.

SYNTH is a package for synthetic spectra modelling. The software uses the main atmospheric parameters as an input to build the interpolated model of atmosphere, and the similar list of atomic and molecular data like in the previously described program, except for the equivalent width measurement. Also, the list of abundances for all elements, which are present in the wavelength range of the analysis, if their abundances differ from the abundances in the model. This software calculates equivalent widths according to the input and constructs the superposition of theoretical line profiles for all lines presented in the wavelength range of the analysis. SYNTH can use several types of profiles for the convolution, depending on stellar characteristics (in our case – Gaussian). This final superposition is the so-called *synthetic spectrum*, that should be compared with an observed spectrum.

2.3.2 Developments and adaptations of computing programs

The previously mentioned software packages are a single core based tools, historically used and designed to work in the DOS environment. Since modern needs are

much different, we made further developments of the WIDTH and SYNYH packages.

The WIDTH package was reassembled and implemented to UNIX/Linux operating system, allowing its usage in the High Performance environment. The main aims of this development were: (1) the implementation of the tools to the standard scientific environment, making them compatible to other scientific applications working usually on UNIX/Linux machines and (2) an automatisation of derivation of main atmospheric parameters, enabling to save the procedure time at least by the factor of 10.

The SYNTH package was reassembled and redesigned to work on UNIX/Linux and, especially, in High Performance environment. Usually, the synthetic spectra modelling is quite time demanding procedure. Therefore the High Performance Computing (HPC) machines working in the GRID infrastructure were chosen, that was on the fast developement stage in the projects LitGrid, Balticgrid & BalticGrid-II (Tautvaišienė, Mikolaitis & Puzeras 2009). The redesigned SYNTH was combined together with the similar code BSYN (Gustafsson et al. 2008) into the SYNTSPEC software package. The main aims of this development were: (1) the implementation of the software into the UNIX/Linux based GRID infrastructure and (2) the creation of a graphical user interface. The SYNTSPEC application consists of two software packages: the MARCS (Gustafsson et al. 2008) atmospheric models work with the software package BSYN, and the ATLAS models with the SYNTH. The SYNTSPEC calculates a number of synthetic spectra, using multicore environment, in the specified wavelength range and provides the graphical output together with the experimental spectrum (Mikolaitis & Tautvaišienė 2011).

The SYNTSPEC software is a set of FORTRAN, PASCAL and C++ coded programs joined together by scripts. A parametric submission is performed under the GRIDCOM interface. A single job runs for 8 – 10 hours. About 50 jobs are required to derive the main atmospheric parameters of a star and about 15 jobs for determining of chemical abundances of every single chemical element. In general, it takes to run more than 400 jobs for one star. The output is not very huge, but a larger amount of temporary memory in every single node is required. The Virtual Observatory alliance provides a nice conception and structure for handling outputs of such calculations (Plez 2008).

The main database for atomic data is the Vienna Atomic Line Database (VALD). The VALD contains line lists compiled by the VALD team from numerous sources (total 1035889 lines for about 60 ions are collected in the SYNTSPEC files), and van der Waals constants calculated by Barklem, Piskunov & O'Mara (2000). It is a comprehensive source of atomic data (for more information see Piskunov et al. 1995; Heiter et al. 2008).

The output follows the VOTABLE standards to be compatible within the Virtual Observatory infrastructure. The International Virtual Observatory alliance (IVOA) provides a valuable possibility to join Grid resources and virtual accessibility of observed or simulated data (for more information see Genova 2009; Taffoni, Vuerli & Pasian 2009).

The SYNTSPEC application is produced under the GRIDCOM interface on the BalticGrid Special Interest Group infrastructure. Integration with the GRIDCOM graphical interface makes the application usage much more intuitive for users and enables scientists to work independently of their physical location. The GRIDCOM interface improved job submission procedures and user interactions. The application can be submitted and analysed by a spread group (for further information, see Juozapavicius & Mažeika 2007; Šešok et al. 2010).

2.4 Equivalent width measurements

The equivalent width measurements by fitting Gaussian profiles were performed using the software package ROSA. The lines suitable for measurement were chosen under the requirement that the profiles be sufficiently clean to provide reliable equivalent widths. Inspection of the solar spectrum by Kurucz et al. (1984), the solar line identifications of Moore, Minnaert & Houtgast (1966) and lists of unblended lines (Gurtovenko & Kostyk 1989) were used to avoid blends. Lines blended by telluric absorption lines were omitted from the treatment as well. In order to avoid the NLTE overionisation effects, mainly weak lines were selected for the analysis.

The definition of the equivalent width of a spectral line is described as a measure of the total absorption of radiant energy as indicated by an absorption line. It may be found by forming a rectangle with a height equal to that of continuum emission, and finding the width such that the area of the rectangle is equal to the area in the

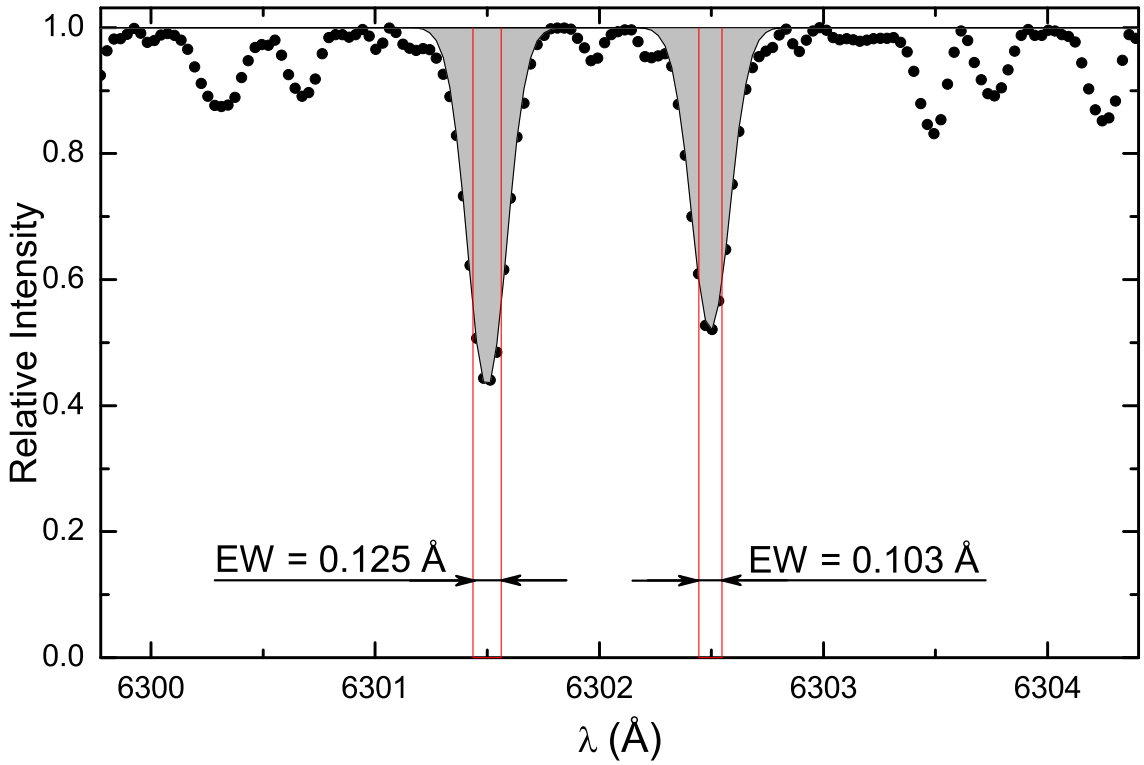

Figure 2.1: An example of fitting Gaussian profile for two neutral iron lines.

spectral line. It is a measure of the strength of spectral features. The equivalent width is described using the equation

$$W_\lambda = \int \left(1 - \frac{F_\lambda}{F_0}\right) d\lambda, \tag{2.1}$$

where F_0 is the continuum intensity at the absorption feature, F_λ is the relative intensity of the absorption or emission feature line profile. W_λ is the width of the hypothetical square shape, which has the constant value of the height equal to 1 and the same area as the absorption line. The example of the equivalent width and the fitting of the Gaussian is provided in Figure 2.1.

2.5 Computing of abundances

The equivalent width analysis software employs equations of principle laws of physics. It is important to know whether a particular line may occur. We need to know the relative population of the exited states of the particles in the gas, to get

information if the particular line can form. The aim is to get the number of atoms per unit volume, N_n, at the energy level n proportion to the total number of atoms, N, of the same atomic species. This relation is described by the Boltzmann Excitation Distribution:

$$\frac{N_n}{N} = \frac{g_n}{u_n(T)} e^{-\frac{\chi_n}{kT}}. \tag{2.2}$$

Denominator $u_n(T)$ is called the partition function of the particle in a gas of temperature T and is defined as

$$u_n(T) = \sum g_i e^{-\frac{\chi_i}{kT}}, \tag{2.3}$$

here statistical weight of n-th level is g_n, and the excitation potential of n-th level is χ_n. To describe the absorption line we need to know the fraction of the atoms of the element which are in the ionised state. The ratio of the atoms in the i state to the atoms in the $i+1$ state is:

$$\frac{N_{i+1}}{N_i} P_e = \frac{(2\pi m_e)^{\frac{3}{2}} (kT)^{\frac{5}{2}}}{h^3} \frac{u_{i+1}(T)}{u_i(T)} e^{-\frac{\chi_i}{kT}}. \tag{2.4}$$

This equation was derived by Saha (1921), developed furthermore by Langmuir & Kingdon (1923), and usually carries the names of its authors (Saha or Saha–Langmuir ionisation equation). The electronic pressure, P_e, explains why stellar spectra are sensitive to pressure. The assumption of LTE is a very important simplification of the general problem, as it allows us to calculate the source function, the population of the atomic energy levels and the ionisation equilibria from only a small number of free physical parameters. In very thin extended atmospheres, or in the case of strong absorption lines which are formed in high atmospheric layers, the LTE assumption breaks down. The calculation of the excitation and ionisation equilibria then becomes enormously more complicated because all interactions between matter and radiation have to be considered in detail (Letarte 2007). Finally the abundance is calculated using equivalent widths of the weak lines and atomic

parameters (log gf and excitation potential χ) by the equation

$$\log\left(\frac{W_\lambda}{\lambda}\right) = \log\left(\frac{\pi e^2}{m_e c^2}\frac{\frac{N_i}{N}}{u(T)}N_H\right) + \log\left(\frac{N}{N_H}\right) + \log(gf\lambda) - \frac{5040}{T}\chi - \log(\kappa_\nu), \tag{2.5}$$

where

$$\frac{5040}{T} = \frac{\log e}{kT} = \theta. \tag{2.6}$$

Here, W_λ is an equivalent width of the line defined by Eq. (2.1), e is the electron charge, N_i/N is a ratio of ionised atoms to the total number of atoms, N_H is the number of hydrogen atoms, N/N_H is the abundance of an element relative to hydrogen, κ_ν is the continuous absorption coefficient and $u(T)$ is the partition function.

2.6 Determination of main atmospheric parameters

Main atmospheric parameters were determined using spectroscopical methods. Spectral lines were restricted to the spectral range 5500–8000 Å in order to minimise problems of line crowding and difficulties in the continuum tracing in the blue region.

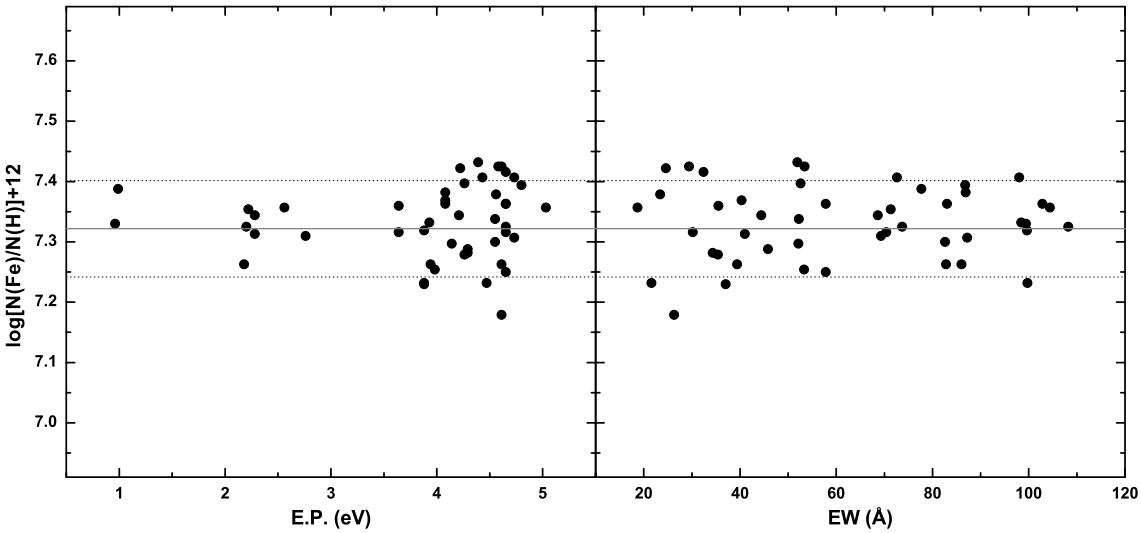

Figure 2.2: The Fe I abundance values versus the lower excitation potential (left) and the equivalent widths (right) for the star NGC 2506 438. The mean abundance is shown as the grey line, and dotted lines are limits of 1σ.

2.6.1 Effective Temperature

The temperature of the stellar atmosphere varies from the bottom to the top. It is essential to use the definition of an effective temperature. The temperature of a black body that radiates the same total energy per unit area as a star is called *effective temperature*:

$$\int_0^\infty F_\nu d\nu = \sigma T_{\rm eff}^4, \tag{2.7}$$

where the total radiant power per unit area is given by the integral and σ is the Stefan-Boltzmann constant. Here F_ν is the flux leaving the surface. The example of the temperature variation over the photosphere of Solar type star is given in the Table 2.1. It is seen, that the temperature $T_{\rm eff}$ equal to Solar is reached between the 53 and 54-th layers of the 72 layers in total.

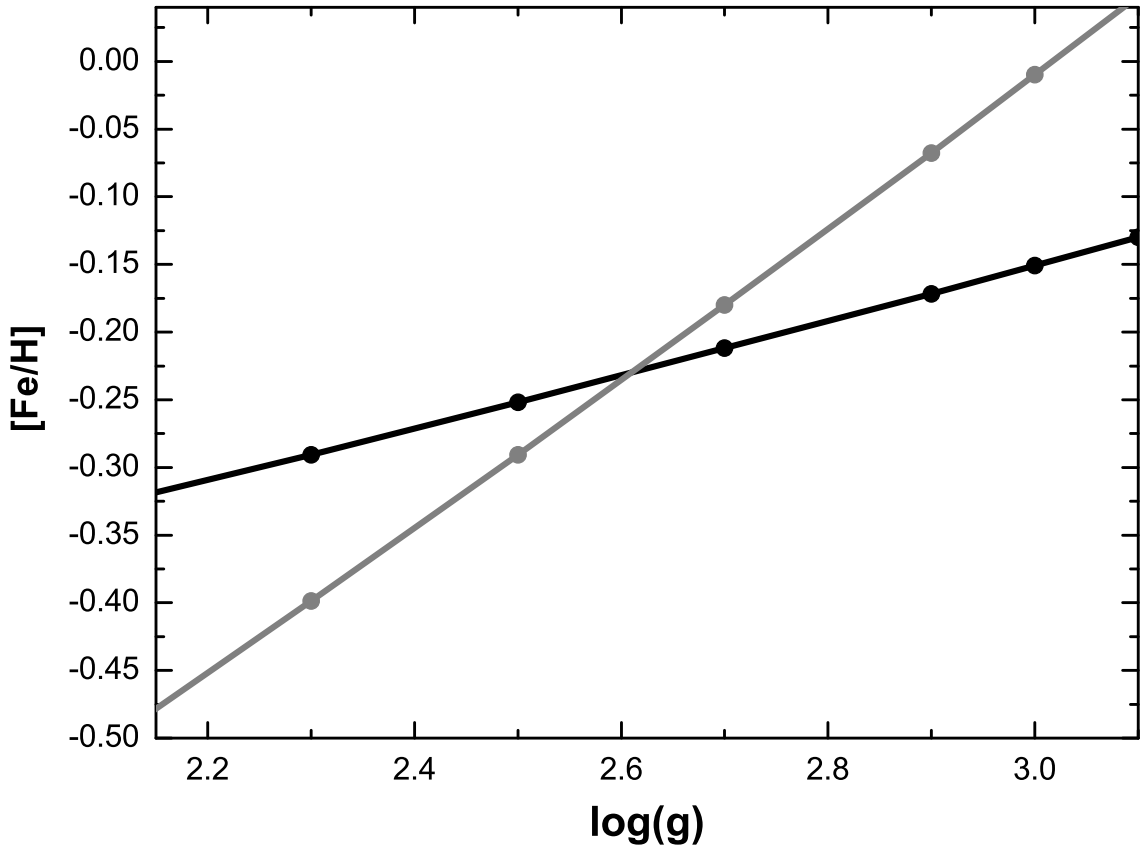

Figure 2.3: Abundances of iron as determined from neutral (black) and ionised (grey) lines for different values of gravity for the star NGC 2506 443.

The preliminary photometric values of the effective temperatures were derived using $(B-V)_0$ colour indices and the temperature calibration by Alonso, Arribas & Martínez-Roger (2001). The interstellar reddening values for the clusters as averaged from four determinations (Marconi et al. 1997; Schlegel, Finkbeiner & Davis 1998; Kim et al. 2001 and Dias et al. 2002), were taken into account.

The spectroscopic determination of effective temperature is based on the fact that the strength of spectral lines of an element depends on the number of atoms in the gas and the temperature. The spectroscopic values of the effective temperatures were derived by minimising a slope of the abundances obtained from neutral Fe I lines with respect to the excitation potential. In general, all the lines of the same element should show the same abundance value. However, the values spread around the mean value, because of uncertain equivalent widths and atomic parameters. So, the effective temperature is defined as correct if the abundances, derived for every line, do not show any dependence on the line excitation potential χ or measured equivalent widths W. An example of the abundance independence test over excitation potentials and measured equivalent widths is shown in Figure 2.2. For example, if too low temperature were used in calculations, less electrons in the higher energy levels should be predicted, and too high abundances for the lines with higher χ would be calculated. The positive slope would be seen in the plot of abundances versus excitation potentials. Thus, the aim is to calibrate the slope towards zero, what means to reach the excitation balance.

2.6.2 Surface gravity

Stellar gravity at the surface, g, is proportional to the ratio of stellar mass M and squared stellar radius R:

$$g = \frac{GM}{R^2}, \tag{2.8}$$

here, G is the gravitational constant. The spectroscopic gravities are calculated using the ionisation equilibria notation. The abundance of the element derived by lines of neutral and ionised atoms must be the same. The spectroscopic values of gravities ($\log g$) were derived by forcing the measured neutral and ionised iron lines to yield the same [Fe/H] value by adjusting the model gravity. An example of neutral and ionised iron abundances for different values of gravity for the star

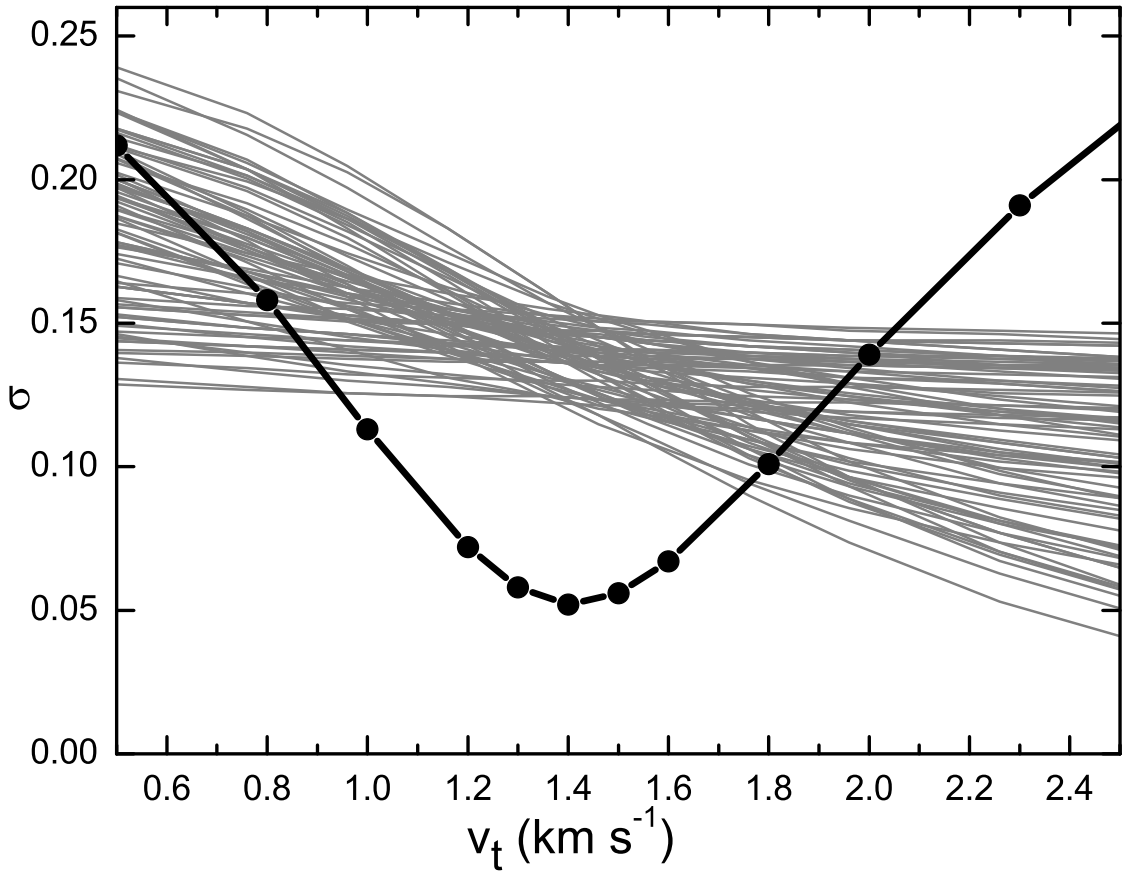

Figure 2.4: Standard deviations of iron abundances as determined from neutral lines for different values of microturbulence velocity for the star NGC 6253 2509 (black line). Abundances of neutral iron lines for different values of microturbulence velocity are shown as grey lines. Graphs are in scale only with the v_t axis for convenience.

NGC 2506 443 is shown in Fig. 2.3.

2.6.3 Metallicity

Each stellar atmosphere model is computed with a parameter representing the chemical composition of a star. It is often referred to as [Fe/H], although it does not only represent the contribution of Fe atoms. It represents also the electronic pressure ($P_{\rm e}$) in the atmosphere of a star with the same chemical element ratios as of the Sun, scaled to a given [Fe/H]. It is the abundance of the elements that contribute to the continuum absorption properties of the atmosphere. A higher metallicity will increase $P_{\rm e}$ in the atmosphere by contributing extra electrons. Some models have different [α/Fe] ratios to represent stars that are systematically different from the

Sun.

2.6.4 Microturbulence velocity

Microturbulence velocity values were determined by forcing Fe I abundances to be independent on the equivalent widths of lines, and minimising the spread of individual abundances of neutral iron lines around the mean value. It is shown in the example in the case of the star NGC 2506 438 in Fig. 2.2. An example of the reaction of the spread σ to the value of microturbulence velocity for the star NGC 6253 4510 is presented in Fig. 2.4.

2.6.5 Non local thermodynamical equilibrium

Abundances of Na and Mg were determined with NLTE taken into account as described by Gratton et al. (1999). Abundances of sodium were determined from equivalent widths of the Na I lines at 5688.22 Å, 6154.23 Å and 6160.75 Å, and magnesium from the Mg I lines at 4730.04 Å, 5711.09 Å, 6318.71 Å, and 6319.24 Å. The oscillator strengths for lines of elements were taken mainly from an inverse solar spectrum analysis done in Kiev (Gurtovenko & Kostyk 1989).

2.7 Synthetic spectra modelling

2.7.1 Carbon, nitrogen and oxygen

For the determination of carbon abundances from C_2 lines in the stars observed with FEROS, we used 5632 – 5636 Å interval to compare with observations of C_2 Swan (0,1) band head at 5630.5 Å (see Fig. 2.5). The same molecular data of C_2 as used by Gonzalez et al. (1998) were adopted for the analysis. For the stars observed with UVES this spectral interval was not available, so we analysed several other Swan (1,0) bands at 4732.8 Å and 4735.3 Å with the molecular input data from Kurucz & Bell (1995). The example of those two features, together with synthetic spectra, is shown in Figure 2.8.

The interval 7940 – 8130 Å, containing strong $^{12}C^{14}N$ features, was used for nitrogen abundance analysis. The molecular data for $^{12}C^{14}N$ and $^{13}C^{14}N$ bands

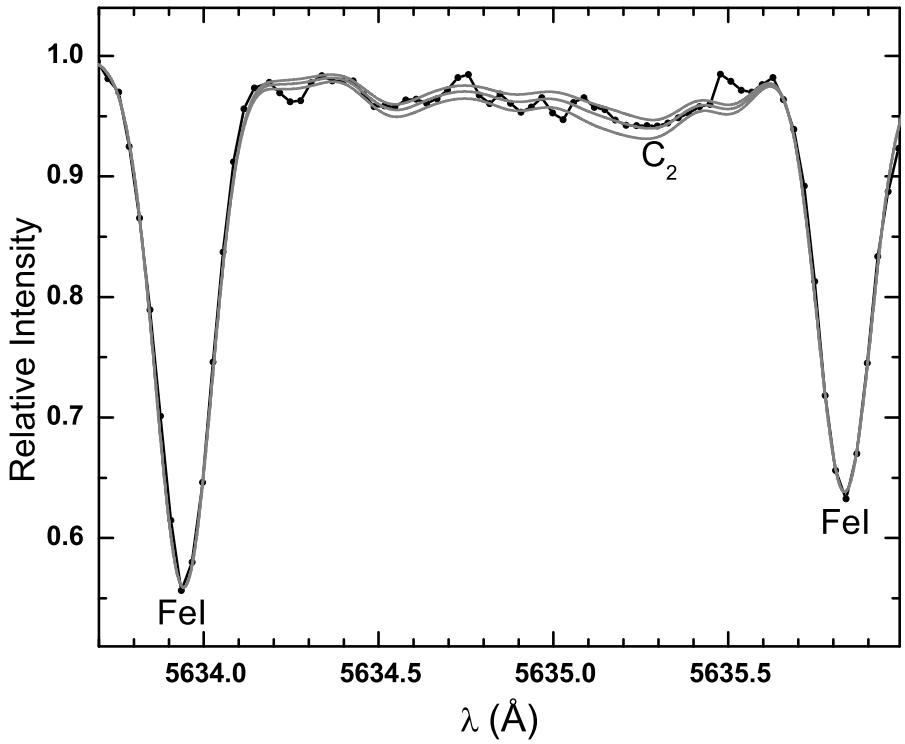

Figure 2.5: Small region of NGC 2506 459 spectrum (solid black line with black dots) at the C_2 Swan (0,1) band head 5635.5 Å, plotted together with synthetic spectra (grey lines) with [C/Fe] values at -0.19 ± 0.05 dex.

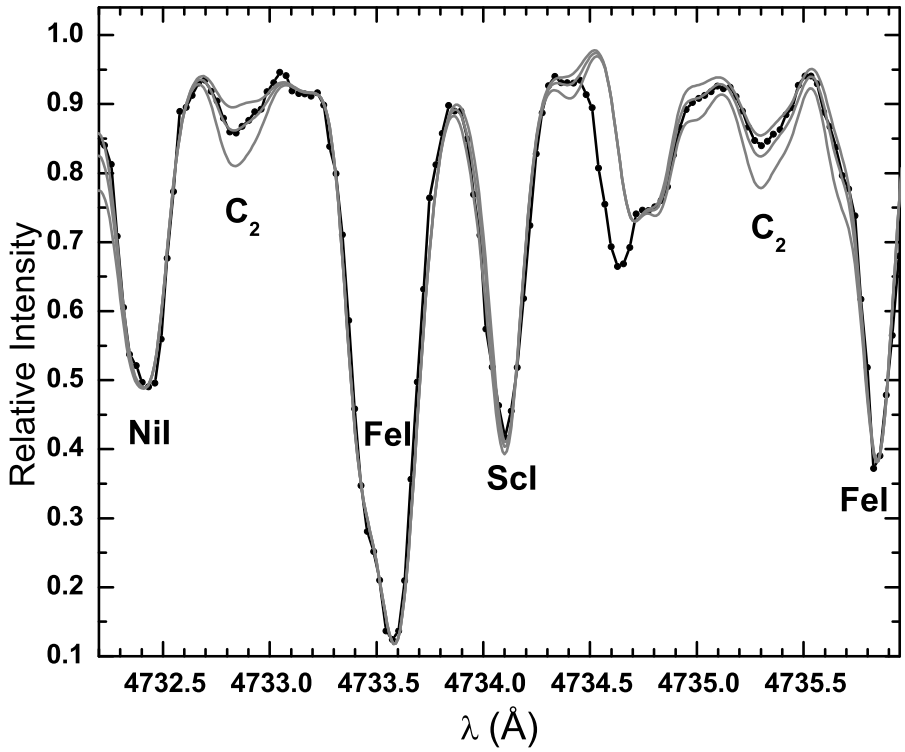

Figure 2.6: Small region of NGC 6253 2885 spectrum (solid black line with black dots) with C_2 features, plotted together with synthetic spectra with [C/Fe] values -0.1 dex (lower grey line), -0.2 dex (middle grey line) and -0.3 dex (upper grey line).

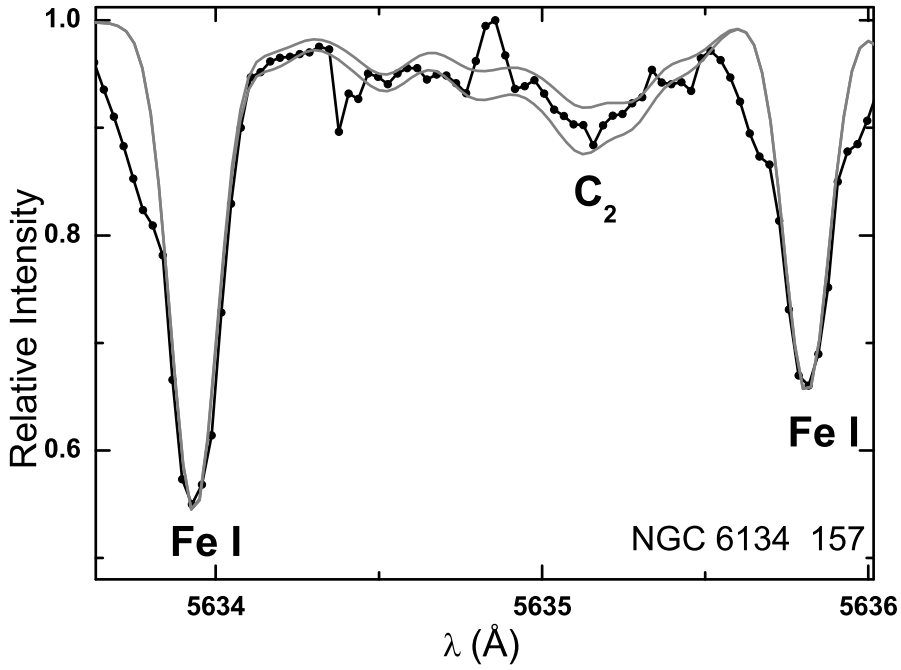

Figure 2.7: Small region of NGC 6134 57 spectrum (solid black line with black dots) at C_2 Swan (0,1) band head 5635.5 Å, plotted together with synthetic spectra with [C/Fe] values lowered by -0.2 dex (lower grey line) and -0.25 dex (upper grey line).

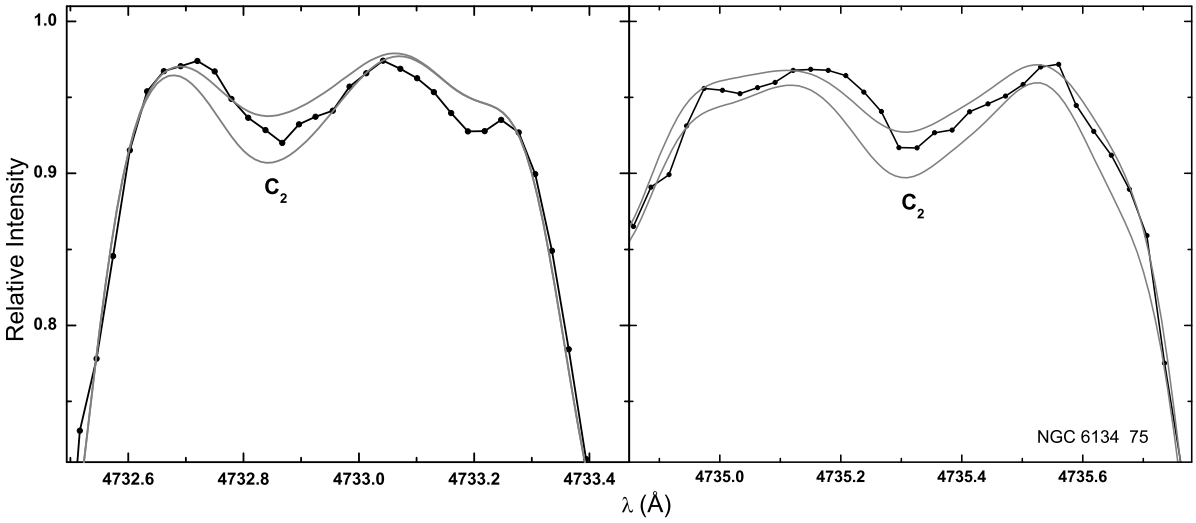

Figure 2.8: Small region of NGC 6134_75 spectrum (solid black line with black dots) at C_2 Swan (1,0) band heads 4732.8 Å and 4735.3 Å, plotted together with synthetic spectra with [C/Fe] values lowered by -0.2 dex (lower grey line) and -0.25 dex (upper grey line).

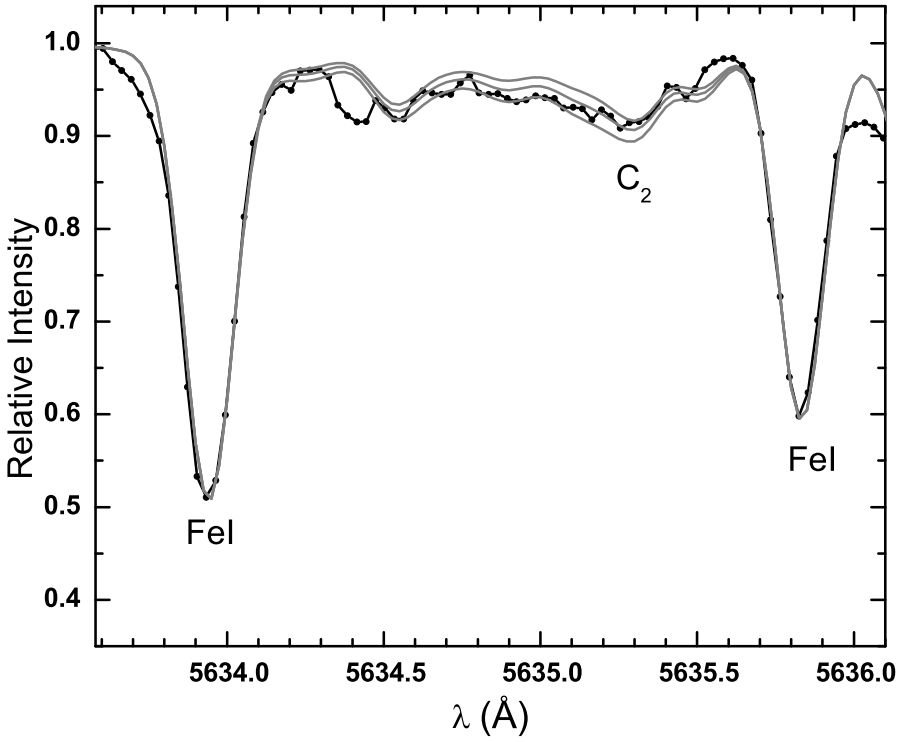

Figure 2.9: Small region of IC 4651 27 spectrum (solid black line with black dots) at C_2 Swan (0,1) band head 5635.5 Å, plotted together with synthetic spectra with [C/Fe] values lowered by -0.2 dex (lower grey line), -0.25 dex (middle grey line) and -0.3 dex (upper grey line).

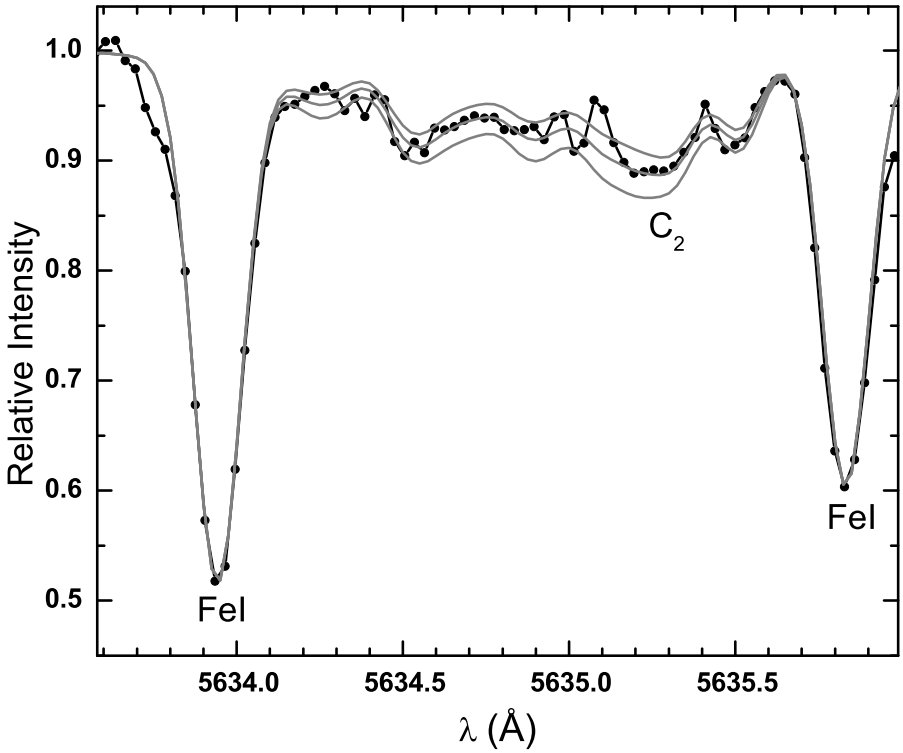

Figure 2.10: Small region of Cr 261 2001 spectrum (solid black line with black dots) at C_2 Swan (0,1) band head 5635.5 Å, plotted together with synthetic spectra with [C/Fe] values of -0.10 dex (lower grey line), -0.15 dex (middle grey line) and -0.20 dex (upper grey line).

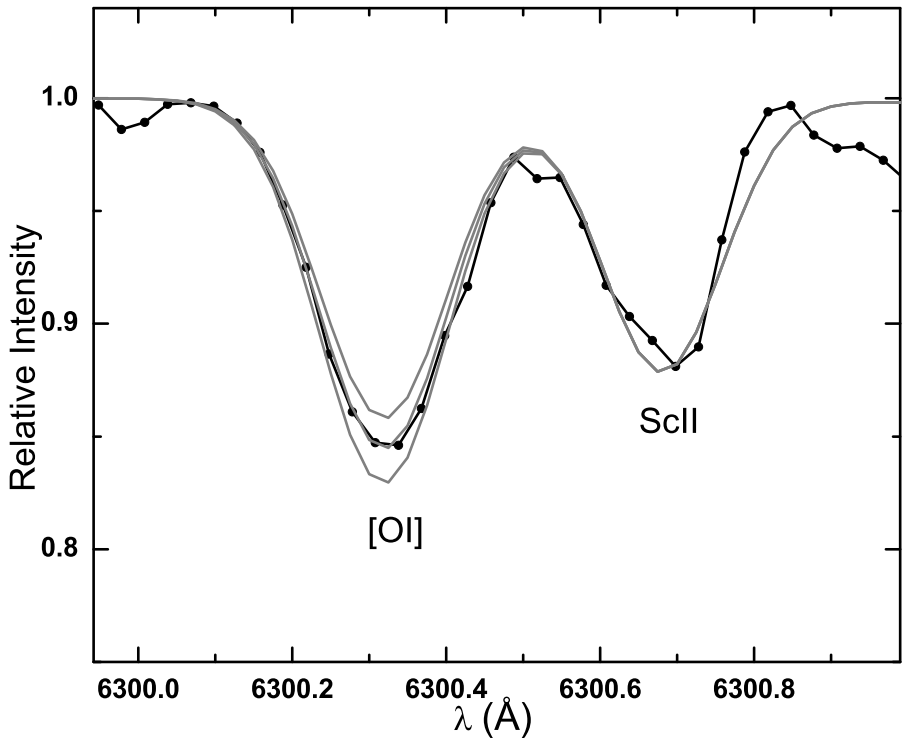

Figure 2.11: Fit to the forbidden [O I] line at 6300.1 Å in NGC 2506 443. The observed spectrum is shown as a solid line with black dots. The synthetic spectra with [O/Fe]= 0.02 ± 0.03 are shown as solid grey lines.

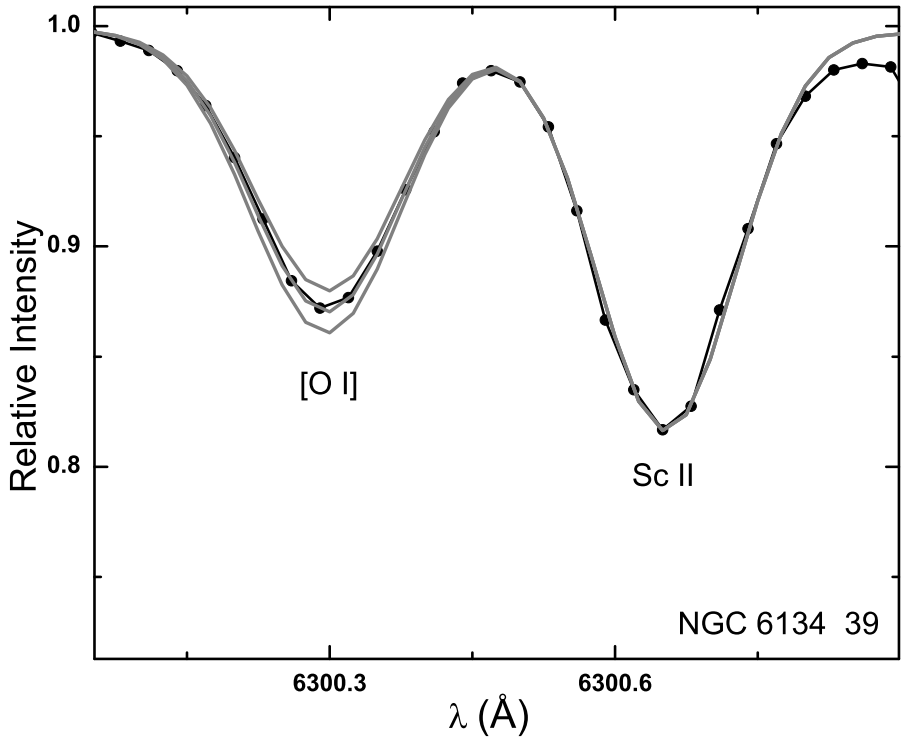

Figure 2.12: Fit to the forbidden [O I] line at 6300 Å in NGC 6134 39. The observed UVES spectrum is shown as a solid line with black dots. Synthetic spectra with [O/Fe]= -0.3, -0.25, and -0.2 are shown as solid grey lines.

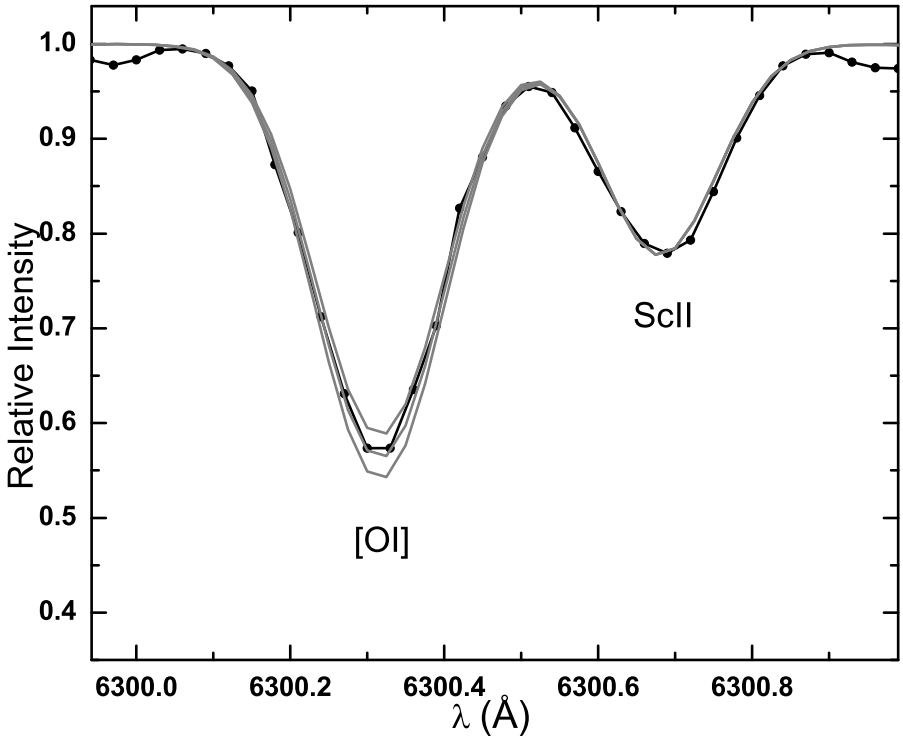

Figure 2.13: Fit to the forbidden [O I] line at 6300 Å in IC 4651 56. The observed spectrum is shown as a solid line with black dots. Synthetic spectra with [O/Fe]= 0.3, 0.08, and 0.13 are shown as solid grey lines.

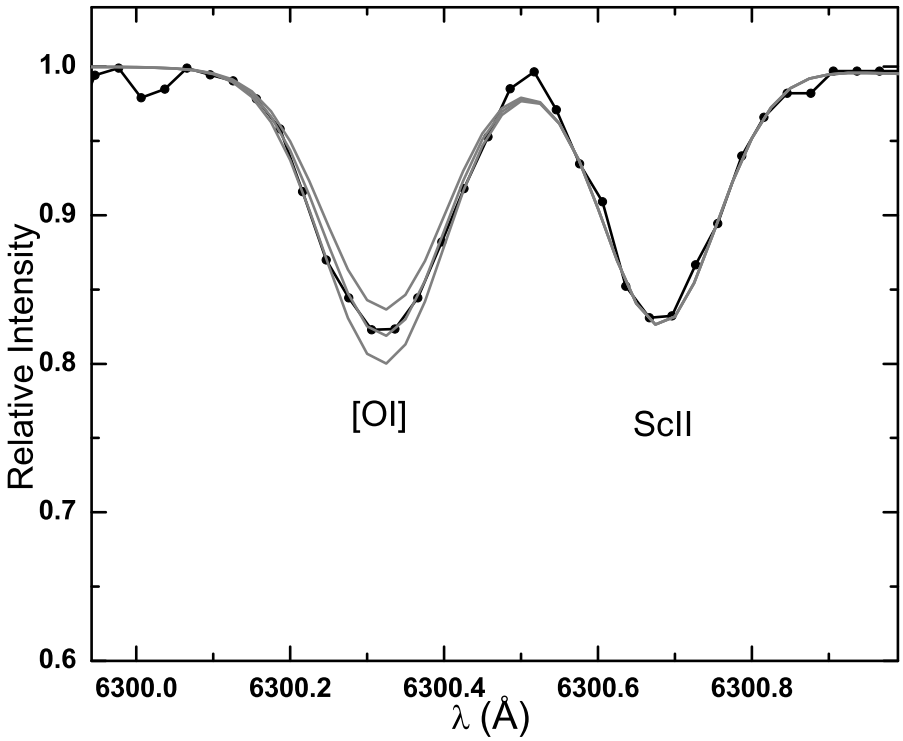

Figure 2.14: Fit to the forbidden [O I] line at 6300 Å in Cr 261 1080. The observed spectrum is shown as a solid line with black dots. Synthetic spectra with [O/Fe]= 0.05, −0.05, and −0.15 are shown as solid grey lines.

were provided by Bertrand Plez (University of Montpellier II). All gf values were increased by +0.021 dex to fit the model spectrum to the Solar flux atlas of Kurucz et al. (1984).

We derived oxygen abundances from synthesis of the forbidden [O I] line at 6300.3 Å. The gf values for ^{58}Ni and ^{60}Ni isotopic line components, which blend the oxygen line, were taken from Johansson et al. (2003). In Figures 2.11, 2.12, 2.13 and 2.14, we show examples of spectrum synthesis for the [O I] line. In spectra of stars of all five clusters the [O I] line was not contaminated by telluric lines.

2.7.2 $^{12}C/^{13}C$ ratio

The $^{12}C/^{13}C$ ratios were mainly determined from the $^{13}C^{14}N$ feature at 8004.7 Å. This feature was analysed in four open clusters: NGC 6134, NGC 6253, IC 4651 and Collinder 261. Figures 2.17, 2.16 and 2.18 show samples of the spectra with $^{12}C^{14}N$ and $^{13}C^{14}N$ features at 8004 Å.

Unfortunately, a $^{12}C/^{13}C$ ratio analysis using the $^{13}C^{14}N$ feature at 8004.7 Å was not possible because of blending by telluric lines for the stars in the open cluster NGC 2506. Thus, we selected another $^{13}C^{14}N$ feature at 7940.4 Å. The example of this feature is shown in Figure 2.15. Three synthetic spectra with the $^{12}C/^{13}C = 10, 14$ and 18 are shown together with the observed spectrum of the NGC 2056 459.

2.7.3 Heavier elements

Determinations of copper, zirconium, yttrium, barium, lanthanum, cerium, neodymium, praseodymium and europium abundances were performed by a spectral synthesis method. The copper abundances were derived using the Cu I line at 5218.2 Å, for which we adopted the hyperfine structure data by Steffen (1985). The zirconium abundances were determined from the Zr I lines at 4687.8 and 6127.5 Å. We adopted the barium hyperfine structure and isotopic composition for the Ba II lines at 5853.7 and 6141.7 Å from McWilliam (1998) and for the line at 6496.9 Å from Mashonkina & Gehren (2000). Lanthanum abundances were determined from the La II lines at 6320.4 and 6390.5 Å, and theat for cerium from the Ce II lines at 5274.2 and 6043.4 Å. Neodymium abundances were determined using atomic parameters presented by Den Hartog et al. (2003). Due to the line crowding in the region of

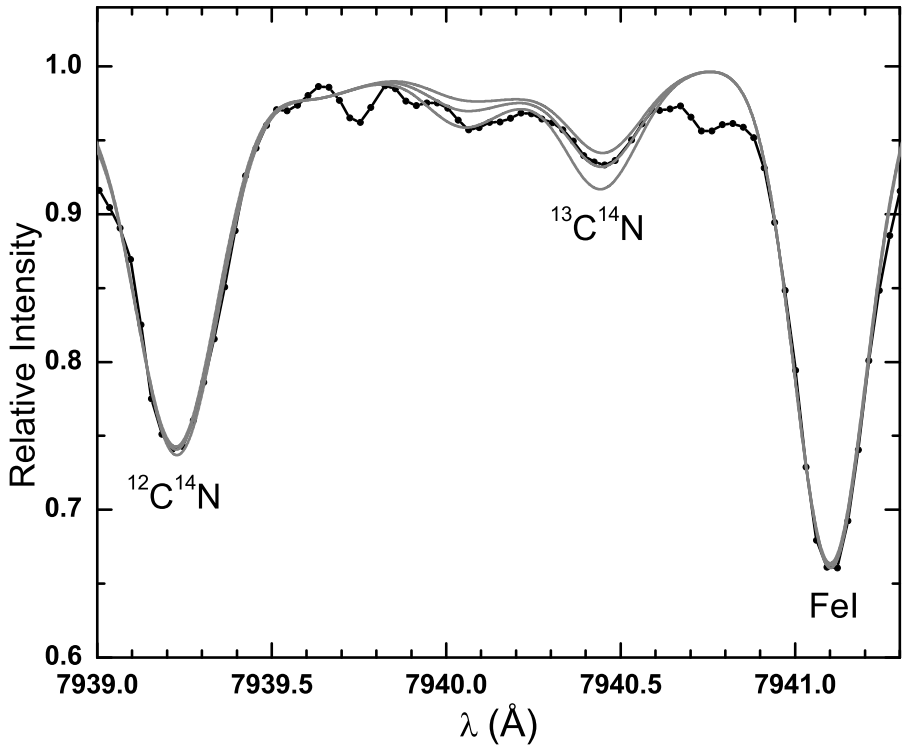

Figure 2.15: Small region of NGC 2506 459 spectrum (solid black line with black dots) with $^{13}C^{14}N$ feature. Grey lines show synthetic spectra with $^{12}C/^{13}C$ ratios equal to 10 (lowest line), 14 (middle line) and 18 (upper line).

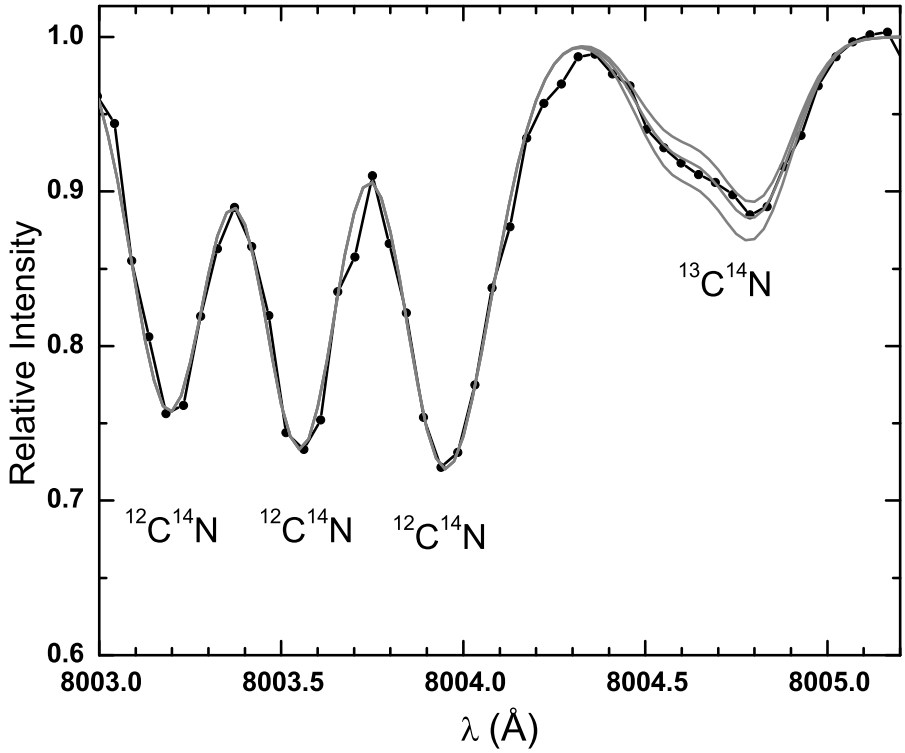

Figure 2.16: Small region of NGC 6253 4510 spectrum (solid black line with black dots) including a $^{13}C^{14}N$ feature. Grey lines show synthetic spectra with $^{12}C/^{13}C$ ratios equal to 12 (lower line), 15 (middle line) and 18 (upper line).

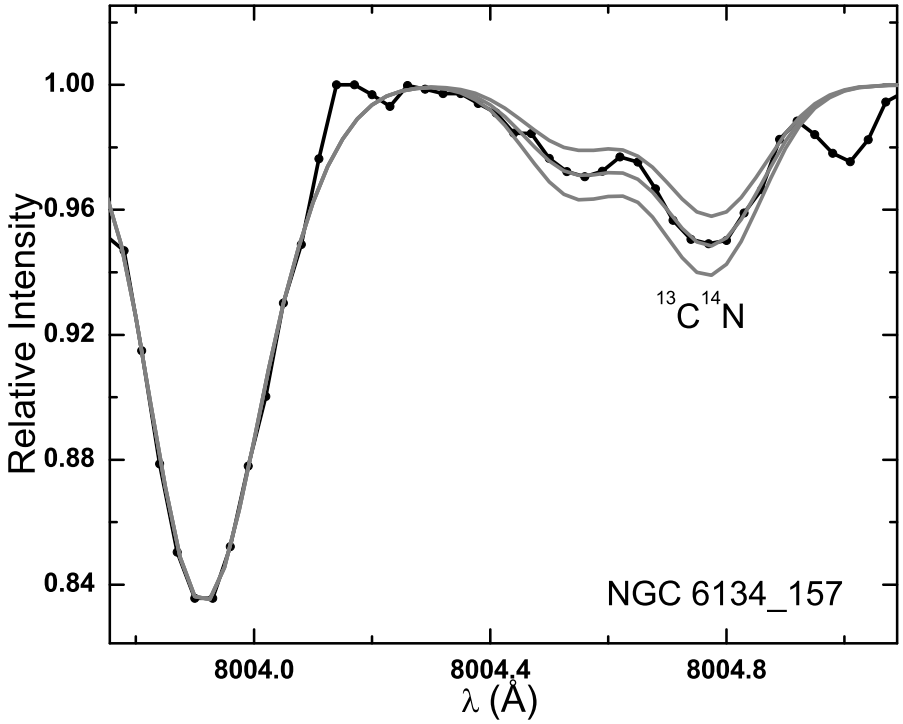

Figure 2.17: Small region of NGC 6134 57 spectrum (solid black line with black dots) with $^{13}C^{14}N$ feature. Grey lines show synthetic spectra with $^{12}C/^{13}C$ ratios equal to 10 (lower line), 12 (middle line) and 14 (upper line).

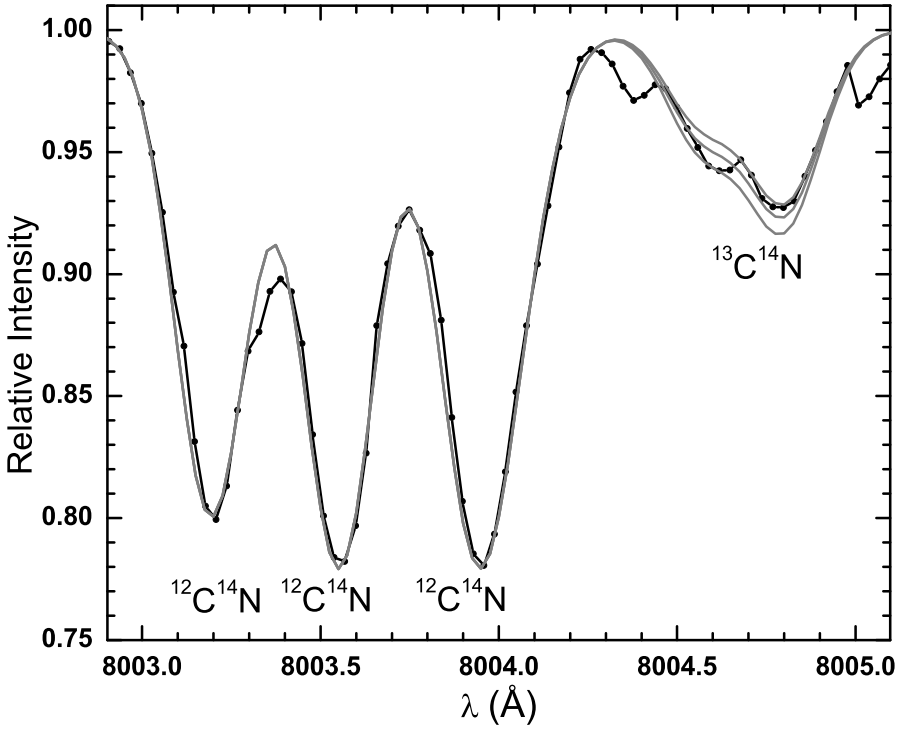

Figure 2.18: Small region of IC 4651 72 spectrum (solid black line with black dots) with $^{13}C^{14}N$ feature. Grey lines show synthetic spectra with $^{12}C/^{13}C$ ratios equal to 13 (lower line), 15 (middle line) and 17 (upper line).

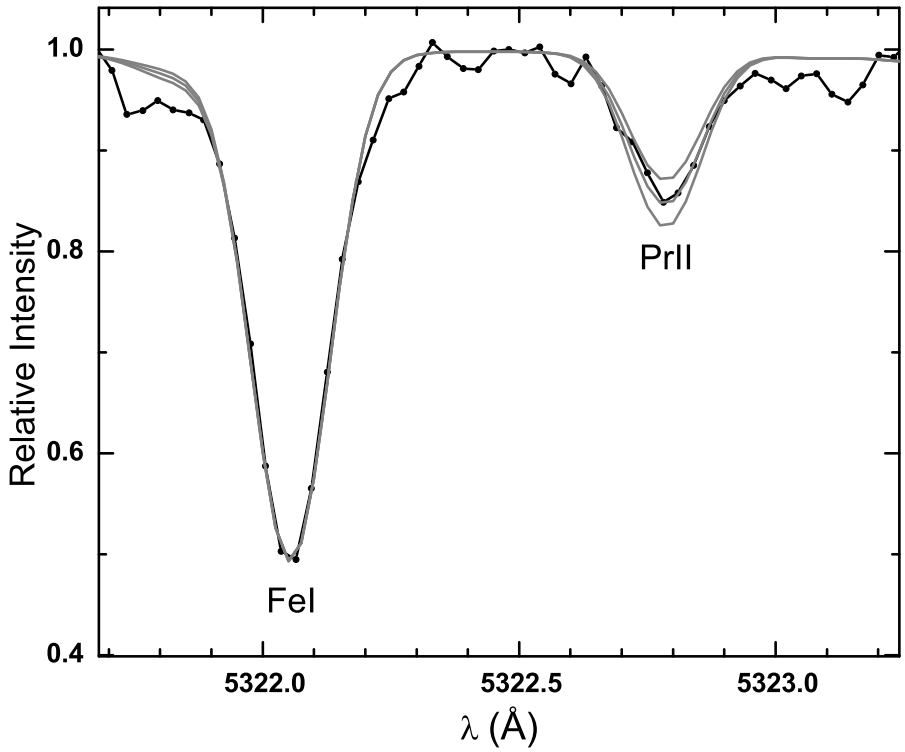

Figure 2.19: Fit to the Pr II line at 5322.8 Å in NGC 2506 438. The observed spectrum is shown as a solid line with black dots. The synthetic spectra with [Pr/Fe]$= 0.13 \pm 0.10$ are shown as solid grey lines.

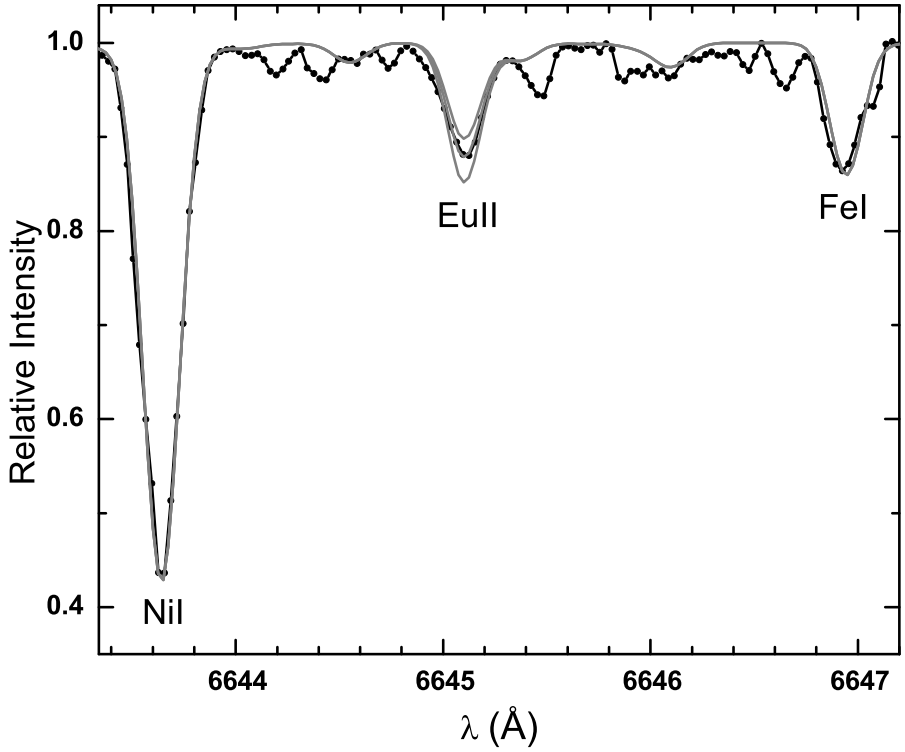

Figure 2.20: Fit to the Eu II line at 6645.1 Å in NGC 2506 438. The observed spectrum is shown as a solid line with black dots. The synthetic spectra with [Eu/Fe]$= 0.17 \pm 0.10$ are shown as solid grey lines.

neodymium lines, only three Nd II lines were chosen: 5092.8, 5249.6 and 5319.8 Å. The praseodymium abundances were determined from the Pr II line at 5322.8 Å. A fit to the NGC 2506 438 spectrum of Pr II line is shown in Fig. 2.19. Europium abundances were determined using the Eu II line at 6645.1 Å. A hyperfine structure for the Eu II line was used for the line synthesis. In Fig. 2.20, a fit to the Eu II line in the NGC 2506 438 spectrum is shown.

2.8 Uncertainties and sensitivity to input parameters

The sources of uncertainty can be divided into two categories. The first category includes the errors that affect a single line (e.g. random errors in the measurements of equivalent widths , oscillator strengths), i.e. uncertainties of the line parameters. The second category includes the errors which affect all the lines together, i.e. mainly the model errors (such as errors in the effective temperature, surface gravity, microturbulence velocity, etc.).

Table 2.2: Effects on the derived abundances, resulting from model changes for the star NGC 6253 2509.

Species	$\Delta T_{\rm eff}$ ± 100 K	$\Delta \log g$ ± 0.3	$\Delta v_{\rm t}$ ± 0.3 km s^{-1}	Total
C (C_2)	0.07	0.05	0	0.09
N (CN)	0.07	0.05	0.03	0.09
O ([O I])	0.03	0.03	0	0.04
$^{12}C/^{13}C$	1.5	1.5	0	2.12

Typical internal error estimates of the atmospheric parameters are: $\pm$ 100 K for $T_{\rm eff}$, ± 0.3 dex for log g and ± 0.3 km s^{-1} for $v_{\rm t}$. The sensitivity of the abundance estimates to changes in the atmospheric parameters by the assumed errors is illustrated for the selected typical stars in this analysis (Tables 2.2, 2.4, 2.5, 2.6). There the "Total" stands for summed (in quadrature) sensitivities to the atmospheric pa-

rameters. Possible parameter errors do not affect the abundances seriously. The table entries show the effects on the logarithmic abundances relative to hydrogen, Δ[El/H]. Note that the effects on "relative" abundances, for example [El/Fe], are often considerably smaller than on abundances relative to hydrogen, [El/H]

Since abundances of C, N and O are bound together by the molecular equilibrium in the stellar atmosphere, we have also investigated how an error in one of them typically affects the abundance determination of another (see Table 2.3).

Table 2.3: Effects of C, N or O abundance error on the abundance determination of another element.

Species	$\Delta[C/H] = 0.10$	$\Delta[N/H] = 0.10$	$\Delta[O/H] = 0.10$
		NGC 2506	
$\Delta[C/H]$	–	0.00	0.05
$\Delta[N/H]$	–0.15	–	–0.10
$\Delta[O/H]$	0.02	0.00	–
		NGC 6134	
$\Delta[C/H]$	–	0.00	0.05
$\Delta[N/H]$	–0.15	–	–0.10
$\Delta[O/H]$	0.05	0.00	–
		NGC 6253	
$\Delta[C/H]$	–	0.00	0.05
$\Delta[N/H]$	–0.15	–	–0.15
$\Delta[O/H]$	0.05	0.00	–
		IC 4651	
$\Delta[C/H]$	–	0.00	0.05
$\Delta[N/H]$	–0.15	–	–0.10
$\Delta[O/H]$	0.02	0.00	–

Table 2.4: Effects on the derived abundances, resulting from model changes for the star NGC 2506 438.

Species	$\Delta T_{\rm eff}$ ± 100 K	$\Delta \log g$ ± 0.3	$\Delta v_{\rm t}$ ± 0.3km s^{-1}	Total
C (C_2)	0.03	0.03	0.00	0.04
N (CN)	0.03	0.01	0.02	0.04
O ([O I])	0.02	0.03	0.01	0.04
Na I	0.07	0.03	0.06	0.10
Mg I	0.06	0.01	0.06	0.09
Al I	0.06	0.01	0.03	0.07
Si I	0.01	0.04	0.04	0.05
Ca I	0.09	0.02	0.10	0.13
Sc II	0.01	0.13	0.08	0.15
Ti I	0.14	0.01	0.08	0.16
Ti II	0.01	0.13	0.11	0.17
V I	0.15	0.01	0.06	0.16
Cr I	0.10	0.01	0.09	0.14
Cr II	0.05	0.12	0.07	0.15
Mn I	0.08	0.02	0.10	0.13
Fe I	0.08	0.00	0.09	0.12
Fe II	0.07	0.14	0.10	0.19
Co I	0.05	0.02	0.06	0.08
Ni I	0.03	0.02	0.08	0.09
Cu I	0.03	0.02	0.08	0.09
Zn I	0.02	0.07	0.08	0.11
Y II	0.02	0.10	0.11	0.15
Zr I	0.04	0.09	0.04	0.11
Ba II	0.02	0.12	0.08	0.15
La II	0.08	0.11	0.02	0.13
Ce II	0.01	0.13	0.05	0.14
Pr II	0.02	0.13	0.01	0.13
Nd II	0.02	0.11	0.06	0.12
Eu II	0.00	0.13	0.02	0.13
$^{12}C/^{13}C$	1.5	1.3	0.5	2

Table 2.5: Effects on the derived abundances, resulting from model changes for the star NGC 6134 114.

Species	$\Delta T_{\rm eff}$ +100 K	$\Delta \log g$ +0.3	$\Delta v_{\rm t}$ +0.3km s^{-1}	Total
C (C_2)	–0.05	0.03	–0.01	0.06
N (CN)	0.05	0.01	0.04	0.06
O ([O I])	–0.02	–0.05	–0.01	0.05
Na I	0.08	–0.08	–0.11	0.16
Mg I	0.05	–0.03	–0.08	0.10
Al I	0.07	–0.01	–0.05	0.09
Si I	–0.01	0.04	–0.04	0.06
Ca I	0.1	–0.01	–0.07	0.12
Sc II	–0.01	0.14	–0.08	0.16
Ti I	0.14	–0.01	–0.06	0.15
Ti II	0.1	–0.03	–0.08	0.13
V I	0.16	0	–0.06	0.17
Cr I	0.09	–0.01	–0.09	0.13
Cr II	0.1	–0.03	–0.07	0.13
Mn I	0.08	–0.02	–0.05	0.10
Co I	–0.09	0.03	–0.05	0.11
Ni I	–0.05	0.03	–0.12	0.13
Cu I	0.01	0.02	0.01	0.02
Zn I	–0.02	0.04	–0.09	0.10
Y II	–0.02	0.11	–0.13	0.17
Zr I	–0.18	0	–0.03	0.18
Ba II	–0.1	0.09	–0.1	0.17
La II	0.01	–0.01	0.04	0.04
Ce II	0	0.13	–0.01	0.13
Nd II	–0.02	0.11	–0.01	0.11
Eu II	0	0.1	–0.01	0.10
$^{12}C/^{13}C$	–1	–1	0	1.41

Table 2.6: Effects on the derived abundances, resulting from model changes for the star IC 4651 72.

Species	$\Delta T_{\rm eff}$ +100 K	$\Delta \log g$ +0.3	$\Delta v_{\rm t}$ +0.3km s^{-1}	Total
C (C_2)	–0.05	0.05	0	0.07
N (CN)	0.05	0	0.05	0.07
O ([O I])	–0.05	–0.05	0	0.07
Na I	0.09	–0.05	–0.04	0.11
Mg I	0.03	0	–0.03	0.04
Al I	0.08	0	–0.03	0.09
Si I	–0.06	0.07	–0.02	0.09
Ca I	0.11	–0.04	–0.06	0.13
Sc II	–0.02	0.13	–0.05	0.14
Ti I	0.16	–0.02	–0.08	0.18
Ti II	–0.03	0.13	–0.06	0.15
V I	0.16	0.01	–0.09	0.18
Cr I	0.1	0	–0.06	0.12
Cr II	–0.09	0.14	–0.03	0.17
Mn I	0.08	–0.04	–0.06	0.11
Co I	0.02	0.05	–0.07	0.09
Ni I	0	0.07	–0.05	0.09
Cu I	0.02	0.03	–0.06	0.07
Zn I	–0.05	0.07	–0.07	0.11
Y II	0.16	–0.02	–0.14	0.21
Zr I	0	0.12	–0.07	0.14
Ba II	–0.03	0.14	–0.02	0.14
La II	0.03	0.08	–0.10	0.13
Ce II	0.02	0.12	–0.03	0.13
Nd II	0.01	0.13	–0.04	0.14
Eu II	0.03	0.13	–0.07	0.15
$^{12}C/^{13}C$	–2	–2	1	3.00

Chapter 3

Results and discussion

3.1 Atmospheric parameters

We present in this section the results of stellar atmospheric parameter estimations. The values of effective temperature, gravity, metallicity and microturbulence velocity for stars of the clusters NGC 6134, IC 4651 were adopted from the paper by Carretta et al. (2004), and for stars of the cluster Collinder 261 from Carretta et al. (2005). The main atmospheric parameters for stars of clusters NGC 2506 and NGC 6253 were determined in this thesis work. The open clusters are presented in Table 3.1.

Since the signal to noise ratios of stellar spectra observed in the open cluster NGC 2506 were much lower than in the other open clusters observed by Carretta et al. (2004) and investigated in our previous papers (Mikolaitis et al. 2010, 2011a), we decided to try to redetermine the main atmospheric parameters of stars in NGC 2506 using more strictly selected lines. After a careful selection, the number of Fe I lines initially analysed by Carretta et al. (2004) was reduced from 137–102 to 47–49 in the brighter stars and from 83 to 35 in the fainter star NGC 2506 456. The number of Fe II lines was reduced from 13–10 to 6–5, respectively. This allowed us to minimise the scatter and increase the accuracy of the abundance and stellar atmospheric parameter determinations. The determined atmospheric parameters and iron abundances for the observed stars in NGC 2506 are presented in Table 3.1.

For the cluster NGC 6253 the atmospheric parameters have been determined by Carretta, Bragaglia & Gratton (2007) previously, however a photometric method was used. In order to have our study as much homogeneous as possible we decided to redetermine them spectroscopically. The determined atmospheric parameters and iron abundances for the observed stars in NGC 6253 are presented in Table 3.1.

Table 3.1: Adopted atmospheric parameters for programme stars.

Star*	$T_{\rm eff}$ (K)	log g	v_t (km s^{-1})	[Fe/H]	$\sigma_{\rm FeI}$	$n_{\rm FeI}$	$\sigma_{\rm FeII}$	$n_{\rm FeII}$
NGC 2506 determined in this work								
438	5050	2.64	1.5	−0.18	0.08	49	0.07	5
443	5050	2.60	1.6	−0.24	0.07	47	0.06	5
456	4960	2.96	1.8	−0.23	0.06	45	0.05	5
459	4660	2.16	1.7	−0.29	0.06	49	0.05	6
* Star numbers from Marconi et al. (1997)								
NGC 6134 adopted from Carretta et al. (2004)								
39	4980	2.52	1.17	+0.24	0.16	117	0.19	11
69	5000	2.98	1.11	+0.05	0.11	83	0.12	8
75	5000	3.10	1.10	+0.22	0.16	82	0.14	9
114	4940	2.74	1.14	+0.11	0.16	128	0.12	12
129	4950	2.83	1.13	+0.11	0.12	81	0.13	9
157	5050	2.92	1.12	+0.16	0.14	126	0.15	13
* Star numbers from Mermilliod (1995)								
NGC 6253 determined in this work								
2509	4494	2.57	1.42	0.46	0.06	63	0.07	5
2885	4490	2.43	1.38	0.43	0.05	63	0.06	5
3595	4535	2.44	1.40	0.44	0.07	63	0.07	5
4510	4509	2.52	1.38	0.47	0.05	63	0.06	5
* Star numbers from Bragaglia et al. (1997)								
IC 4651 adopted from Carretta et al. (2004)								
27	4610	2.52	1.17	+0.10	0.15	128	0.17	10
56	3950	0.29	1.46	−0.34	0.17	89	0.15	6
72	4500	2.23	1.21	+0.13	0.13	120	0.21	9
76	4620	2.26	1.21	+0.11	0.17	129	0.17	11
146	4730	2.14	1.21	+0.10	0.16	125	0.16	11
* Star numbers from Lindoff (1972)								
Collinder 261 adopted from Carretta et al. (2005)								
1045	4470	2.07	1.23	0.00	0.16	126	0.19	10
1080	4500	2.09	1.23	0.00	0.15	114	0.26	11
1485	4340	1.76	1.27	–0.06	0.13	113	0.17	12
1871	3980	0.43	1.44	–0.31	0.14	94	0.19	9
2001	4580	1.83	1.26	–0.02	0.12	122	0.19	11
2105	4180	1.59	1.29	–0.08	0.15	124	0.19	8
* Star numbers from Marconi et al. (1997)								

The differences between the photometric and spectroscopic parameters appeared to be quite small and lie within uncertainties of the determinations. There is no systematic difference in $T_{\rm eff}$, just a mean scatter of $\pm$30 K, our log g values are by about 0.07 dex larger, $v_{\rm t}$ by about 0.2 km s^{-1} larger, and differences in [Fe/H] do not exceed $\pm$0.05 dex.

3.2 Evolutionary effects of chemical composition

Nuclear reactions in stellar interiors are the main processes leading the stellar evolution. Various phases of evolution have different physical properties. Therefore, on some evolutionary phases the internal structure and its behaviour can change in such a way that the material transport emerge and change the surface abundance pattern. According to standard theories of stellar evolution, the only episode of such behaviour, modifying the surface abundance pattern of low-mass stars during their ascent on the Red Giant Branch (RGB) is the first dredge-up (Iben 1967) occurring at the base of the RGB. At this stage the convective envelope deepens and the products of hydrogen fusion, mainly CN-cycle products, are dredged-up to the stellar surface, causing the decrease of the ^{12}C/^{13}C and ^{12}C/^{14}N surface ratios. The regions reached by the convective envelope are also lithium free and the surface lithium abundance therefore drops significantly (Canto Martins et al. 2011). Several chemical elements are known that can be involved in surface abundance alterations caused by mixing.

Lithium: Nuclear reactions destroy the lithium isotopes (^{6}Li and ^{7}Li) in stellar interiors at temperatures 2×10^6 (^{6}Li) and 2.5×10^6 K (^{7}Li). Convection cleans the upper atmosphere of Li nuclei by transporting them to deeper, hotter layers where they are rapidly destroyed. Young low-mass stars are entirely convective and most of the primordial Li nuclei are burned in their interiors in a mere few million years (Israelian et al. 2003). The rest of the Li abundance is affected by the further processes. As soon as a star evolves to the red giant phase, the convective envelope deepens and brings to the stellar surface material that has been exposed to high temperatures in the stellar interior, causing an overall dilution of Li in a giant's atmosphere. Red giant stars are, therefore, expected to present a low amount of Li. Starting from the meteoritic abundance of A(Li) of 3.3 dex (Grevesse & Sauval

1998), standard models predict the dilution of Li in the giant's atmosphere down to a level of about 1.5 dex, depending on the stellar mass and metallicity (Iben 1967, Monaco et al. 2011). However, the large number of abundance anomalies detected in main-sequence and giant stars provide evidences pointing to one or more processes of extra-mixing occurring in stellar interiors. Several extra-mixing processes were suggested with the intention of explaining the Li depletion in F- and G-type stars. However, the physical parameters that control this extra-mixing are subjects of debate (Canto Martins et al. 2011). Also, the quality of spectra for the Li investigation requires to be extraordinary. Mainly the analysis of Li includes the blend of two Li (^{6}Li and ^{7}Li) lines 6707.76 Å and 6707.98 Å, together with other blending features (Cr, Ti, CN, Fe) in the region (Israelian et al. 2003). The analysis of the Lithium isotopic ratio (^{6}Li/^{7}Li) requires even higher accuracy and signal to noise ratio.

Beryllium: The destruction temperature of beryllium (3.5×10^6 K) is higher than for lithium. The destruction happens in different depths in the stellar interior. Both elements (Li and Be) could help in constraining the transport mechanisms by performing a stellar tomography. In the study of mixing processes as a function of mass and evolutionary status, cluster stars are ideal because they have well defined masses and share the same age and initial chemical composition (Smiljanic et al. 2009). The beryllium is a very promising element for mixing and extra-mixing theory testing. For evolved stars, beryllium abundances can only be determined using the Be II 2S–2P0 resonance lines at 3131.065 Å and 3130.420 Å. This near-UV region is extremely crowded with atomic and molecular lines, some of them are still lacking a proper identification.

Boron: Other element of the "fragile trio" is boron, which is destructed at a temperature of 5×10^6 K. The degree to which Li, Be and B are depleted from a stellar atmosphere could serve as a subtle tracer of internal stellar kinematics (Puglia 2011). There were attempts to analyse the B III resonance lines at 2066 Å (Cunha 2010), ^{7}B I and ^{6}B I lines at 2089 and 2497 Å (Thorén & Edvardsson 2000) for metal poor stars. However, the spectra of our programme stars are not suitable for this challenging analysis.

Carbon and nitrogen: Surface abundances of carbon and nitrogen are modified in deep mixing processes. The abundance values and the ratios of abundances be-

tween CNO elements and specific isotopes are key tools for mixing investigations in low- and intermediate-mass giants. The alterations of carbon and oxygen isotopic and carbon to nitrogen ratios are used as a valued output from mixing models. The spectroscopic features of nitrogen (CN molecular bands) and carbon (C_2 molecular bands) are investigated by a number of scientists in Galactic globular or open clusters and field stars (Smiljanic et al. 2009; Tautvaišienė et al. 2000; Tautvaišienė et al. 2001; Tautvaišienė et al. 2005; Tautvaišienė, Mikolaitis & Puzeras 2009; Tautvaišienė et al. 2010b; Barisevičius et al. 2010, 2011; Gratton et al. 1999, 2006; Gilroy 1989; Gilroy & Brown 1991; Luck 1994; Gonzalez et al. 1998; Gonzalez & Wallerstein 2000; Origlia et al. 2006; Sneden & Pilachowski 1986, etc.). In this work we aim to study these elements.

3.2.1 Carbon and nitrogen abundances, C/N and $^{12}C/^{13}C$ ratios

The interpretation of the carbon abundances in the investigated open clusters can be done by a comparison with carbon abundances determined for dwarf stars in the Galactic disk. Shi, Zhao & Chen (2002) performed an abundance analysis of carbon for a sample of 90 F and G type main-sequence disk stars using C I and [C I] lines and found [C/Fe] to be about solar at the solar metallicity. The same result was found by Gustafsson et al. (1999) who analysed a sample of 80 late F and early G type dwarfs using the forbidden [C I] line. The solar carbon and nitrogen abundances used in our work are $\log A_{\rm C} = 8.52$ and $\log A_{\rm N} = 7.92$ (Grevesse & Sauval 2000), so the solar $C/N = 3.98$. The $^{12}C/^{13}C$ ratio in the solar photosphere is equal to 89 (Coplen & Mermilliod 2002). The star-to-star results of carbon and nitrogen abundances, C/N and $^{12}C/^{13}C$ ratios are presented Tables 3.2, 3.3, 3.4, 3.5. The mean cluster abundances are presented in Table 3.6.

NGC 2506 The average value of carbon to iron ratio in NGC 2506 is $[C/Fe] = -0.19 \pm 0.08$. We compared the carbon abundance in NGC 2506 with carbon abundances determined for dwarf stars in the Galactic disc. The ratios of [C/Fe] in our stars lie about 0.3 dex below the values obtained for dwarf stars of the Galactic disc. The mean nitrogen to iron abundance ratio in NGC 2506 is $[N/Fe] = 0.32 \pm 0.03$. This shows that nitrogen is overabundand in these evolved stars of NGC 2506 by 0.3 dex, since [N/Fe] values in the Galactic main sequence stars are about solar at

the solar metallicity (c.f. Shi, Zhao & Chen 2002). The mean $^{12}C/^{13}C$ and C/N ratios in the investigated NGC 2506 stars are equal to 11 ± 3 and 1.25 ± 0.27, respectively. It is worth to note that two investigated stars in NGC 2506 belong to the clump (438 and 443) and the remaining star is in the RGB-tip. The mean $^{12}C/^{13}C$ ratio is equal to 9 ± 1 in the clump stars and to 14 in the RGB-tip giant.

NGC 6134 The ratios of [C/Fe] in our stars lie about 0.2 dex below the trend obtained for dwarf stars of the Galactic disk. Smiljanic et al. (2009) analysed carbon abundances in two stars of our sample clusters, NGC 6134 30 and NGC 6134 202, and also found [C/Fe] abundance ratios to be lowered by about the same amount. The mean nitrogen to iron abundance ratio in NGC 6134 is [N/Fe]=0.25 ± 0.10. Nitrogen to iron abundance ratios in the two clump stars investigated in NGC 6134 by Smiljanic et al. (2009) are enhanced too by (0.42 and 0.36 dex). This shows that nitrogen is overabundand in these clump stars of NGC 6134, while [N/Fe] values in the main-sequence stars are about solar at the solar metallicity (c.f. Shi, Zhao & Chen 2002). Reddy et al. (2003) investigated nitrogen abundances in a sample of 43 F–G dwarfs in the Galactic disk by means of weak N I lines. At a value of [Fe/H] of about -0.2 dex, which was well represented in their sample, [N/Fe] is about 0.2 dex. There were few stars of solar metallicity investigated in their study. Nevertheless, the authors make the extrapolation that at solar metallicity [N/Fe] values should be solar. We find that for the open cluster NGC 6134, the mean $^{12}C/^{13}C$ ratios are lowered to about 9 ± 2.5 in the clump stars investigated. Smiljanic et al. (2009) found for this ratio the value of 12 and 13 for their two stars in NGC 6134.

NGC 6253 The average value of carbon to iron ratios in NGC 6253 stars is $[C/Fe] = -0.20 \pm 0.01$. So, the ratios of [C/Fe] in the investigated stars of this cluster lie below the values obtained for dwarf stars of the Galactic disk by the factor of 0.3 dex. The mean nitrogen to iron abundance ratio in NGC 6253 stars is $[N/Fe] = 0.29 \pm 0.03$. This shows that the nitrogen abundances are enhanced in these evolved stars, since [N/Fe] values in the Galactic main-sequence stars are about solar at the solar metallicity (c.f. Shi, Zhao & Chen 2002). The C/N and $^{12}C/^{13}C$ ratios depend on stellar turn-off mass, which is 1.40 $M_{\odot}$ (Bragaglia & Tosi 2006) for NGC 6253. The mean C/N ratio in NGC 6253 is equal to 1.37 ± 0.09. The mean $^{12}C/^{13}C$ ratio

in four clump stars investigated in NGC 6253 is equal to 16 ± 1.

IC 4651 The average value of carbon to iron ratio in IC 4651 is $[C/Fe] = -0.27 \pm 0.02$. If we compare the carbon abundance in IC 4651 with those determined for dwarf stars in the Galactic disk, we see that the ratios of [C/Fe] in our stars lie about 0.3 dex below the values obtained for field dwarf stars. The mean nitrogen to iron abundance ratio in IC 4651 is $[N/Fe] = 0.21 \pm 0.04$. This shows that nitrogen is, again, overabundand in these evolved stars of IC 4651, since [N/Fe] values in the Galactic main-sequence stars are about solar at the solar metallicity (c.f. Shi, Zhao & Chen 2002). Unfortunately, neither carbon, neither nitrogen abundances were investigated in the main sequence stars of IC 4651 by Pace, Pasquini & François (2008) and Pasquini et al. (2004). The mean C/N ratio in IC 4651 is equal to 1.36 ± 0.11. The smallest value, $C/N = 1.12$, was obtained for the star IC 4651 56. We find that the mean $^{12}C/^{13}C$ ratio is about 16 ± 2 in the evolved stars investigated. We did not find differences in the carbon isotopic ratios between clump and other two giant stars in this cluster.

Collinder 261 The average value of carbon to iron ratios in Cr 261 stars is $[C/Fe] = -0.13 \pm 0.02$. So, the ratios of [C/Fe] in investigated stars of this cluster lie below the values obtained for dwarf stars of the Galactic disk by about of 0.1 dex. The mean nitrogen to iron abundance ratio in Cr 261 is $[N/Fe] = 0.23 \pm 0.02$, therefore, the nitrogen abundances are enhanced. The C/N and $^{12}C/^{13}C$ ratios depend on stellar turn-off mass, which for Cr 261 is 1.10 $M_{\odot}$ (Bragaglia & Tosi 2006). In this cluster both, the first-ascent giants after the red giant branch (RGB) luminosity bump and the clump stars were analysed, thus it is worth to check whether the carbon isotope ratios are similar or not. Two investigated stars in Cr 261 belong to the clump (1080 and 2001) and the remaining stars are giants located above the bump. We see that carbon isotope ratios are lowered more in the clump stars than in the giants. The mean $^{12}C/^{13}C$ ratio is equal to 12 ± 1 in the clump stars and 18 ± 2 in the giants.

3.2.2 Theoretical models of mixing

A huge amount of energy is produced by fusion processes in a star. This energy is driven towards the surface by convection and radiation. Turbulent motions are created by convection inside a star. These motions of material can transport chemical elements upwards and downwards. Therefore, we can expect the surface composition alterations to appear. In order to understand the full dynamics of elements and, most important, the observable surface abundances, the processes of mixing should be modelled numerically.

A low-mass star, $M < 2.5M_{\odot}$, approaches the red giant branch after the turn-off from the main sequence. The convective envelope deepens towards the hydrogen burning shell. The point of the deepest convection is the end of the first dredge-up (Iben 1967). A sharp composition discontinuity leaves after this event. The result is the altered surface abundances of ^{3}He and previously described mixing tracers such as $\mathrm{Li}, \mathrm{Be}, \mathrm{B}, \mathrm{C}, \mathrm{N}$, depending on the initial stellar mass and chemical composition (Charbonnel 1994; Charbonnel & Zahn 2007; Charbonnel & Lagarde 2010; Boothroyd & Sackmann 1999). After the completion of the first dredge-up, canonical mixing models, where the rotation is not included and the convection is the only tool of mixing inside the stellar interior, do not predict any further alter-

Table 3.2: Elemental abundances relative to iron, [El/Fe], of carbon, nitrogen, oxygen and C/N, $^{12}\mathrm{C}/^{13}\mathrm{C}$ ratios of open clusters Cr 261 and NGC 6253.

Cluster	Star	[C/Fe]	[N/Fe]	σ^{*}	n^{**}	[O/Fe]	C/N	$^{12}\mathrm{C}/^{13}\mathrm{C}$
Cr 261	1045	–0.15	0.23	0.05	16	–0.05	1.66	15
Cr 261	1080	–0.15	0.26	0.05	10	–0.05	1.58	11
Cr 261	1485	–0.15	0.23	0.05	16	–0.05	1.66	18
Cr 261	1871	–0.10	0.20	0.04	20	–0.20	2.04	18
Cr 261	2001	–0.15	0.20	0.07	10	–0.10	1.66	13
Cr 261	2105	–0.10	0.24	0.06	16	–0.05	1.78	19
NGC 6253	2509	–0.20	0.33	0.03	21	–0.10	1.17	15
NGC 6253	2885	–0.22	0.30	0.05	21	–0.20	1.20	16
NGC 6253	3595	–0.20	0.25	0.04	19	–0.10	1.40	17
NGC 6253	4510	–0.20	0.28	0.03	21	–0.18	1.32	15

* The standard deviations in the mean value due to the line-to-line scatter.
** The number of CN molecular features used.

Table 3.3: Elemental abundances relative to iron, [El/Fe], in NGC 2506 stars. The quoted errors, σ, are the standard deviations in the mean value due to the line-to-line scatter within the species. The number of lines used is indicated by n.

	438 (clump)			443 (clump)		
Species	[El/Fe]	σ	n	[El/Fe]	σ	n
C (C_2)	–0.24		1	–0.27		1
N (CN)	0.30	0.09	12	0.36	0.08	12
O ([O I])	–0.03		1	0.02		1
Na I	0.01	0.07	2	0.03	0.06	2
Mg I	0.04	0.06	3	0.09	0.06	3
Al I	0.04	0.04	2	–0.01	0.05	2
Si I	–0.05	0.09	10	–0.01	0.06	12
Ca I	–0.06	0.06	6	–0.08	0.06	6
Sc II	–0.02	0.08	6	–0.04	0.08	8
Ti I	–0.01	0.08	18	–0.02	0.10	23
Ti II	0.00	0.09	6	–0.04	0.08	7
V I	–0.02	0.08	6	0.00	0.09	7
Cr I	–0.12	0.09	17	–0.11	0.09	19
Cr II	–0.03	0.08	9	0.02	0.06	8
Mn I	–0.17	0.08	6	–0.15	0.07	4
Co I	–0.03	0.07	5	–0.03	0.09	5
Ni I	–0.12	0.09	31	–0.13	0.09	32
Cu I	–0.13		1	–0.13		1
Zn I	0.01	0.08	3	0.00	0.08	3
Y II	–0.09	0.02	5	0.01	0.07	5
Zr I	0.13		1	0.13	0.07	2
Ba II	0.08	0.08	3	0.10	0.07	2
La II	0.11	0.07	2	0.13	0.04	2
Ce II	0.02		1	0.14	0.04	2
Pr II	0.13		1	0.19		1
Nd II	0.01	0.04	2	0.05	0.04	2
Eu II	0.17		1	0.24		1
C/N	1.14			0.93		
$^{12}C/^{13}C$	10			8		

Table 3.3: Continued

	456 (giant)			459 (RGB-tip)		
Species	[El/Fe]	σ	n	[El/Fe]	σ	n
C (C_2)	–0.15		1	–0.10		1
N (CN)	0.30	0.09	10	0.31	0.09	19
O ([O I])	0.03		1	0.15		1
Na I	–0.11	0.06	2	0.14	0.05	2
Mg I	–0.01		1	0.05	0.07	3
Al I	–0.06	0.00	1	0.12	0.04	2
Si I	–0.01	0.03	4	0.12	0.07	12
Ca I	–0.12	0.03	3	0.02	0.07	6
Sc II	0.10	0.08	4	0.06	0.09	9
Ti I	–0.08	0.94	10	0.07	0.09	25
Ti II	0.08	0.09	4	0.09	0.09	10
V I	–0.11	0.08	4	0.04	0.09	7
Cr I	–0.08	0.09	8	–0.02	0.09	26
Cr II	0.13	0.06	2	–0.04	0.09	9
Mn I	–0.17	0.04	3	0.00	0.09	6
Co I	0.00	0.02	2	0.09	0.04	7
Ni I	–0.07	0.09	19	–0.01	0.09	32
Cu I	–0.14		1	–0.21		1
Zn I	0.05		1	0.04	0.04	3
Y II	0.09	0.03	3	–0.14	0.04	5
Zr I	0.13		1	–0.03	0.03	2
Ba II	0.07	0.05	3	–0.11	0.05	3
La II				–0.06	0.07	2
Ce II	–0.04		1	0.19	0.04	2
Pr II				0.14		1
Nd II	0.10		1	0.19	0.09	3
Eu II	0.20		1	0.19		1
C/N	1.39			1.55		
$^{12}C/^{13}C$				14		

Table 3.4: Elemental abundances relative to iron, [El/Fe], in NGC 6134 stars. The quoted errors, σ, are the standard deviations in the mean value due to the line-to-line scatter within the species. The number of lines used is indicated by n.

	114			39			157		
Species	[El/Fe]	σ	n	[El/Fe]	σ	n	[El/Fe]	σ	n
C (C_2)	–0.26		1	–0.20		1	–0.23		1
N (CN)	0.32	0.14	11	0.23	0.16	10	0.33	0.14	11
O ([OI])	–0.15		1	–0.23		1	–0.13		1
Na I	0.02	0.07	3	–0.07	0.06	3	0.01	0.06	3
Mg I	–0.04	0.06	4	–0.09	0.06	4	–0.05	0.07	4
Al I	–0.03	0.08	2	0.08	0.07	2	0.12	0.06	2
Si I	0.09	0.08	12	–0.07	0.07	12	0.05	0.06	12
Ca I	0.10	0.06	12	0.14	0.08	12	0.04	0.05	12
Sc II	0.09	0.05	9	0.01	0.08	9	0.04	0.08	9
Ti I	0.14	0.07	18	0.03	0.08	18	0.07	0.03	18
Ti II	–0.01	0.05	8	–0.02	0.06	8	–0.12	0.04	8
V I	0.12	0.03	9	0.15	0.04	9	0.08	0.05	9
Cr I	–0.03	0.08	24	0.01	0.08	24	–0.05	0.07	24
Cr II	–0.08	0.06	6	0.00	0.03	6	–0.06	0.06	6
Mn I	0.17	0.03	6	0.08	0.08	6	0.16	0.05	6
Co I	0.13	0.07	8	0.11	0.06	8	0.24	0.05	8
Ni I	0.06	0.08	36	0.03	0.07	36	0.15	0.07	36
Cu I	0.02	0.06	3	0.00	0.07	3	0.11	0.05	3
Zn I	–0.08	0.05	2	–0.13	0.05	2	–0.05	0.05	2
Y II	–0.01	0.03	6	–0.08	0.02	6	0.11	0.06	6
Zr I	–0.10		1	–0.09		1	0.07		1
Ba II	0.13	0.01	2	0.07	0.02	2	0.24	0.05	2
La II	0.00		1	–0.07		1	0.13		1
Ce II	0.10	0.07	2	0.06	0.06	2	0.21	0.05	2
Nd II	0.22	0.05	3	0.16	0.06	3	0.19	0.03	3
Eu II	0.04		1	–0.09		1	0.04		1
C/N	1.05			1.48			1.1		
$^{12}C/^{13}C$	6	±1		9	±1		12	±1	

Table 3.4: Continued

	75			129			69		
Species	[El/Fe]	σ	n	[El/Fe]	σ	n	[El/Fe]	σ	n
C (C_2)	–0.27	0.04	2	–0.25	0.07	2	–0.36	0.04	2
N (CN)	0.18	0.05	11	0.36	0.07	11	0.10	0.06	11
O ([O I])	–0.14		1	–0.10		1	–0.11		1
Na I	0.06	0.04	2	0.20	0.07	2	0.04	0.04	2
Mg I	0.01	0.04	3	0.12	0.03	3	–0.01	0.01	3
Al I	–0.07	0.02	2	0.03	0.04	2	–0.11	0.04	2
Si I	0.14	0.09	5	0.16	0.07	5	0.01	0.09	5
Ca I	–0.12	0.07	9	0.01	0.04	9	–0.11	0.07	9
Sc II	0.09	0.03	3	0.08	0.03	3	–0.06	0.05	3
Ti I	–0.04	0.08	5	0.00	0.06	5	–0.12	0.09	5
Ti II	0.08	0.09	2	0.35	0.07	2	0.19	0.01	2
V I	0.10	0.09	2	0.17	0.08	2	–0.01	0.07	2
Cr I	0.08	0.08	12	0.22	0.05	12	0.04	0.09	12
Cr II	0.03		1	0.20		1	0.06		1
Mn I	0.03	0.08	2	0.10	0.04	2	–0.06	0.07	2
Co I	0.09	0.07	4	0.13	0.02	4	–0.03	0.02	4
Ni I	0.02	0.07	21	0.06	0.07	21	–0.12	0.08	21
Cu I	0.10		1	0.25		1	–0.01		1
Zn I	–0.04	0.04	2	0.13	0.09	2	–0.11	0.08	2
Y II	0.13		1	0.20		1	0.19		1
Zr I	–0.02	0.07	2	0.00	0.07	2	–0.06	0.07	2
Ba II	0.08	0.05	2	0.05	0.07	2	–0.01	0.05	2
La II	0.23	0.07	2	0.24	0.01	2	0.11	0.05	2
Ce II	0.08		1	0.15		1	0.04		1
Nd II	0.18		1	0.35		1	0.19		1
Eu II	0.13		1	0.20		1	0.01		1
C/N	1.41			0.98			1.38		
$^{12}C/^{13}C$	7	±1		8	±1		12	±1	

Table 3.5: Elemental abundances relative to iron, [El/Fe], in IC 4651 stars. The quoted errors, σ, are the standard deviations in the mean value due to the line-to-line scatter within the species. The number of lines used is indicated by *n*.

	27			56			72		
Species	[El/H]	σ	*n*	[El/H]	σ	*n*	[El/H]	σ	*n*
C (C_2)	–0.25		1	–0.30		1	–0.25		2
N (CN)	0.26	0.07	24	0.25	0.11	18	0.22	0.07	24
O ([O I])	–0.05		1	0.07		1	–0.04		1
Na I	–0.01	0.05	3	0.09	0.02	3	–0.03	0.04	3
Mg I	–0.05	0.07	4	–0.06	0.08	4	–0.08	0.09	4
Al I	0.01	0.05	4	0.12	0.07	4	0.00	0.02	4
Si I	0.15	0.08	9	–0.01	0.09	6	0.12	0.10	8
Ca I	0.07	0.05	9	0.06	0.08	6	0.00	0.09	10
Sc II	0.07	0.02	9	–0.16	0.05	9	0.01	0.06	8
Ti I	0.15	0.08	24	0.14	0.07	9	0.10	0.09	24
Ti II	0.11	0.09	6	0.04	0.09	8	0.06	0.07	7
V I	0.10	0.07	9	–0.24	0.02	9	0.04	0.09	5
Cr I	0.00	0.05	19	–0.17	0.06	11	–0.05	0.09	25
Cr II	–0.05	0.04	6	–0.16	0.05	6	–0.13	0.09	9
Mn I	0.10	0.04	6	–0.13	0.01	6	0.08	0.05	5
Co I	0.15	0.07	8	0.16	0.09	5	0.07	0.07	9
Ni I	0.07	0.08	34	0.09	0.10	30	0.07	0.09	34
Cu I	–0.05	0.06	3	0.01	0.07	3	–0.05	0.02	3
Zn I	–0.10	0.06	2	0.06	0.02	2	–0.03	0.09	2
Y II	–0.03	0.05	6	0.09	0.03	6	–0.03	0.04	6
Zr I	–0.07	0.08	2	0.00	0.01	2	–0.13	0.05	2
Ba II	–0.07	0.03	3	0.05	0.04	2	–0.05	0.07	3
La II	0.08	0.02	2	0.01	0.02	2	–0.03	0.05	2
Ce II	0.12	0.08	2	0.04	0.02	2	0.07	0.07	2
Nd II	0.17	0.08	3	0.16	0.04	2	0.15	0.06	3
Eu II	0.04		1	0.09		1	–0.03		1
C/N	1.23			1.12			1.34		
$^{12}C/^{13}C$	17			14			15		

Table 3.5: Continued

	76			146		
Species	[El/Fe]	σ	n	[El/Fe]	σ	n
C (C_2)	–0.28		1	–0.25		1
N (CN)	0.19	0.06	24	0.17	0.09	23
O ([O I])	0.05		1	0.08		1
Na I	–0.01	0.05	3	–0.03	0.04	3
Mg I	–0.02	0.05	4	–0.02	0.09	4
Al I	0.06	0.04	4	–0.01	0.03	4
Si I	0.09	0.07	9	0.11	0.09	9
Ca I	0.06	0.09	8	0.07	0.10	8
Sc II	0.04	0.06	9	0.08	0.05	9
Ti I	0.07	0.08	26	0.11	0.10	28
Ti II	0.12	0.09	11	0.04	0.09	11
V I	0.14	0.05	9	0.17	0.04	9
Cr I	–0.01	0.09	24	0.00	0.09	24
Cr II	–0.03	0.09	6	–0.03	0.04	6
Mn I	0.04	0.01	6	0.08	0.06	6
Co I	0.13	0.08	8	0.17	0.08	8
Ni I	0.06	0.07	36	0.07	0.08	36
Cu I	0.05	0.01	3	0.00	0.02	3
Zn I	–0.04	0.07	2	–0.03	0.08	2
Y II	–0.07	0.01	6	0.04	0.04	6
Zr I	–0.07	0.02	2	–0.10	0.05	2
Ba II	–0.06	0.05	3	–0.05	0.05	3
La II	0.04	0.03	2	0.05	0.05	2
Ce II	0.13	0.01	2	0.10	0.07	2
Nd II	0.04	0.05	3	0.08	0.03	3
Eu II	0.02		1	0.00		1
C/N	1.35			1.5		
$^{12}C/^{13}C$	14			18		

Table 3.6: Mean cluster abundances relative to iron, [El/Fe], and standard deviations for the clusters stars.

	NGC 2506		NGC 6134		IC 4651	
Species	[El/Fe]	σ	[El/Fe]	σ	[El/Fe]	σ
C (C_2)	–0.19	0.08	–0.26	0.11	–0.26	0.02
N (CN)	0.32	0.03	0.25	0.10	0.21	0.04
O ([O I])	0.04	0.08	–0.14	0.05	0.01	0.06
Na I	0.02	0.10	0.04	0.06	–0.02	0.01
Mg I	0.04	0.04	–0.01	0.06	–0.04	0.03
Al I	0.02	0.07	0.00	0.12	0.02	0.03
Si I	0.01	0.07	0.06	0.08	0.12	0.03
Ca I	–0.06	0.06	0.01	0.14	0.05	0.04
Sc II	0.03	0.07	0.04	0.09	0.05	0.03
Ti I	–0.01	0.06	0.01	0.12	0.11	0.03
Ti II	0.03	0.07	0.08	0.14	0.08	0.04
V I	–0.02	0.06	0.10	0.10	0.11	0.05
Cr I	–0.08	0.05	0.05	0.09	–0.01	0.02
Cr II	0.02	0.08	0.03	0.09	–0.06	0.05
Mn I	–0.12	0.08	0.08	0.11	0.07	0.03
Co I	0.01	0.06	0.11	0.12	0.13	0.04
Ni I	–0.08	0.06	0.03	0.12	0.07	0.01
Cu I	–0.15	0.04	0.08	0.09	–0.01	0.05
Zn I	0.02	0.02	–0.05	0.07	–0.05	0.03
Y II	–0.03	0.10	0.09	0.09	–0.02	0.05
Zr I	0.09	0.08	–0.03	0.09	–0.09	0.03
Ba II	0.04	0.10	0.09	0.12	–0.06	0.01
La II	0.06	0.10	0.11	0.12	0.03	0.05
Ce II	0.08	0.11	0.11	0.08	0.11	0.03
Pr II	0.15	0.03	–	–	–	–
Nd II	0.09	0.08	0.22	0.04	0.11	0.06
Eu II	0.20	0.03	0.06	0.09	0.01	0.03
C/N	1.25	0.27	1.23	0.22	1.36	0.11
$^{12}C/^{13}C$	11	3	9	2.5	16	2

Table 3.6: Continued

	NGC 6253		Collinder 261	
Species	[El/Fe]	σ	[El/Fe]	σ
C (C_2)	–0.19	0.08	–0.26	0.11
N (CN)	0.32	0.03	0.25	0.10
O ([O I])	0.04	0.08	–0.14	0.05
C/N	1.25	0.27	1.23	0.22
$^{12}C/^{13}C$	11	3	9	2.5

ations in the surface abundances until the giant reaches the asymptotic giant branch (AGB). Many observations of star in the Galactic field and open or globular clusters show the signature of some non-canonical mixing process that happens after the low-mass star reaches the RGB bump (Sneden & Pilachowski 1986; Gilroy 1989; Gilroy & Brown 1991; Luck 1994; Charbonnel 1994; Charbonnel, Brown & Wallerstein 1998; Gratton et al. 2000; Tautvaišienė et al. 2000, 2005; Smiljanic et al. 2009; Mikolaitis et al. 2010, 2011a,b, 2012).

Main models of extra-mixing were calculated by several scientific groups. In this thesis work we compare our results with the most recent thermohaline instability induced mixing model by Charbonnel & Lagarde (2010), and the cool-bottom processing model by Boothroyd & Sackmann (1999).

Model of thermohaline instability induced mixing

The model of thermohaline instability induced mixing is based on ideas of Eggleton, Dearborn & Lattanzio (2006) and Charbonnel & Zahn (2007). Eggleton, Dearborn & Lattanzio (2006) found a mean molecular weight (μ) inversion in their 1 $M_{\odot}$ stellar evolution model, occurring after the so-called luminosity bump on the RGB, when the hydrogen-burning shell reaches the chemically homogeneous part of the envelope. The μ-inversion is produced by the reaction $^3\mathrm{He}(^3\mathrm{He}, 2\mathrm{p})^4\mathrm{He}$, as predicted by Ulrich (1972). It does not occur earlier, because the magnitude of the μ-inversion is low and negligible compared to a stabilising μ-stratification. Following Eggleton, Dearborn & Lattanzio, Charbonnel & Zahn (2007) computed stellar models including the prescription by Ulrich (1972) and extended them to the case

of a non-perfect gas for the turbulent diffusivity produced by that instability in a stellar radiative zone. They found that a double diffusive instability referred to as thermohaline convection, which has been discussed long ago in the literature (Stern 1960), is important in evolution of red giants. This mixing connects the convective envelope with the external wing of the hydrogen-burning shell and induces surface abundance modifications in red giant stars. The Kippenhahn diagram and evolutionary tracks are provided as examples in Figs. 3.1 and 3.2.

The thermohaline instability induced mixing is widely used in oceanology. It is used to model the regions of cooler, less salty water below the warmer water where the salinity is higher because of the evaporation from the surface. The so-called "long fingers" of the warmer water penetrate the cooler water; mixing occurs when the heat excess is exchanged (e.g., Schmitt 1983, 2003; Ruddick 2003; Kunze 2003; Radko 2010).

Charbonnel & Lagarde (2010) also computed the models of rotation-induced mixing for stars at the zero age main sequence (ZAMS) with rotational velocities of $110\,\mathrm{km\,s^{-1}}$, $250\,\mathrm{km\,s^{-1}}$ and $300\,\mathrm{km\,s^{-1}}$. Typical initial ZAMS rotation velocities were chosen depending on the stellar mass, based on observed rotation distributions in young open clusters, see Gaigé (1993). The convective envelope was supposed to rotate as a solid body through the evolution. The transport coefficients for chemicals associated to thermohaline and rotation-induced mixings were simply added in the diffusion equation and the possible interactions between the two mechanisms were not considered. The rotation-induced mixing modifies the internal chemical structure of main sequence stars, although its signatures are revealed only later in the stellar evolution. These models lie closer to the observational data but yet not close enough.

As an alternative to the pure ^{3}He-driven thermohaline convection, the model of magneto-thermohaline mixing was proposed by Denissenkov, Pinsonneault & MacGregor (2009). On the basis of three-dimensional numerical simulations of thermohaline convection, it was suggested that the salt-finger spectrum might be shifted towards larger diameters by a toroidal magnetic field (Denissenkov & Merryfield 2011).

Wachlin, Miller Bertolami & Althaus (2011) have computed full evolutionary sequences of red giant branch stars close to the luminosity bump and also found that

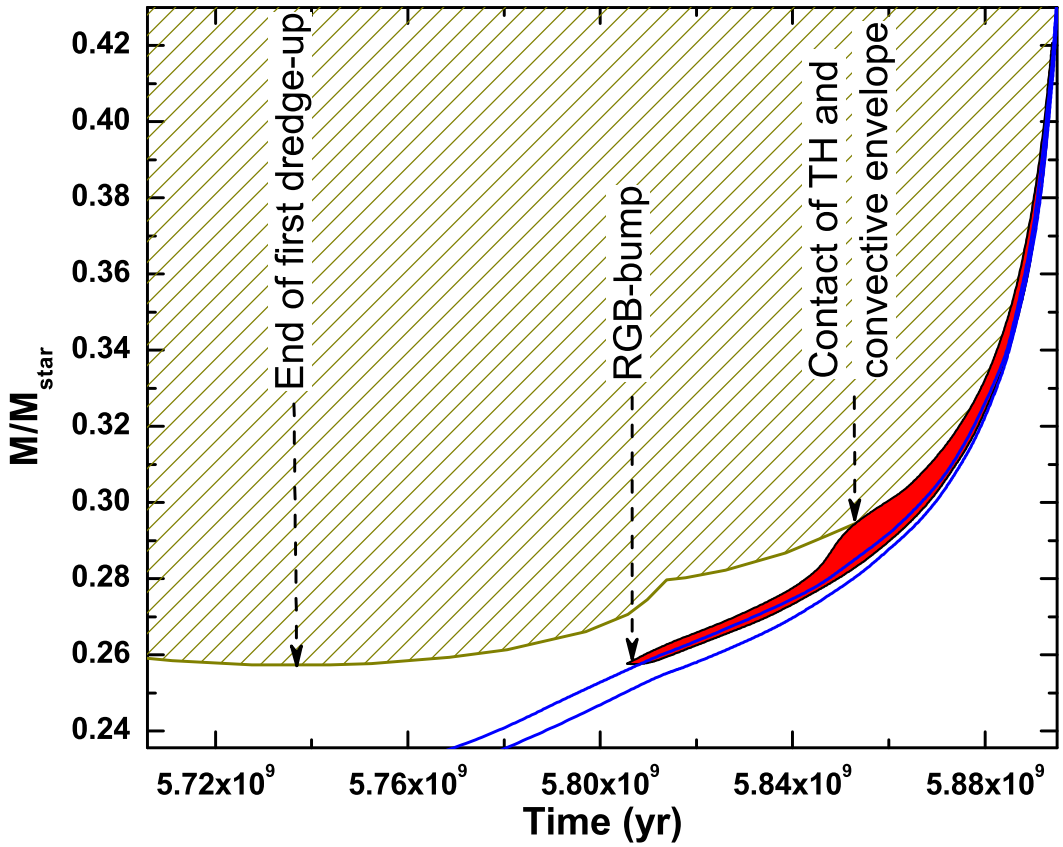

Figure 3.1: Kippenhahn diagram for the $M = 1.25 M_{\odot}$ Population I star evolution from the first dredge-up up to the RGB-tip. Hatched area indicates the convective envelope. A zone where the thermohaline instability develops is shown in red. Blue lines delimit the hydrogen-burning shell above the degenerate helium core. Diagram is taken from Charbonnel & Lagarde (2010).

thermohaline mixing is not efficient enough for fingering convection to reach the bottom of the convective envelope of red giants. To reach the contact, the diffusion coefficient has to be artificially increased by about four orders of magnitude.

Cool-bottom processing model

The Cool-bottom processing model, which includes a deep circulation mixing below the base of the standard convective envelope, was proposed more than a decade ago (Boothroyd, Sackmann & Wasserburg 1995; Wasserburg, Boothroyd & Sackmann 1995; Boothroyd & Sackmann 1999 and references therein). In this model, an extra-mixing takes material from the convective envelope, transports it down to the regions hot enough for some nuclear processing in the outer wing of H-burning

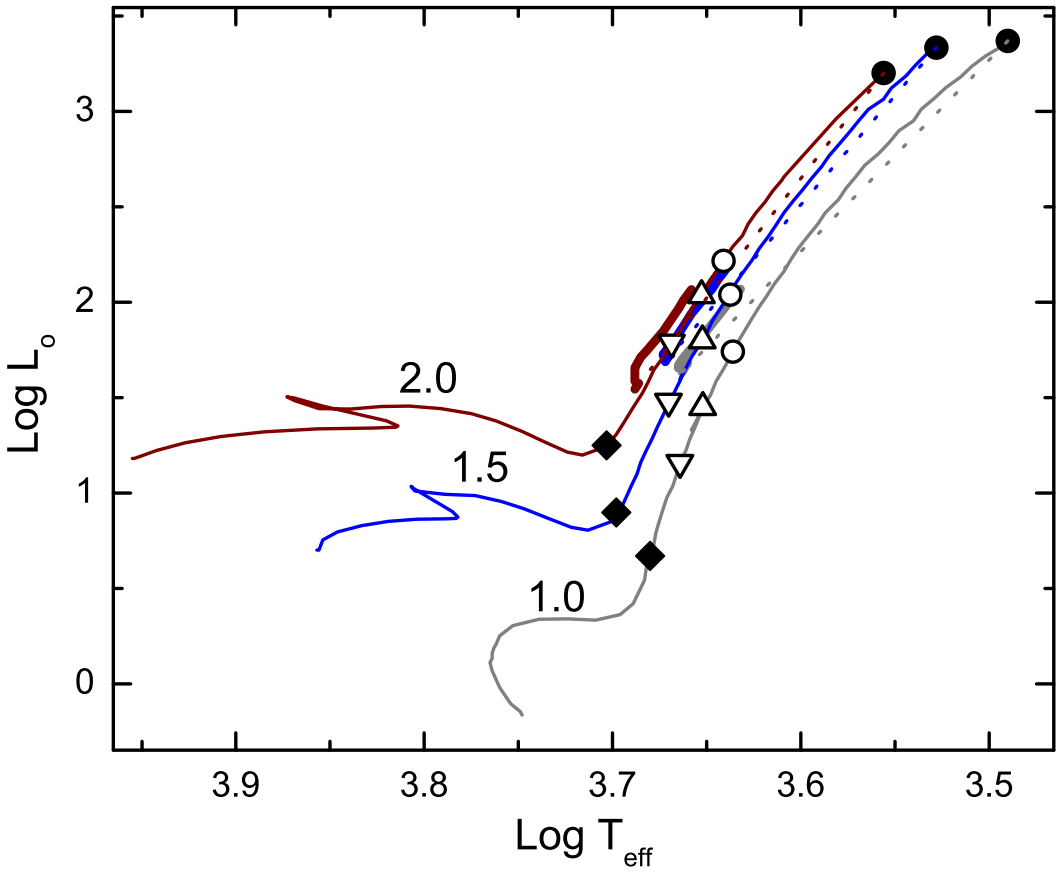

Figure 3.2: Evolutionary tracks for Population I low-mass stars $Z = 0.02$. Tracks (Girardi et al. 2000) in the H-R diagram are labelled by their initial masses. Solid diamonds indicate the points where the convective envelope sinks deep enough to reach the ^{13}C rich region. Reversed triangles on the RGB indicate the end of the first dredge-up, it is the point on the RGB when the convective envelope penetrates he deepest into the star. Open triangles show the point where the advancing hydrogen-burning shell has reached the composition discontinuity ("μ-barrier") left behind by the first dredge-up, cool-bottom processing is expected after this last point. Open circles indicate the point where thermohaline instability reaches the bottom of the convective envelope, thermohaline mixing is expected after this point up to the helium flash (marked as open circles). Short and heavy solid path to the left of the RGB tracks indicate the helium-core-burning (clump) phase.

shell, and then transports it back up to the convective envelope. The cool-bottom processing induced mixing is expected to appear after the star reaches RGB-bump phase (see Fig. 3.2). For computations of the extra-mixing, a "conveyor-belt" circulation model was used. The temperature difference between the bottom of mixing and the bottom of the H-burning shell was considered a free parameter, to be determined by comparison with observations, to open cluster M 67 (Gilroy 1989; Gilroy & Brown 1991), in particular.

Table 3.7: $^{12}C/^{13}C$ and C/N ratios along with the values of turn-off mass, age, galactocentric distance and atmospheric parameters for the clump stars in open clusters

Star	T_{eff}(K)	log g	[A/H]	$^{12}C/^{13}C$	C/N	Ref.*
NGC 752						
M_{TO}=1.6 $M_\odot$; Age = 2.0 Gyr; R_{gc} = 8.75 kpc.						
1	5000	2.85	0.1	16	–	1
75	4900	2.85	0.1	13	–	1
77	4900	2.85	0.2	16	–	1
213	5000	2.90	0.1	14	–	1
295	5000	2.90	0.2	15	–	1
NGC 2360						
M_{TO}=2.02 $M_\odot$; Age = 1.15 Gyr; R_{gc} = 6.32 kpc.						
50	5015	2.90	–0.03	–	1.04	5
62	5105	3.15	0.12	–	1.38	5
86	4960	2.65	–0.06	–	0.93	5
12	4800	2.70	0.2	14.5	–	1
NGC 2447						
M_{TO}=1.90 $M_\odot$; Age = 0.45 Gyr; R_{gc} = 6.51 kpc.						
28	5060	2.70	–0.01	–	0.69	5
34	5120	2.90	–0.01	–	0.87	5
NGC 2506						
M_{TO}=1.69 $M_\odot$; Age = 1.7 Gyr; R_{gc} = 10.38 kpc.						
438	5050	2.64	–0.18	10	1.14	8
443	5050	2.60	–0.24	8	0.93	8
NGC 2682						
M_{TO}=1.20 $M_\odot$; Age = 5.0 Gyr; R_{gc} = 9.05 kpc.						
F84	4750	2.4	–0.02	20	1.15	3
F141	4730	2.4	–0.01	16	1.32	3
F151	4760	2.4	–0.03	17	1.32	3
F164	4700	2.5	0.00	18	1.62	3
F224	4710	2.4	–0.11	8	1.58	3
F226	4730	2.4	–0.02	15	1.62	3
F84	4800	2.70	0.0	11.5	–	1
F141	4800	2.70	0.0	10.5	–	1
F164	4800	2.70	0.0	10.5	–	1

* 1 – Gilroy (1989); 2 – Luck (1994); 3 – Tautvaišienė et al. (2000);
4 – Tautvaišienė et al. (2005); 5 – Smiljanic et al. (2009); 6 – Mikolaitis et al. (2010);
7 – Mikolaitis et al. (2011a); 8 – Mikolaitis et al. (2011b); 9 – Mikolaitis et al. (2012).

Table 3.7: Continued

Star	T_{eff}(K)	log g	[A/H]	$^{12}C/^{13}C$	C/N	Ref.*
NGC 3532						
M_{TO}=3.03 $M_{\odot}$; Age = 0.35 Gyr; R_{gc} = 7.87 kpc.						
19	4995	2.65	0.11	12	1.02	5
122	5045	2.60	–0.02	–	0.93	5
596	5020	2.50	0.04	–	0.95	5
HD95879	5000	2.25	0.08	10	1.10	2
HD96174	5000	2.17	0.00	15	0.59	2
HD96175	5100	2.25	0.12	15	0.44	2
HD96445	5000	2.36	0.13	10	1.51	2
NGC 5822						
M_{TO}=2.19 $M_{\odot}$; Age = 0.9 Gyr; R_{gc} = 8.1 kpc.						
201	5035	2.85	0.05	13	0.87	5
316	5110	3.05	0.16	–	1.00	5
NGC 6134						
M_{TO}=2.34 $M_{\odot}$; Age = 0.7 Gyr; R_{gc} = 7.6 kpc.						
39	4980	2.52	0.24	9	1.48	6
69	4950	2.83	0.11	12	1.38	6
75	5000	3.10	0.22	7	1.41	6
114	4940	2.74	0.11	6	1.05	6
129	5000	2.98	0.05	8	0.98	6
157	5050	2.92	0.16	12	1.10	6
30	4980	2.95	0.21	12	0.93	5
NGC 6253						
M_{TO}=1.40 $M_{\odot}$; Age = 3.0 Gyr; R_{gc} = 6.6 kpc.						
2509	4494	2.57	0.46	15	1.20	9
2885	4490	2.43	0.43	17	1.12	9
3595	4535	2.44	0.44	17	1.39	9
4510	4509	2.52	0.47	15	1.20	9
NGC 6281						
M_{TO}=3.18 $M_{\odot}$; Age = 0.3 Gyr; R_{gc} = 8.47 kpc.						
3	4915	2.30	0.01	12	0.64	5
4	5015	2.50	0.09	12	0.95	5

Table 3.7: Continued

Star	T_{eff}(K)	log g	[A/H]	$^{12}C/^{13}C$	C/N	Ref.*
NGC 6633						
M_{TO}=2.79 $M_{\odot}$; Age = 0.45 Gyr; R_{gc} = 8.42 kpc.						
100	5015	2.85	0.11	21	0.91	5
NGC 7789						
M_{TO}=1.60 $M_{\odot}$; Age = 1.4 Gyr; R_{gc} = 9.43 kpc.						
K605	4860	2.4	–0.02	10	1.05	4
K665	4970	2.4	0.00	9	1.45	4
K732	4900	2.3	0.02	7	1.51	4
Collinder 261						
M_{TO}=1.10 $M_{\odot}$; Age = 6.0 Gyr; R_{gc} = 7.5 kpc.						
1080	4500	2.09	0.00	11	1.58	9
2001	4580	1.83	–0.02	13	1.66	9
IC 2714						
M_{TO}=2.85 $M_{\odot}$; Age = 0.50 Gyr; R_{gc} = 8.34 kpc.						
5	5070	2.70	0.12	–	0.83	5
IC 4651						
M_{TO}=1.69 $M_{\odot}$; Age = 1.7 Gyr; R_{gc} = 7.1 kpc.						
27	4610	2.52	0.10	17	1.23	7
76	4620	2.26	0.11	14	1.35	7
146	4730	2.14	0.10	18	1.50	7
IC 4756						
M_{TO}=2.37 $M_{\odot}$; Age = 0.7 Gyr; R_{gc} = 7.23 kpc.						
12	5030	2.75	–0.01	11	0.91	5
14	4720	2.47	0.03	17	1.02	5
38	5075	3.00	0.05	10	1.20	5
69	5130	3.00	0.08	5	1.15	5
144	5200	3.20	0.0	18	–	1
176	5200	3.00	0.0	12	–	1
228	5000	2.90	0.0	21	–	1
296	5000	2.90	0.0	18	–	1

3.2.3 Comparison of observed $^{12}C/^{13}C$ and C/N values with theoretical models of mixing

In Table 3.7 we present a compilation of recent data on $^{12}C/^{13}C$ and C/N ratios in clump stars of open clusters, investigated by Mikolaitis et al. (2010, 2011a,b, 2012); Smiljanic et al. (2009); Tautvaišienė et al. (2000, 2005); Luck (1994) and Gilroy (1989). From Gilroy (1989) we selected four clusters with well defined red clump stars. Luck (1994) derived carbon isotope ratios for eight open clusters, however only one cluster was included to our comparison since for other clusters it was very difficult to identify stars of the red clump. The turn-off masses, ages and galactocentric distances were chosen from the most recent studies and used to display the results of the other $^{12}C/^{13}C$ and C/N investigations for the same cluster, if available.

In Figures 3.3 and 3.4, we compare the mean carbon isotope and C/N ratios of clump stars in different open clusters as a function of turn-off mass with the theoretical models of the first dredge-up, the thermohaline mixing (TH) model, thermohaline mixing together with rotation-induced mixing for stars at the zero age main sequence (ZAMS) having rotational velocities of $110\,\mathrm{km\,s^{-1}}$, $250\,\mathrm{km\,s^{-1}}$ and $300\,\mathrm{km\,s^{-1}}$ computed by Charbonnel & Lagarde (2010); and the cool-bottom Processing model (CBP) by Boothroyd & Sackmann (1999). For NGC 6134 we plot the mean $^{12}C/^{13}C$ ratio 10 ± 3 as averaged from clump stars investigated in our study and by Smiljanic et al. (2009).

We confirm the observational evidence that theoretical models for stars with turn-off masses of 2–3 $M_{\odot}$ should consider the larger extra-mixing, probably dominated by the former rotation on the main sequence. This is seen from the results of NGC 6134 in this study, also form NGC 3532, NGC 5822, NGC 6134, NGC 6281 and IC 4756 (Smiljanic et al. 2009), and from NGC 3532 (Luck 1994). For clusters with stars of smaller turn-off masses, the $^{12}C/^{13}C$ and C/N values agree with models of extra-mixing used for the comparison.

3.2.4 Helium flash influence to mixing

For the clusters in which both the first-ascent giants after the red giant branch (RGB) luminosity bump and the clump stars were analysed, it is worth to check whether

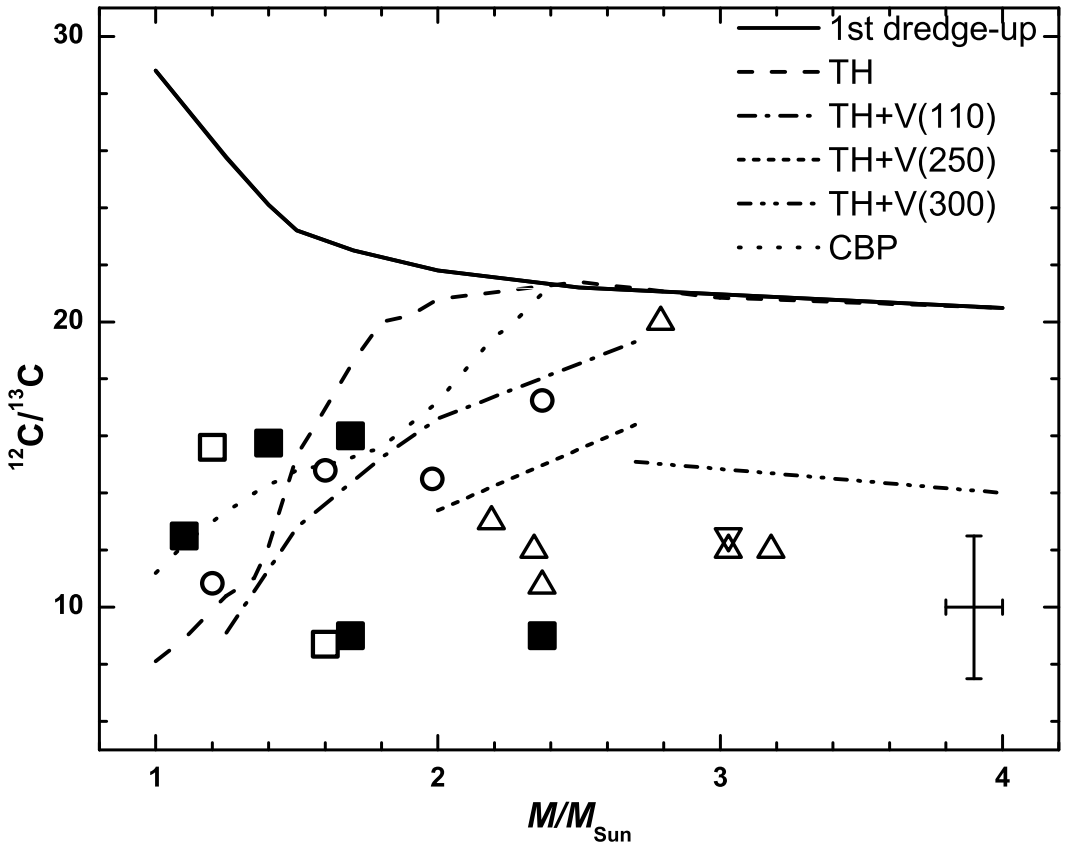

Figure 3.3: The average carbon isotope ratios in clump stars of open cluster as a function of stellar turn-off mass. The models of the first dredge-up, thermohaline mixing (TH) and rotation-induced mixing (V) are taken from Charbonnel & Lagarde (2010). The CBP model of extra-mixing is taken from Boothroyd & Sackmann (1999). The results of this work are marked by the filled square; from Mikolaitis et al. (2010, 2011a,b, 2012) and Tautvaišienė et al. (2000, 2005) – open squares; from Smiljanic et al. (2009) – open triangles; from Luck (1994) – reversed open triangle; from Gilroy (1989) – open circles. A typical error bar is indicated.

the carbon isotope ratios are similar or not. Two investigated stars in Collinder 261 belong to the clump and the remaining stars are giants located above the bump. We see that the carbon isotope ratios are lowered more in the clump stars than in the giants. The mean $^{12}C/^{13}C$ ratio is equal to 12 ± 1 in the clump stars and to 18 ± 2 in the giants. In NGC 2506, the mean C/N ratio in the clump stars is lowered slightly more (1.04 ± 0.11) than in the first ascent giants (1.47 ± 0.08). In the clump stars the $^{12}C/^{13}C$ ratios are also lowered to the smaller values (8 and 10) than in the RGB-tip star 459, which is equal to 14.

The He-flash influence to the extra-mixing of CN-cycled material to stellar sur-

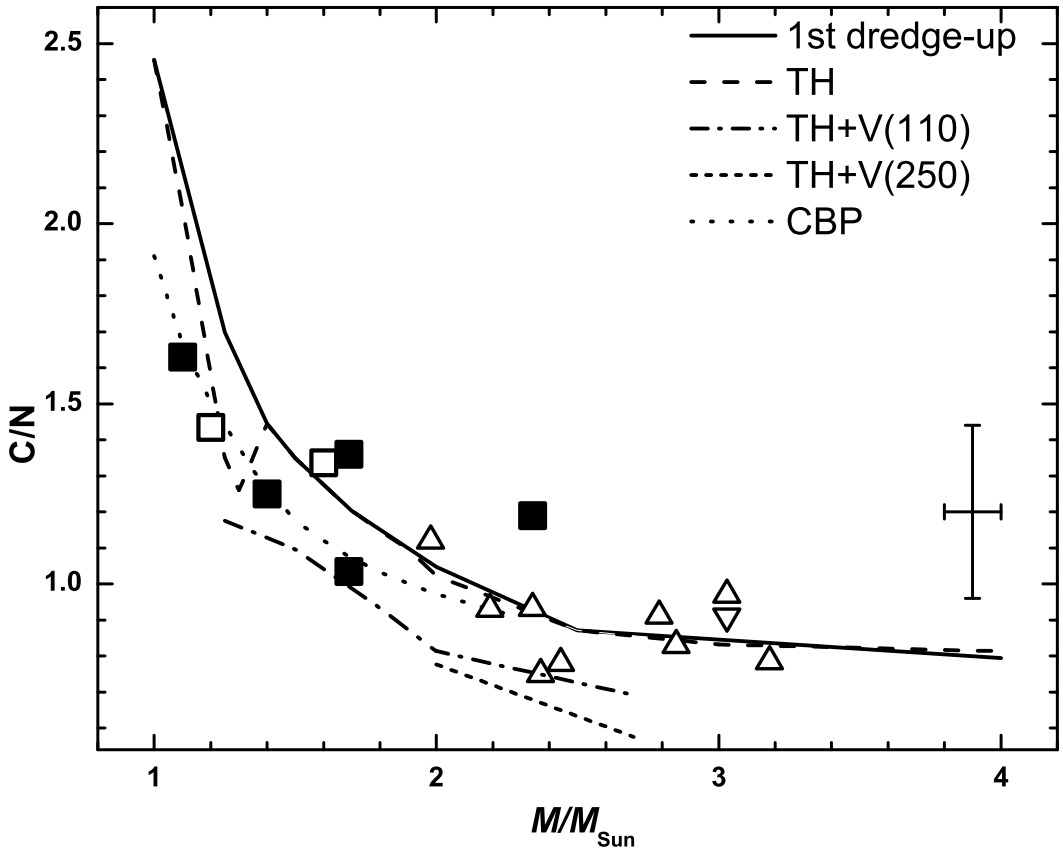

Figure 3.4: The average carbon to nitrogen ratios in the clump stars of open clusters as a function of stellar turn-off mass. The symbols are the same as in Fig. 3.3.

faces has yet to be investigated both theoretically and observationally. The theoretical calculations indicate that the nature of nucleosynthesis and mixing depend upon the degree of degeneracy in the He-core and, hence, intensity of the explosion: intermediate flashes produce most efficient mixing (Despain 1982; Deupree 1986; Deupree & Wallace 1987). Attempts to model this violent event of stellar evolution are continuing (e.g. Schlattl et al. 2001; Cassisi et al. 2003; Dearborn, Lattanzio & Eggleton 2006; Mocák et al. 2010 and references therein). Precise observations of RGB-tip stars and clump stars in clusters are most useful in order to uncover the effects of the He-core flash.

In the previously investigated open cluster NGC 7789 we also found some differences in the mean $^{12}C/^{13}C$ and $^{12}C/^{14}N$ ratios when comparing giants and clump stars (Tautvaišienė et al. 2005). In NGC 7789 we also investigated the first-ascent giants located above the red giant bump and more evolved clump stars. The mass of turn-off stars is of about 1.6 $M_{\odot}$. The mean $^{12}C/^{14}N$ ratio is 1.9 ± 0.5 in the

giants, and 1.3 ± 0.2 in the clump stars; however, the $^{12}C/^{13}C$ ratios are very similar for all the stars investigated, 9 ± 1. One RGB-tip star and two clump stars were investigated in the cluster NGC 3532 by Smiljanic et al. (2009). The mean $^{12}C/^{13}C$ ratio in the clump stars is 11 ± 1, while in the RGB-tip star is larger and equal to 20. However, the C/N ratios are about the same. $^{12}C/^{13}C$ ratios depend little on stellar atmospheric parameters and are sensitive indicators of mixing processes, their analysis has to be continued. We plan to address this topic in our forthcoming studies.

3.3 Galactic radial abundance gradients

The open cluster radial abundance gradient was analysed and discussed many times during several decades (see e.g. Friel 1995; Twarog, Ashman & Anthony-Twarog 1997; Bragaglia et al. 2001, 2008; Friel et al. 2002; Friel, Jacobson & Pilachowski 2005; Carretta et al. 2004, 2005; Carretta, Bragaglia & Gratton 2007; Yong, Carney & Teixera de Almeida 2005; Sestito et al. 2006; Sestito, Randich & Bragaglia 2007; Sestito et al. 2008; Jacobson, Friel & Pilachowski 2008, 2009; Smiljanic et al. 2009; Pancino et al. 2010 and references therein). Twarog, Ashman & Anthony-Twarog (1997) first proposed that the open cluster abundance distribution is not a negative linear gradient but two separate distributions, each of constant metallicity, divided at $R_{gc} = 10$ kpc. Clusters in the inner part are of solar metallicity, while in the outer part the mean metallicity is about -0.3 dex. The recent investigations of open clusters, reaching also the more distant parts of the disk, show that maybe the gradient is not the same across the whole disk: it is rather steep in the inner disk ($R_{gc} < 12 - 14$ kpc), and it flattens in the outer disk (c.f., Carraro et al. 2004, 2007; Yong, Carney & Teixera de Almeida 2005; Sestito et al. 2006; Sestito, Randich & Bragaglia 2007; Sestito et al. 2008; Jacobson, Friel & Pilachowski 2009; Jacobson, Pilachowski & Friel 2011).

Recently, Magrini et al. (2009) used a set of literature abundances of open clusters, based on high resolution spectroscopy, to compare the gradient, and its time evolution, with their models of chemical evolution. However, their sample is not homogeneous (distances, ages, and abundances were taken from papers of many different groups) so it is not an ideal set, since systematics can mask or produce features in the distribution. The BOCCE project aims at collecting a homogeneous

sample, well spread over the Galactic plane, covering a wide range of ages, and metallicities. Figures 3.5, 3.6, 3.7, 3.8, and 3.9 display the radial distribution of some elemental abundances for the targets analysed so far by BOCCE and for other clusters in recent studies. The scatter is quite large at all radii, but the results of our sample clusters agree well with the data on other open clusters at similar $R_{\rm gc}$.

3.3.1 Oxygen

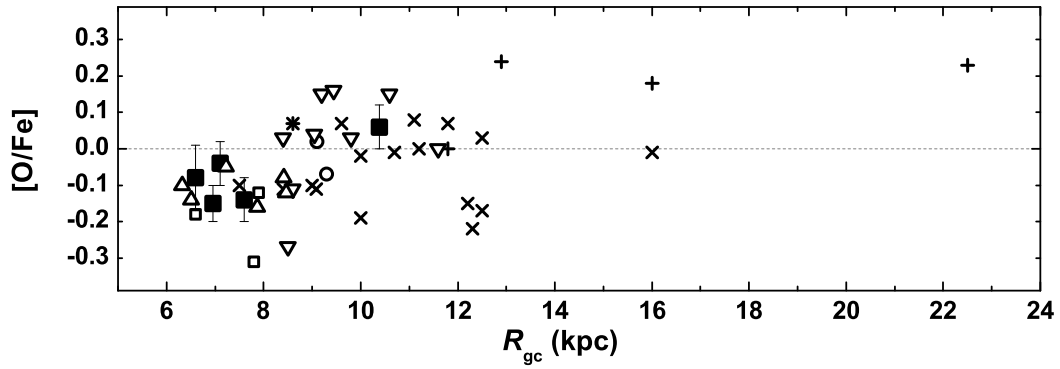

Figure 3.5: Radial distribution of oxygen abundances in open cluster. Open squares show the results by Carretta et al. (2005); Carretta, Bragaglia & Gratton (2007). The results of this study are marked as filled squares. Crosses represent the results presented in the papers by Friel, Jacobson & Pilachowski (2005) and Jacobson, Friel & Pilachowski (2008, 2009); Jacobson, Pilachowski & Friel (2011), pluses – Yong, Carney & Teixera de Almeida (2005), circles – Tautvaišienė et al. (2000, 2005), triangles – Smiljanic et al. (2009), and reversed triangles – Pancino et al. (2010) and Carrera & Pancino (2011).

The analysis of oxygen abundance was performed using the most popular forbidden [O I] line at 6300 Å. While determining the carbon abundance, we also had to analyse oxygen since carbon and oxygen are bound together by the molecular equilibrium in the stellar atmosphere. The mean oxygen to iron abundance ratios are presented in Tables 3.2, 3.3, 3.4, 3.5 and the mean cluster abundances are presented in Table 3.6. These results are in agreement with oxygen abundances in metal rich dwarfs (Bensby, Feltzing & Lundström 2004 and references therein). The results for oxygen are also in good agreement with the values found by Carretta et al. (2005) and Carretta, Bragaglia & Gratton (2007). The increase in [O/Fe] values (see

Fig. 3.5) towards larger Galactocentric distances till about R_{gc} = 12 kpc is a mirror image of the [Fe/H] trend (Friel, Jacobson & Pilachowski 2005; Jacobson, Friel & Pilachowski 2008, 2009; Jacobson, Pilachowski & Friel 2011). This is due to a relationship between [O/Fe] and [Fe/H] that has been seen in numerous field star studies (see, e.g., Bensby et al. 2005; Jacobson, Pilachowski & Friel 2011), and which has been attributed to the increased contribution of Type Ia supernovae over time to the chemical enrichment of the disk. However, the appearance of the trend is driven by the innermost ($R_{gc} \leq 8$ kpc) and outermost ($R_{gc} \geq 15$ kpc) objects; the [O/Fe] distribution for $R_{gc} = 9 - 14$ kpc clusters is quite flat, consistent with the solar ratio (Jacobson, Friel & Pilachowski 2009; Jacobson, Pilachowski & Friel 2011).

3.3.2 Sodium and aluminum

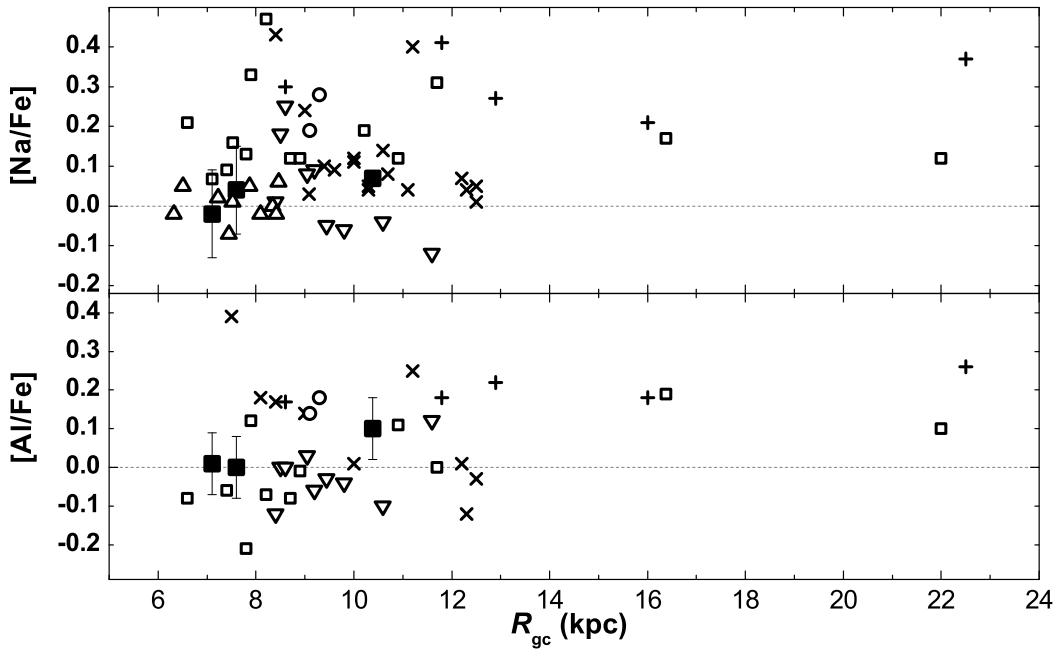

Figure 3.6: Radial distribution of sodium and aluminium abundances in open clusters. Open squares show results by Bragaglia et al. (2001, 2008), Carretta et al. (2004, 2005); Carretta, Bragaglia & Gratton (2007), and Sestito et al. (2006); Sestito, Randich & Bragaglia (2007); Sestito et al. (2008). Other symbols are the same as in Fig. 3.5.

Sodium and aluminium are among the chemical elements for which observa-

tions of abundance anomalies are also present. The O-Na anticorrelation has been observed among the brightest red giants in Galactic globular clusters for a long time (see Kraft 1994; Da Costa 1998; Denissenkov & Herwig 2003 and references therein). An overabundance of Na could appear, due to the deep mixing from layers of the NeNa cycle of H burning. Extensive theoretical studies of deep mixing in stellar atmospheres have been carried out Denissenkov & Weiss (1996); Denissenkov & Tout (2000); Denissenkov & Herwig (2003); Gratton, Sneden & Carretta (2004), and references therein. However, the explanation of abundance changes by deep mixing has been eliminated by the determination of an Na–O anticorrelation in less evolved stars down to the main sequence (Gratton et al. 2001; Thévenin et al. 2001; Ramirez & Cohen 2002; D'Orazi et al. 2010). For a recent discussion of Na and O abundances in open clusters, see Denissenkov, Pinsonneault & MacGregor (2009), who explicitly addressed the problem of the (not seen) Na–O anticorrelation.

Abundances of sodium were determined from the NLTE analysis of Na I lines at 5682.64 Å, 6154.23 Å and 6160.75 (Å). The Na I line at 5682.64 Å was not available for the analysis of UVES spectra. Abundances of aluminium were determined from Al I lines at 6696.03 Å, 6698.67 Å, 7835.30 Å and 7836.13 Å. The stars of the three clusters in our sample, where the elements heavier than oxygen were investigated (NGC 2506, NGC 6134 and IC 4651) do not show overabundances either of sodium or of aluminium (Fig. 3.6).

There are two studies, where the same open cluster IC 4651 was investigated. Pasquini et al. (2004) investigated spectra of both giants and main-sequence stars in IC 4651, and Pace, Pasquini & François (2008) studied the main-sequence stars in this cluster. The authors expressed their strong believe that [Na/Fe] ratio is comprehensively higher in the giants in comparison to the main-sequence stars and that this is due to internal nucleosynthesis and mixing. However, neither Pace, Pasquini & François (2008) nor our study can confirm this statement. In Table 3.8, we present the mean [El/Fe] for giant and main-sequence stars of IC 4651 investigated in our work, Pasquini et al. (2004) and Pace, Pasquini & François (2008). In our work, the abundances of Na and Mg were determined with NLTE taken into account, and we do not find an overabundance of these chemical elements. Aluminium is close to solar in all three studies. The [Na/Fe] and [Al/Fe] ratios confirm observational evidences by other authors that the radial abundance distributions of these elements

Table 3.8: The mean [El/Fe] for giant (G) and main-sequence (MS) stars of IC 4651 investigated in this work, Pasquini et al. (2004) and Pace, Pasquini & François (2008).

	This work	Pasquini et al.		Pace et .al.
Species	[El/Fe]	[El/Fe]	[El/Fe]	[El/Fe]
	G	G	MS	MS
Na I	0.00	0.19	–0.09	–0.03
Mg I	–0.05	0.09	0.13	
Al I	0.03	0.07	–0.07	–0.10
Si I	0.09	0.08	0.07	–0.02
Ca I	0.05	0.00	0.04	0.04
Sc II	0.01	0.11	–0.11	
Ti I	0.11	0.12	0.08	–0.02
Ti II	0.07	0.18	0.00	
Cr I	–0.05	–0.02	0.11	
Ni I	0.07	0.10	0.01	–0.02

are essentially flat.

3.3.3 α-elements

According to observations of main sequence stars in the Galactic disk, abundance ratios of α-elements to iron at the solar metallicity are solar or slightly higher. In the study by Edvardsson et al. (1993), [Mg/Fe], [Si/Fe] and [Ti/Fe] for almost all of the stars lie slightly above the solar ratio, [Ca/Fe] are solar. In the study of Reddy et al. (2003), [Mg/Fe] and [Si/Fe] values are above solar, while [Ca/Fe] and [Ti/Fe] are exactly solar. The mean [α/Fe] ratios in most of the open clusters investigated are slightly higher than in the Sun, and, especially, the overabundance of silicon is noticeable (c.f. Brown et al. 1996; Bragaglia et al. 2001; Friel et al. 2003, but see, also, Bragaglia et al. 2008; Sestito et al. 2008). There has also been a claim that [α/Fe] is higher for the outer disk clusters (e.g., Yong, Carney & Teixera de Almeida 2005), but this has not been confirmed by other studies (Carraro et al. 2007; Sestito et al. 2008).

In the cluster NGC 2506, the mean cluster abundances of four α-elements is $[\alpha/\mathrm{Fe}] \equiv \frac{1}{4}([\mathrm{Mg/Fe}]+[\mathrm{Si/Fe}]+[\mathrm{Ca/Fe}]+[\mathrm{Ti/Fe}]) = 0.0 \pm 0.06$ (s.d.). In NGC 6134, the mean cluster $[\alpha/\mathrm{Fe}] = 0.02 \pm 0.03$ (s.d.), which is very close to the solar value. For IC 4651, the mean $[\alpha/\mathrm{Fe}] = 0.06 \pm 0.07$ (s.d.) is also close to the solar value.

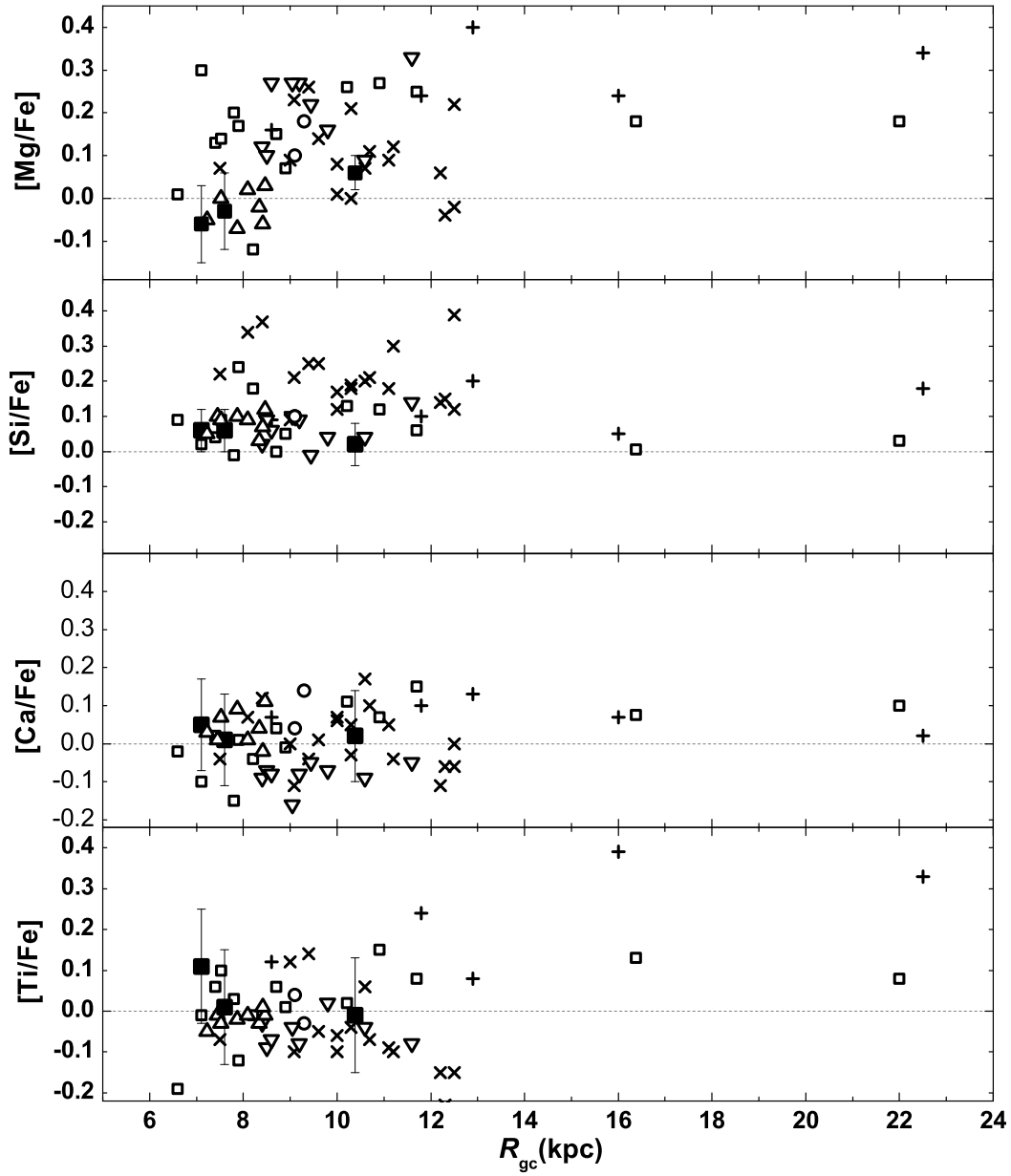

Figure 3.7: Radial distribution of magnesium, silicon, calcium and titanium abundances in open clusters. Symbols are the same as in Fig. 3.6.

The study of Pasquini et al. (2004) (see Table 3.8) also revealed a closely similar $[\alpha/\mathrm{Fe}]$ value for giants, 0.07 ± 0.05 (s.d.), and for main-sequence stars, 0.08 ± 0.04 (s.d.).

The radial dependence of element-to-iron ratios are shown in Figure 3.7. With the exception of oxygen and magnesium, the range of all element abundances appears roughly constant and independent of Galactic radial distance, with no evidence of a

change from the inner to the outer disk. The flat distributions of abundances relative to iron with Galactic radial distances for the α-elements are consistent with that seen in the inhomogeneous cluster sample of Pancino et al. (2010). They found that the clusters beyond $R_{gc} = 15$ kpc have slightly larger [α/Fe] ratios than the clusters inside this R_{gc}, but emphasised that the distribution is also consistent, within the errors, with that having a zero slope. As seen in Figure 3.7, the outer disk clusters have slightly enhanced [Mg/Fe] ratios compared to some inner disk clusters, but this is not the case for Si, Ca, or Ti (accounting for the dispersion in individual cluster Ti abundances from different studies). The magnitude of abundance dispersions, seen in Figure 3.7, varies from element to element, with the α-elements generally ranging between 0.3–0.4 dex. Many of the clusters are enhanced in Mg and Si. The [Si/Fe], [Ca/Fe] and [Ti/Fe] ratios confirm observational evidences by other authors that radial abundance distributions of these elements are essentially flat. The radial distribution of [Mg/Fe] have a tendency to increase towards larger Galactocentric distances till about R_{gc} = 12 kpc.

3.3.4 Iron group elements

We measured abundances of scandium, vanadium, chromium, manganese, cobalt and nickel. The scandium and vanadium were derived from up to nine lines of ScII and VI. Scandium is not overabundant. Vanadium shows some overabundance in the clusters NGC 6134 and IC 4651. We derived chromium from both neutral and ones-ionised species. Both CrI and CrII abundance to iron ratios do not show significant differences from the solar ratios. The manganese abundances were derived from two to six spectral lines, depending on the spectrograph properties. Manganese is slightly underabundant in the open cluster NGC 2506. The cobalt abundance to iron ratio is slightly overabundant in the clusters NGC 6134 and IC 4651. The [NiI/Fe] values (as expected) do not show any differences from the solar ratio. The radial distribution of nickel abundances in the open clusters is shown in Fig. 3.8.

For the cluster IC 4651Pasquini et al. (2004) and Pace, Pasquini & François (2008) (see Table 3.8) also presented the nickel abundances. Our value is close to that found for giants by Pasquini et al. (2004).

The small dispersion in [Ni/Fe] seen for the clusters across the entire range of

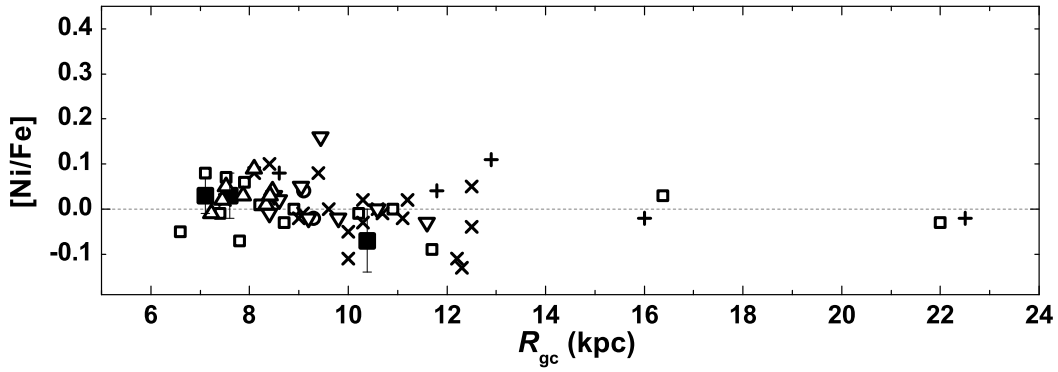

Figure 3.8: Radial distribution of nickel abundances in open clusters. Symbols are the same as in Fig. 3.6.

Galactic radial distances is reassuring: [Ni/H] generally follows [Fe/H] in the metallicity range spanned by open clusters, therefore, the values of [Ni/Fe] around 0 and a small dispersion indicate robustness in the Fe analysis. [Ni/Fe] ratios confirm observational evidences by other authors that radial abundance distribution of this element is essentially flat.

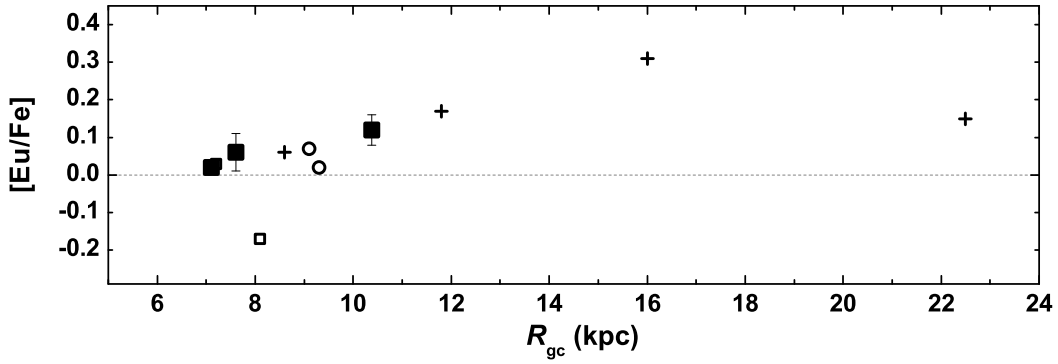

Figure 3.9: Radial distribution of open cluster europium abundances. Open squares show results by Carretta, Bragaglia & Gratton (2007). The results of this study are marked as a filled squares. Pluses show results presented in the paper by Yong, Carney & Teixera de Almeida (2005), and circles – Tautvaišienė et al. (2000, 2005).

3.3.5 *s*- and *r*-process elements

There are no many lines of *s*- and *r*-process elements for the abundance derivation in the analysed spectra. We derived abundances of zinc, yttrium, zirconium, barium, lanthanum, cerium, praseodymium, neodymium and europium in three clusters (NGC 2506, NGC 6134 and IC 4651). As it is seen from Tables 3.3, 3.4, and 3.5, the ratios of abundances of iron group, *s*- and *r*-process elements to iron are close to solar. Only the europium abundance in the more distant cluster NGC 2506 is overabundant by 0.2 dex. The open cluster IC 4651 was investigated later on by Maiorca et al. (2011) they analysed abundances of yttrium, zirconium, lanthanum and cerium, and confirmed our results. *s*- and *r*-process elemental analyses in open clusters are very scarce. The radial distribution of europium abundances in the open clusters is shown in Fig. 3.9.

Chapter 4

Main results and conclusions

1. Photospheric abundances of up to 26 chemical elements determined in three open clusters (NGC 2506, NGC 6132, and IC 4651). Atmospheric parameters determined for stars in the open clusters NGC 2506 and NGC 6253.

2. $^{12}C/^{13}C$ and $^{12}C/^{14}N$ ratios determined in evolved stars of five open clusters:
   - NGC 2506 $^{12}C/^{13}C=9\pm1$, C/N=1.04 ± 0.11 in two clump stars, and $^{12}C/^{13}C$=14, C/N=1.55 in the RGB-tip star;
   - NGC 6134 $^{12}C/^{13}C=9\pm2.5$ and C/N=1.2 ± 0.2 in six clump stars;
   - NGC 6253 $^{12}C/^{13}C=16\pm2.5$ and C/N=1.37 ± 0.09 in four clump stars;
   - IC 4651 $^{12}C/^{13}C=16\pm2$, C/N=1.36 ± 0.14 in three clump stars, and $^{12}C/^{13}C=15\pm1$, C/N=1.23 ± 0.15, in two first ascent giants;
   - Collinder 261 $^{12}C/^{13}C=12\pm1$, C/N=1.62 ± 0.06 in two clump stars, and $^{12}C/^{13}C=18\pm2$, C/N=1.79 ± 0.18, in four first ascent giants.

3. The $^{12}C/^{13}C$ ratios in helium-core-burning clump stars for the clusters with turn-off masses lower than 2 $M_{\odot}$ are in agreement with the Cool-bottom processing (CBP) model and the Thermohaline mixing (TH) model.

4. The observed $^{12}C/^{13}C$ ratios of the helium-core-burning stars in the open cluster NGC 6134 support the observational evidence for extra-mixing in stars heavier than 2.5 $M_{\odot}$ and are in dissagreament with the theoretical models of mixing which state that extra-mixing is not possible for stars with higher turn-off mass than 2.5 $M_{\odot}$.

5. In the open clusters NGC 2506 and NGC 6253, the $^{12}C/^{13}C$ ratios in core-helium-burning stars are lower than in the first ascent giants, located above the

RGB luminosity bump. This could be caused by the further material mixing during a very violent helium flash event.

6. The [Na/Fe], [Al/Fe], [Si/Fe], [Ca/Fe], [Ti/Fe] and [Ni/Fe] ratios confirm observational evidences by other authors that the radial abundance distributions of these elements are essentially flat. The radial distributions of [O/Fe] and [Mg/Fe] have a tendency to increase towards larger Galactocentric distances till about R_{gc} = 12 kpc.

References

Angelou G. C., Stancliffe R. J., Church R. P., Lattanzio J. C., Smith G. H., 2012, ApJ, 749, 128

Ahumada J. A. 2002, ASP Conference Series, 274, 307

Alonso A., Arribas S., Martínez-Roger C., 1999, A&AS, 140, 261

Alonso A., Arribas S., Martínez-Roger C., 2001, A&A, 376, 1039

Anthony-Twarog B. J. & Twarog B. A., 1987, AJ, 94, 1222

Anthony-Twarog B. J. & Twarog B. A., 2000, AJ, 119, 2282

Anthony-Twarog B. J., Mukherjee K., Twarog B. A., Caldwell N., 1988, AJ, 95, 1453

Anthony-Twarog B. J., Deliyannis C. P., Twarog B. A., Cummings J. D., Maderak R. M., 2010, AJ, 139, 2034

Barisevičius G., Tautvaišienė G., Berdyugina S., Chorniy Y., Ilyin I., 2010, BaltA, 19, 157

Barisevičius G., Tautvaišienė G., Berdyugina S., Chorniy Y., Ilyin I., 2011, BaltA, 20, 53

Barklem P. S., Piskunov N., O'Mara B. J., 2000, A&AS, 142, 467

Bensby T., Feltzing S., Lundström I., 2004, A&A, 415, 155

Bensby T., Feltzing S., Lundström I., Ilyin I., 2005, A&A, 433, 185

Biazzo K., Pasquini L., Girardi L., Frasca A., da Silva L., Setiawan, J., Marilli, E., Hatzes, A. P., Catalano, S.

Biehl D., 1976, Diplomarbeit, Christian-Albrechts-Universitaet Kiel, Institut fuer Theoretishe Physik und Sternwarte

Boothroyd A. I., Sackmann I.-J., Wasserburg G. J., 1995, ApJ, 442, L21

Boothroyd A. I., Sackmann I. J., 1999, ApJ, 510, 232

Bragaglia A., Tessicini G., Tosi M., Marconi G., Munari U., 1997, MNRAS, 284, 477

Bragaglia A., Tosi M. 2006, AJ, 131, 1544

Bragaglia A., Tosi M., 2007, ASPC, 374, 175

Bragaglia A., et al. 2001, AJ, 121, 327

Bragaglia A., Sestito P., Villanova S., Carretta E., Randich S., Tosi M., 2008, A&A, 480, 79

Brown J. A., Wallerstein G., Geisler D., Oke J. B., 1996, AJ, 112, 1551

Bruntt H., Frandsen S., Kjeldsen H., Andersen M. I., 1999, A&AS, 140, 135

Cayrel R., 1988, IAUS, 132, 345

Cantiello M. & Langer N., 2010, A&A, 521, 9

Canto Martins B. L., Lèbre A., Palacios A., de Laverny P., Richard O., Melo C. H. F., Do Nascimento J. D., Jr., de Medeiros J. R., 2011, A&A, 527, A94

Carraro G., Chiosi C., 1994, A&A, 288, 751

Carraro G., Ng Y. K., Portinari L., 1998, MNRAS, 296, 1045

Carraro G., Bresolin F., Villanova S., Matteucci F., Patat F., Romaniello M., 2004, AJ, 128, 1676

Carraro G., Geisler D., Villanova S., Frinchaboy P. M., Majewski S. R., 2007, A&A, 476, 217

Carrera R., Pancino E., 2011, arXiv, arXiv:1107.2242

Carretta E., Bragaglia A., Gratton R., Tosi M., 2004, A&A, 422, 951

Carretta E., Bragaglia A., Gratton R., Tosi M., 2005, A&A, 441, 131

Carretta E., Bragaglia A., Gratton R. 2007, A&A, 473, 129

Cassisi S., Schlattl H., Salaris M., Weiss A., 2003, ApJ, 582, L43

Castelli F., 1988, Pubblicazione Osservatorio Astronomico di Trieste, 1164

Chanamé J., Pinsonneault M., Terndrup D. M., 2005, ApJ, 631, 540

Charbonnel C. & Lagarde N., 2010, A&A, 522, 10

Charbonnel, C. & Zahn, J.-P. 2007, A&A, 467, 15

Charbonnel C., 1994, A&A, 282, 811

Charbonnel C., Brown J. A., Wallerstein G., 1998, A&A 332, 204

Chen W.P., Chen C.W., Shu C.G., 2004, AJ, 128, 2306

Charbonnel C., 2006, EAS, 19, 125

Chiu L.-T. G., van Altena W. F., 1981, ApJ, 243, 827

Claria J. J., Mermilliod J. C., 1992, A&AS, 92, 429

Cunha K., 2010, IAUS, 268, 243

Coplen T. et al. 2002, Pure & Appl. Chem. 74:1987-2017

D'Orazi V., Lucatello S., Gratton R., Bragaglia A., Carretta E., Shen Z., Zaggia S., 2010, ApJ, 713, L1

Da Costa G.S., 1998, IAUS, 189, 193

De Silva G. M., Freeman K. C., Asplund M., Bland-Hawthorn J., Bessell M. S., Collet R., 2007, AJ, 133, 1161

De Silva G. M., Gibson B. K., Lattanzio J., Asplund M., 2009, A&A, 500, L25

Dearborn D. S. P., Lattanzio J. C., Eggleton P. P. 2006, ApJ, 639, 405

Den Hartog E. A., Lawler J. E., Sneden C., Cowan J. J., 2003, ApJS, 148, 543

Denissenkov P. A., Weiss A., 1996, A&A, 308, 581

Denissenkov P. A., Tout C. A., 2000, MNRAS, 316, 395

Denissenkov P. A., Herwig F., 2003, ApJ, 590, L99

Denissenkov P. A., 2010, ApJ, 723, 563

Denissenkov P. A., Pinsonneault M., MacGregor K. B., 2009, ApJ, 696, 1823

Denissenkov P. A., Merryfield W. J., 2011, ApJ, 727, L8

Despain K. H. 1982, ApJ, 253, 811

Deupree R.G., Wallace R. K. 1987, ApJ, 317, 724

Deupree R.G. 1986, ApJ, 303, 649

Dias W. S., Alessi B. S., Moitinho A., Lépine J. R. D., 2002, A&A, 389, 871

Edvardsson B., Andersen J., Gustafsson B., Lambert D. L., Nissen P. E., Tomkin J., 1993, A&A 275, 101

Eggen, O. J., 1971, ApJ, 166, 87

Eggleton P. P., Dearborn D. S. P., Lattanzio J. C., 2006, Sci, 314, 1580

Friel E. D., Janes K. A., 1993, A&A, 267, 75

Friel E. D., 1995, ARA&A, 33, 381

Friel E. D., Janes K. A., Tavarez M., Scott J., Katsanis R., Lotz J., Hong L., Miller N., 2002, AJ, 124, 2693

Friel E. D, Jacobson H. R., Barrett E., Fullton L., Balachandran S. C., Pilachowski C. A., 2003, AJ, 126, 2372

Friel E. D., Jacobson H. R., Pilachowski C. A., 2005, AJ, 129, 2725

Gaigé Y., 1993, A&A, 269, 267

Geisler D., Claria J. J., Minniti D., 1992, AJ, 104, 1892

Geisler D., 1984, ApJ, 287, L85

Genova F., 2009, MmSAI, 80, 548

Gilroy K. K., 1989, ApJ, 347, 835

Gilroy K. K., Brown J. A., 1991, ApJ, 371, 578

Girardi L., Bressan A., Bertelli G., Chiosi C., 2000, A&AS, 141, 371

Gonzalez, G., Lambert, D.L., Wallerstein, G., Rao, N.K., Smith, V.V., McCarthy, J.K., 1998, ApJS 114, 133

Gonzalez G., Wallerstein G., 2000, PASP, 112, 774

Gozzoli E., Tosi M., Marconi G., Bragaglia A., 1996, MNRAS, 283, 66

Gratton R.G., 1988, Rome Obs. Preprint Ser., 29

Gratton R.G., Carretta, E., Eriksson, K., Gustafsson, B., 1999, A&A, 350, 955

Gratton R.G., Sneden C., Carretta E., Bragaglia A. 2000, A&A, 345, 169

Gratton R.G., et al. 2001, A&A, 369, 87

Gratton R.G., Sneden C., Carretta E. 2004, ARA&A, 42, 385

Gratton R.G., Bragaglia A., Carretta E., Tosi M. 2006, ApJ, 642, 462

Grevesse N., Sauval A. J., 1998, SSRv, 85, 161

Grevesse N., Sauval A. J., 2000, "Origin of Elements in the Solar System, Implications of Post-1957 Observations, O. Manuel (ed.), Kluwer, 261

Gurtovenko E. A., Kostyk R. I., 1989, "Fraunhofer's spectrum and a system of solar oscillator strengths", Kiev, Naukova Dumka, 200

Gustafsson B., Karlsson T., Olsson E., Edvardsson B., Ryde N., 1999, A&A, 342, 426

Gustafsson B., Edvardsson B., Eriksson K., Jørgensen U. G., Nordlund Å., Plez B., 2008, A&A, 486, 951

Heiter U., et al., 2008, JPhCS, 130, 012011

Iben I., Jr., 1965, ApJ, 142, 1447

Iben I., Jr., 1967, ApJ, 147, 624

Yong D., Carney B. W., Teixera de Almeida M. L., 2005, AJ, 130, 597

Israelian G., Santos N. C., Mayor M., Rebolo R., 2003, A&A, 405, 753

Jacobson H. R., Friel E. D., Pilachowski C. A., 2008, AJ, 135, 2341

Jacobson H. R., Friel E. D., Pilachowski C.A., 2009, AJ, 137, 4753

Jacobson H. R., Pilachowski C. A., Friel E. D., 2011, AJ, 142, 59

Janes K. A., Phelps R. L., 1994, AJ, 108, 1773

Johansson S., Litzén U., Lundberg H., Zhang Z., 2003, ApJ, 584, 107

Juozapavičius, A., Mažeika, D. 2007, Baltic IT&T Review, 3, 5

Kim S. et al., 2001, AcA, 51, 49

Kjeldsen H., Frandsen S., 1991, A&AS, 87, 119

Kraft R. P., 1994, PASP, 106, 553

Kunze E., 2003, PrOce, 56, 399

Kupka F. G., Ryabchikova T. A., Piskunov N. E., Stempels H. C., Weiss W. W., 2000, BaltA, 9, 590

Kurucz R. L., Furenlid I., Brault J., Testerman L., 1984, ”Solar Flux Atlas from 296 to 1300 nm.”, National Solar Observatory, Sunspot, New Mexico

Kurucz R., 1993, KurCD, 13,

Kurucz R. L., Bell B., 1995, Atomic Line Data, Kurucz CD-ROM No. 23, Cambridge Mass.: Smithsonian Asatrophysical Observatory.

Kurucz R. L., 2005, MSAIS, 8, 189

Lawler J. E., Wickliffe M.E., Den Hartog E. A., 2001, ApJ, 563, 1075

Langmuir I., Kingdon K. H., 1923, Phys. Rev., 22, 148

Lagarde N., Charbonnel C., Decressin T., Hagelberg J., 2011, A&A, 536, A28

Letarte B., 2007, PhD dissertation, Univ. Groningen, Netherlands

Lindoff U., 1972, A&AS, 7, 231

Luck R. E., 1994, ApJS, 91, 309

Magrini L., Sestito P., Randich S., Galli D., 2009, A&A, 494, 95

Maiorca E., Randich S., Busso M., Magrini L., Palmerini S., 2011, ApJ, 736, 120

Marconi G., Hamilton D., Tosi M., Bragaglia A., 1997, MNRAS, 291, 763

Mashonkina L. & Gehren T, 2000, A&A, 364, 249

Mazur B., Krzeminski W., Kaluzny J., 1995, MNRAS, 273, 59

McClure R. D., 1974, ApJ, 194, 355

McClure R. D., Twarog B. A., Forrester W. T., 1981, ApJ, 243, 841

McWilliam A. 1998, AJ, 115, 1640

Meibom S., Andersen J., Nordström B., 2002, A&A, 386, 187

Meibom S., 2000, A&A, 361, 929

Mermilliod J.-C., 1995, ASSL, 203, 127

Mermilliod J.-C., Paunzen E., 2003, A&A, 410, 511

Minniti D., 1995, A&AS, 113, 299

Mikolaitis Š., Tautvaišienė G., Gratton R., Bragaglia A., Carretta E., 2010, MNRAS, 407, 1866

Mikolaitis Š., Tautvaišienė G., Gratton R., Bragaglia A., Carretta E., 2011a, MNRAS, 413, 2199

Mikolaitis Š., Tautvaišienė G., Gratton R., Bragaglia A., Carretta E., 2011b, MNRAS, 416, 1092

Mikolaitis Š., Tautvaišienė G., Gratton R., Bragaglia A., Carretta E., 2012, A&A, 541, A137

Mikolaitis Š., Tautvaišienė G., 2011, EAS, 45, 413

Mocák M., Campbell S. W., Müller E., Kifonidis K. 2010, A&A, 520, 114

Monaco L., et al., 2011, A&A, 529, A90

Montalto M., Piotto G., Desidera S., Platais I., Carraro G., Momany Y., de Marchi F., Recio Blanco A., 2009, yCat, 350, 51129

Moore C. E., Minnaert M. G. J., Houtgast J., 1966, The Solar Spectrum 2935 Å to 8770 Å, NBS Monogr., No. 61

Nissen P. E., 1988, A&A, 199, 146

Origlia L., Valenti E., Rich R. M., Ferraro F. R., 2006, AJ, 646, 499

Pace G., Pasquini L., François P., 2008, A&A, 489, 403

Pagel B. E. J., 1974, MNRAS, 167, 413

Palacios A., Gebran M., Josselin E., Martins F., Plez B., Belmas M., Lèbre A., 2010, A&A, 516, A13

Pallavicini R., 2003, MSAIS, 3, 74

Palmerini S., La Cognata M., Cristallo S., Busso M., 2011, ApJ, 729, 3

Pancino E., Carrera R., Rossetti E., Gallart C., 2010, A&A, 511, 56

Pasquini L., Randich S., Zoccali M., Hill V., Charbonnel C., Nordström B., 2004, A&A, 424, 951

Paunzen E., 2008, CoSka, 38, 435

Phelps R. L., Janes K. A., Montgomery K. A., 1994, AJ, 107, 1079

Piatti A. E., Claria J. J., Abadi M. G., 1995, AJ, 110, 2813

Piatti A. E., Clariá J. J., Bica E., Geisler D., Minniti D., 1998, AJ, 116, 801

Piskunov N. E., Kupka F., Ryabchikova T. A., Weiss W. W., Jeffery C. S., 1995, A&AS, 112, 525

Plez B., 2008, asvo.proc, 169

Puglia S. M. R., 1973, PhD thesis, Univ. of Catania

Purgathofer A., 1964, Zeitschrift fr Astrophysik, 59, 79

Radko T., 2010, JFM, 645, 121

Ramirez S.V., Cohen J.G., 2002, AJ, 123, 3277

Reddy, B.E., Tomkin J., Lambert D.L., Allende Prieto C., 2003, MNRAS, 340, 304

Ruddick B., 2003, PrOce, 56, 483

Santos N. C., Lovis C., Pace G., Melendez J., Naef D., 2009, A&A, 493, 309

Saha M. N., 1921, RSPSA, 99, 135

Sbordone L., Bonifacio P., Castelli F., Kurucz R. L., 2004, MSAIS, 5, 93

Schaller G., Schaerer D., Meynet G., Maeder, A., 1992, A&AS, 96, 269

Schlattl H., Cassisi S., Salaris M., Weiss A. 2001, ApJ, 559, 1082

Schlegel D. J., Finkbeiner D. P., Davis M., 1998, ApJ, 500, 525

Schmitt R. W., 1983, PhFl, 26, 2373

Schmitt R., 2003, PrOce, 56, 419

Sestito P., Bragaglia A., Randich S., Carretta E., Prisinzano L., Tosi M., 2006, A&A, 458, 121

Sestito P., Randich S., Bragaglia A., 2007, A&A, 465, 185

Sestito P., Bragaglia A., Randich S., Pallavicini R., Andrievsky, S. M., Korotin S. A., 2008, A&A, 488, 943

Shi J. R., Zhao G., Chen Y. Q., 2002, A&A, 381, 982

Smiljanic R., Gauderon R., North P., Barbuy, B., Charbonnel C., Mowlavi N., 2009, A&A, 502, 267

Smiljanic R., Pasquini L., Charbonnel C., Lagarde N., 2010, A&A, 510, A50

Sneden C., Pilachowski C. A., 1986, ApJ, 301, 860

Steffen M., 1985, A&AS, 59, 403

Stern, M. E. 1960, Tellus, 12, 172

Šešok, D., Belevičius, R., Kačeniauskas, A., Mockus, J. 2010, Mechanika, No. 2(82), 63

Taffoni G., Vuerli C., Pasian F., 2009, MSAIS, 13, 147

Tautvaišienė G. Edvardsson B., Tuominen I., Ilyin I., 2000, A&A, 360, 499

Tautvaišienė G., Edvardsson B., Tuominen I., Ilyin I., 2001, A&A, 380, 578

Tautvaišienė G. Edvardsson B., Puzeras E., Ilyin I., 2005, A&A, 431, 933

Tautvaišienė G., Mikolaitis Š., Puzeras E., 2009, MmSAI, 80, 534

Tautvaišienė G., Edvardsson B., Puzeras E., Barisevičius G., Ilyin I., 2010a, MNRAS, 409, 1213

Tautvaišienė G., Barisevičius G., Berdyugina S., Chorniy Y., Ilyin I., 2010b, BaltA, 19, 95

Thévenin F., Charbonnel C., de Freitas Pacheco J. A., Idiart T. P., Jasniewicz G., de Laverny, P. & Plez B., 2001, A&A, 373, 905

Thorén P., Edvardsson B., 2000, A&A, 363, L33 s

Tosi M., Greggio L., Marconi G., Focardi P., 1991, AJ, 102, 951

Twarog B. A., Ashman K. M., Anthony-Twarog B. J., 1997, AJ, 114, 2556

Twarog B. A., Anthony-Twarog B. J., De Lee N., 2003, AJ, 125, 1383

Ulrich, R. K. 1972, ApJ, 172, 165

van den Bergh S., Sher D., 1960, Pub. David Dunlap Obs., 2, 203

Wachlin F. C., Miller Bertolami M. M., Althaus L. G., 2011, A&A, 533, A139

Wasserburg G. J., Boothroyd A. I., Sackmann I.-J., 1995, ApJ, 447, L37

Wyller A. A., 1966, ApJ 143, 828

Acknowledgements

First of all I express my gratefulness to my supervisor Gražina Tautvaišienė for leading through all the study process, encouragement and support. I am especially thankful to my colleagues and co-authors Raffaele Gratton, Angela Bragaglia and Eugenio Carretta for the valuable observational material. Bertrand Plez (University of Montpellier II) and Guillermo Gonzalez (Washington State University) were particularly generous in providing us with atomic data for CN and C_2 molecules, respectively. This research has made use of SIMBAD (operated at CDS, Strasbourg, France), VALD (Kupka et al. 2000) and NASA's Astrophysics Data System. I thank the referees of all papers and this thesis for a careful reading of the manuscript and constructive suggestions for the improvement of the work.